CIVIL ENGINEERING STUDIES
Illinois Center for Transportation Series No. 16-012
UILU-ENG-2016-2012
ISSN: 0197-9191

LOAD RATING AND FRP RETROFITTING OF BRIDGE ABUTMENT TIMBER PILES

Prepared By
Kun-Ho Eugene Kim
Bassem Andrawes
University of Illinois at Urbana-Champaign

Research Report No. FHWA-ICT-16-011

A report of the findings of

ICT PROJECT R27-134
Strengthening of Bridge Wood Piling Retrofits for Moment Resistance, Phase II

Illinois Center for Transportation

May 2016

TECHNICAL REPORT DOCUMENTATION PAGE

1. Report No.	2. Government Accession No.	3. Recipient's Catalog No.
FHWA-ICT-16-011		

4. Title and Subtitle	5. Report Date
Load Rating and FRP Retrofitting of Bridge Abutment Timber Piles	May 2016
	6. Performing Organization Code

7. Author(s)	8. Performing Organization Report No.
Kun-Ho E Kim, Bassem O. Andrawes	ICT-16-012 UILU-ENG-2016-2012

9. Performing Organization Name and Address	10. Work Unit No.
Illinois Center for Transportation Department of Civil and Environmental Engineering University of Illinois at Urbana-Champaign 205 North Mathews Avenue, MC-250 Urbana, IL 61801	11. Contract or Grant No. R27-134

12. Sponsoring Agency Name and Address	13. Type of Report and Period Covered
Illinois Department of Transportation (SPR) Bureau of Material and Physical Research 126 East Ash Street Springfield, IL 62704	Phase II Final Report November 16, 2012–May 15, 2016
	14. Sponsoring Agency Code FHWA

15. Supplementary Notes

Conducted in cooperation with the U.S. Department of Transportation, Federal Highway Administration.

16. Abstract

This report details Phase II of the study titled Strengthening of Bridge Wood Piling Retrofits for Moment Resistance. Phase I of the research (project R27-082) was focused on developing a load rating method for timber piles under eccentric load and examining FRP retrofitting of pier piles. However, Phase II focused first on numerically assessing the state of the practice of timber pile retrofitting in Illinois. The study next focused on investigating load rating and FRP retrofitting of abutment timber piles as well as studying the long-term performance of FRP-wrapped timber piles. Historically, timber piles have been designed for axial loads only. Under this assumption, conventional load rating procedures considered only the effect of dead and live loads in determining the capacity of a timber pile. Unlike pier timber piles, abutment piles must resist significant lateral forces from earth pressure and surcharge loads in addition to dead and live loads. Currently, there does not exist a separate load rating procedure for abutment timber piles. In this study, a load rating method was developed specifically for abutment timber piles. The combined loading effects were accounted for by using the allowable stress P–M interaction equation in the National Design Specification for Wood Construction (NDS). In addition, a method was developed to account for the effect of FRP retrofits in the load rating. The results showed that deterioration levels as low as 10% could lead to unsatisfactory load ratings for abutment timber piles depending on the backfill soil type and equivalent fluid pressure assumed. FRP retrofitting, however, increased the load rating of deteriorated abutment timber piles by at least 17%. FRP retrofitting techniques for abutment piles were also examined experimentally. Three full-size timber pile specimens with different levels of deterioration were tested. A nondestructive stress wave timing method was used to assess the condition of each specimen. FRP retrofits were designed for two of the specimens based on the results of the condition assessment. The piles were load tested in the axial direction. First, a specified eccentric load was applied to induce a bending moment, then a concentric axial load was applied until the proportional limit. Each pile was tested under a series of eccentric loads varying from 10 kips to 35 kips. Timber condition normalized test results showed that the FRP retrofit was able to at least restore the properties of the piles to their undeteriorated condition properties. Finally, the long-term performance of FRP-wrapped timber piles was studied by examining their performance in uniaxial compression after exposure to long-term degradation. Field-extracted red oak pile specimens with different degrees of initial deterioration were used in the study. The initial condition of the timber was assessed through stress wave timing. To simulate natural degradation in unretrofitted and retrofitted timber piles caused by environmental exposure in a short period of time, an accelerated aging procedure was used. The number of FRP layers and type of resin used (polyester, standard epoxy, and moisture-tolerant epoxy) were varied. Results showed that accelerated aging induces significant deterioration in unretrofitted timber piles but the effects are relatively minor in the FRP-wrapped specimens. It was also proven that FRP composite can significantly improve the performance of timber piles in terms of peak stress and ductility, even after being subjected to extreme degradation.

17. Key Words	18. Distribution Statement
Bridge Abutment, Timber Piles, Load Rating, Fiber-Reinforced Polymer, Retrofit, Long-term Performance	No restrictions. This document is available through the National Technical Information Service, Springfield, VA 22161.

19. Security Classif. (of this report)	20. Security Classif. (of this page)	21. No. of Pages	22. Price
Unclassified	Unclassified	65 pp. plus appendices	N/A

ACKNOWLEDGMENT AND DISCLAIMER

This publication is based on the results of ICT-R27-134**, Strengthening of Bridge Wood Piling Retrofits for Moment Resistance, Phase II**. ICT-R27-134 was conducted in cooperation with the Illinois Center for Transportation; the Illinois Department of Transportation, Division of Highways; and the U.S. Department of Transportation, Federal Highway Administration.

Members of the Technical Review panel were the following:

- Jeff Burke (TRP Chair), IDOT
- Dan Brydl, FHWA
- Jack Elston, IDOT
- Tom Casson, Menard County Highway Department
- James Klein, IDOT
- Bill Kramer, IDOT
- Sheila Moynihan, IDOT
- Micah Loesch, FHWA
- Dan Tobias, IDOT

EXECUTIVE SUMMARY

This report details Phase II of the study titled Strengthening of Bridge Wood Piling Retrofits for Moment Resistance. Phase I (R27-082) focused on developing a load rating method for eccentrically loaded pier timber piles and experimentally examined a retrofitting method for posted timber piles using fiber-reinforced polymer (FRP) composites. Phase II was focused on load rating and FRP retrofitting of abutment timber piles as well as studying the long-term performance of FRP-wrapped timber piles. This report also includes finite element analysis results for three timber pile retrofitting alternatives using wide-flange and round HSS sections.

Historically, timber piles have been designed for axial loads only. Under this assumption, conventional load rating procedures consider only the effect of dead and live loads in determining the capacity of a timber pile. Previous studies have shown that the axial force and bending moment interaction (P–M interaction) represents a critical load case for timber piles (Borello et al. 2009; Caiza et al. 2012). Unlike pier timber piles, abutment piles must resist significant lateral forces from earth pressure and surcharge loads in addition to dead and live loads. Currently, there does not exist a separate load rating procedure for abutment timber piles. In this study, a load rating method was developed specifically for abutment timber piles by taking an approach similar to the eccentric load rating method proposed in Phase I. The combined loading effects were accounted for by using the allowable stress P–M interaction equation in the National Design Specification for Wood Construction (NDS) (AFPA 2005). The equation was modified to include the effect of both earth pressure and live load surcharge loads as specified in the AASHTO Standard Specifications for Highway Bridges (AASHTO 2002). In addition, a method was developed to account for the effect of FRP retrofits in the load rating. Because of the backing wall, FRP retrofits can be applied only to the tension side of abutment timber piles. Using an elastic design approach, the improved bending moment capacity of a retrofitted timber pile was translated into a modified allowable bending stress. The proposed load rating method and the effect of the modified allowable bending stress for FRP-retrofitted abutment piles were demonstrated using a detailed finite element model of a typical timber pile bridge. The results showed that deterioration levels as low as 10% could lead to unsatisfactory load ratings for abutment timber piles, depending on the backfill soil condition. FRP retrofitting, however, increased the load rating of deteriorated abutment timber piles by at least 17%.

FRP retrofitting techniques for abutment piles were also examined experimentally. Three full-size timber pile specimens with different levels of deterioration were tested. To design efficient and effective retrofits, understanding the condition of the substrate is very important. In the case of timber structures, it is difficult to obtain an accurate condition assessment without the use of advanced inspection tools and techniques. In this study, a nondestructive stress wave timing method was used to assess each specimen. Stress wave timing is based on the principle that stress waves propagate rapidly through a dense, stiff material and more slowly through a soft, flexible material. The stress wave velocity was measured at several locations in each specimen, and the velocities were related to dynamic elastic moduli using a one-dimensional simplification. The dynamic elastic modulus was used as an indicator of the timber pile condition. The stress wave timing measurements revealed that two of the specimens were in a more deteriorated state. The least deteriorated timber pile was tested as-is and adopted as the reference condition. FRP retrofits were designed for the other two specimens using an elastic approach based on improving the flexural stiffness to the same

level as the reference timber pile. The moment of inertia required in the retrofitted piles was computed by scaling the moment of inertia of the reference pile by the ratio of dynamic elastic moduli. The thickness of FRP required was then back-calculated from the moment of inertia. Two FRP configurations were considered: strips and a half-shell. The piles were load tested in the axial direction. First, a specified eccentric load was applied to induce a bending moment, then a concentric axial load was applied until the proportional limit. Each pile was tested under a series of eccentric loads varying from 10 kips to 35 kips. A direct comparison of the results showed that the capacity of the retrofitted piles was 15% to 30% lower than the reference as-is timber pile. However, normalizing the results based on the timber condition revealed that for a given timber condition, the FRP strips and half-shell retrofits used in this study were able to improve the axial capacity of the timber piles by 7%. Increasing the thickness of the FRP is required to provide further improvements.

Although FRP composites have been identified as an effective material for retrofitting timber piles, there is still a relatively large knowledge gap in the long-term performance of FRP-retrofitted timber. This experimental study focused on examining the performance of glass FRP (GFRP)-strengthened bridge timber piles under uniaxial compression after exposure to long-term degradation. Field-extracted red oak pile specimens with different degrees of initial deterioration were used in the study. The initial condition of the timber was assessed through stress wave timing. To simulate natural degradation in unretrofitted and retrofitted timber piles caused by environmental exposure in a short period of time, an accelerated aging procedure was used. In total, 24 timber pile specimens were tested in uniaxial compression. The number of FRP layers and type of resin used (polyester, standard epoxy, and moisture-tolerant epoxy) were varied. Results showed that accelerated aging induces significant deterioration in unretrofitted timber piles but the effects are relatively minor in the FRP-wrapped specimens. It was also proven that FRP composite is able to significantly improve the performance of timber piles in terms of peak stress and ductility, even after being subjected to extreme degradation.

CONTENTS

LIST OF FIGURES ..... **VII**

LIST OF TABLES ..... **IX**

CHAPTER 1: INTRODUCTION **1**

1.1 BACKGROUND **1**

1.2 REPORT OUTLINE **2**

CHAPTER 2: IDOT TIMBER PILE POSTING ALTERNATIVES **3**

2.1 RETROFIT SCHEMES **3**

2.2 FINITE ELEMENT ANALYSIS **4**

2.2.1 Timber Pile Model 4

2.2.2 Soil–Pile Interaction 4

2.3.2 ABAQUS Retrofit Models 6

2.3.3 Loading 8

2.4 ANALYSIS RESULTS **9**

2.4.1 Timber Pile 9

2.4.2 Retrofit Schemes 9

2.5 CONCLUSIONS **15**

CHAPTER 3: LOAD RATING OF ABUTMENT TIMBER PILES **17**

3.1 LOAD RATING PROCEDURE FOR AXIALLY LOADED PILES **17**

3.2 PROPOSED LOAD RATING METHOD FOR ABUTMENT PILES **18**

3.3. BRIDGE MODEL **20**

3.3.1 Bridge Parameters 20

3.3.2 Deterioration of Timber Piles 22

3.4 FINITE ELEMENT MODEL DESCRIPTION **23**

3.4.1 Superstructure 23

3.4.2 Pile Caps 23

3.4.3 Abutment Lagging 23

3.4.4 Timber Piles 23

3.4.5 Soil–Pile Interaction 24
3.4.6 Loading 24
3.5. BRIDGE MODEL LOAD RATING 26
3.5.1 Standard Bridge Model 26
3.5.2 Sensitivity Study Results 27
3.6 FRP RETROFIT 30
3.6.1 Design 30
3.6.2 Modified Allowable Bending Stress 30
3.6.3 Effect on Critical Load Rating 32
3.7 CONCLUSIONS 34
CHAPTER 4: EXPERIMENTAL TESTING OF FRP RETROFITS FOR ABUTMENT TIMBER PILES 35
4.1 TIMBER PILE SPECIMENS 35
4.2 INITIAL CONDITION ASSESSMENT 36
4.2.1 Stress Wave Timing 36
4.2.2 Stress Wave Timing Results 38
4.3 FRP RETROFIT 39
4.3.1 Materials 39
4.3.2 Retrofit Design 39
4.4 EXPERIMENTAL TESTING 41
4.4.1 Test Setup 41
4.4.2 Results 42
4.5 CONCLUSIONS 45
CHAPTER 5: LONG-TERM PERFORMANCE TESTING OF FRP RETROFITTED TIMBER PILES 47
5.1 TEST SPECIMENS 47
5.1.1 Timber Piles 47
5.1.2 FRP Wrapping 48
5.2 STRESS WAVE TIMING 50
5.3 ACCELERATED AGING 52
5.4 TEST RESULTS 53
5.4.1 As-Is Timber Piles 54

5.4.2 FRP Retrofitted Piles Without Accelerated Aging 55
5.4.3 Effect of Accelerated Aging 57
5.5 CONCLUSIONS 61
CHAPTER 6: SUMMARY AND CONCLUSIONS 62
REFERENCES 64
APPENDIX A: TIMBER PILE POSTING ALTERNATIVES 67
APPENDIX B: FRP RETROFIT TESTING RESULTS 72

LIST OF FIGURES

Figure 2-1. IDOT timber pile retrofit schemes. 3

Figure 2-2. Timber material model. 4

Figure 2-3. Soil spring models. 5

Figure 2-4. Typical timber pile analysis model: (a) complete timber pile model; (b) soil springs arranged along the embedded length of the pile. 5

Figure 2-5. Finite element models created in ABAQUS: (a) Retrofit Scheme 1; (b) Retrofit Scheme 2; (c) Retrofit Scheme 3; (d) HP 10 × 42 section; (e) Retrofit Scheme 3 HSS assembly weld. 6

Figure 2-6. Weld material behavior. 7

Figure 2-7. Concrete section in Retrofit Scheme 1: (a) concrete section and reinforcement cage; (b) reinforcement embedded. 8

Figure 2-8. Eccentric loading pattern. 8

Figure 2-9. Timber pile analysis results. 10

Figure 2-10. Cross-section stress at (a) maximum deflection above the riverbed; (b) maximum deflection below the riverbed; (c) pile tip. 11

Figure 2-11. Retrofitted pile analysis results. 12

Figure 2-12. HP 10 × 42 compression flange buckling: (a) Retrofit Scheme 1; (b) Retrofit Scheme 2. 13

Figure 2-13. Compression yielding of the HSS assembly in Retrofit Scheme 3 13

Figure 2-14. Maximum stresses in the fillet welds around the H-pile in Retrofit Scheme 2 14

Figure 2-15. Stresses in the timber pile segment: (a) Retrofit Scheme 2; (b) Retrofit Scheme 3. 15

Figure 3-1. Loads applied on abutment timber piles. 19

Figure 3-2. Layout of a typical timber pile bridge: (a) deck, (b) bridge elevation, (c) deck cross-section, (d) typical timber pile bent. 21

Figure 3-3. Timber pile deterioration profiles. 22

Figure 3-4. FE model of a typical timber pile bridge: (a) elevation of FE model; (b) live load vehicle load pattern. 25

Figure 3-5. Load rating sensitivity study results. 29

Figure 3-6. Half-shell FRP retrofit scheme considered in this study. 30

Figure 3-7. Elastic design approach for abutment pile FRP retrofit design 31

Figure 3-8. Projection of the bending moment obtained from transformed section analysis onto an unretrofitted timber pile section. 32

Figure 3-9. Comparison of critical load ratings for unretrofitted and retrofitted timber piles with deterioration Profile I. 33
Figure 4-1. Timber pile specimens used in experimental testing of FRP retrofits. 35
Figure 4-2. Stress wave timing concept (Wang et al. 2004). 36
Figure 4-4. Average stress wave velocity along pile length. 38
Figure 4-6. Possible FRP retrofitting configurations for abutment timber piles. 40
Figure 4-8. FRP-retrofitted timber pile specimens: (a) SP1; (b) SP2. 41
Figure 4-9. P–M interaction test setup. 42
Figure 4-10. Mid-height curvature caused by the eccentric load. 43
Figure 4-11. Peak total axial force attained under each bending moment. 43
Figure 4-12. Normalized test results. 45
Figure 5-1. Typical red oak pile specimens used in the study. 47
Figure 5-2. FRP wet layup process: (a) cutting the fabric; (b) resin application. 49
Figure 5-3. Stress wave timing parallel to grain: (a) UPV instrument; (b) schematic of test setup. 51
Figure 5-4. Test setup for the ASTM D1037 accelerated aging procedure adopted in this study: (a) heated water tank; (b) steam box with steam generator; (c) chest freezer; (d) aggregate drying oven. 53
Figure 5-5. Failure of unretrofitted timber specimens. 54
Figure 5-6. Stress–strain behavior of unretrofitted as-is timber piles. 54
Figure 5-7. Typical FRP-strengthened specimen damage progression: (a) beginning of loading; (b) initial longitudinal rupture of the FRP; (c) rupture propagation; (d) complete rupture of the FRP and crushing of the timber pile. 55
Figure 5-8. Performance of FRP-strengthened timber piles not subjected to accelerated aging: (a) five layers; (b) ten layers. 56
Figure 5-9. Unretrofitted timber piles, as-is and after accelerated aging. 57
Figure 5-10. Stress–strain behavior of unretrofitted and FRP-strengthened timber piles subjected to accelerated aging: (a) five-layer polyester resin; (b) ten-layer polyester resin; (c) five-layer standard epoxy resin; (d) ten-layer standard epoxy resin; (e) five-layer moisture-tolerant epoxy; (f) ten-layer moisture-tolerant epoxy 58

LIST OF TABLES

Table 2-1. Summary of Steel Material Properties 7

Table 3-1. Bridge Design Parameters Used in This Study 20

Table 3-2. Friction Soil Spring Behavior from Borello et al. (2009). 24

Table 3-3. Reference Design Values for Treated Red Oak Timber Piles Under Normal Load Duration and Wet Service Conditions (AWPA 2005) 26

Table 3-4. Typical Analysis Results and Load Rating of the Standard Bridge Model 27

Table 3-5. Modified Allowable Reference Bending Stress for a Red Oak Timber Pile Retrofitted with a Half-Shell FRP 33

Table 4-1. Timber Pile Specimen Details 36

Table 4-2. Stress Wave Transmission Times Through Undeteriorated Red Oak 37

Table 4-3. FRP Composite Material Properties 39

Table 4-5. Condition Scaling Factors and Normalization Loads 44

Table 5-1. FRP Composite Material Properties 48

Table 5-2. Summary of Test Specimens 50

Table 5-3. Average Stress Wave Transmission Times Through Timber Pile Specimens Parallel to Grain 51

Table 5-4. ASTM D1037 Accelerated Aging Procedure Adopted in This Study 52

CHAPTER 1: INTRODUCTION

1.1 BACKGROUND

Bridges supported on timber pile bents are common in low-traffic and rural areas throughout the United States. Although timber piles properly treated with preservatives such as creosote can be very durable—with a service life of over 65 years—environmental and biological degradation is still a major concern, especially when the pile is exposed above the water table and subjected to wet and dry cycles (AWPI 2002). Studies have shown that degradation of the timber can lead to significant reductions in structural capacity (Andrawes and Caiza 2011; Caiza et al. 2012). In addition, many timber pile bridges were constructed based on outdated standard designs and are in need of major rehabilitation efforts. As construction costs increase and funding for civil infrastructure decreases, safe, more cost-effective, and durable repair and retrofitting methods are needed to extend the service life of existing bridges. Phase I of the study considered pier timber piles. In the current phase, Phase II, abutment timber piles were investigated.

The National Bridge Inspection Standards (NBIS) require all highway bridges longer than 20 ft to be load rated to determine safe loading capacities. Load rating requires determining the live load capacity of a bridge from as-built plans and information from field inspections (Mertz 2012). In general, the allowable stress rating (ASR) is used for the load rating of timber bridges, and the maximum stress in a member is compared with the allowable stress. The stress demand is typically determined through simplified analysis methods. Traditionally, the load rating of timber piles was computed based solely on the axial capacity. This method overlooks the importance of combined axial–flexural loading that may significantly reduce the axial load capacity of timber piles (Borello et al. 2009, 2010). Andrawes and Caiza (2011) showed that the conventional load rating method is unconservative for pier timber piles subjected to eccentric loading and proposed a modified load rating method that accounts for deck eccentricity. In contrast to pier piles where bending moments are generated through eccentricities, timber piles supporting the abutments must resist high lateral forces from earth pressure and surcharge loads. Currently there is no load rating method directly applicable to abutment timber piles where the combined axial–flexural loading (P–M interaction) is accounted for. This report proposes P–M interaction based load rating method for abutment timber piles. A detailed finite element (FE) model of a typical timber pile bridge was developed to demonstrate the new load rating method.

Traditionally, posting has been the most widely used repair method for timber piles because it is cheap and easy to implement. Posting consists of simply cutting away the deteriorated sections of a pile and splicing a new timber segment to the existing pile using steel drift pins or nails. However, because the connections have no moment capacity, posting can have catastrophic consequences, especially if the piles are subjected to bending moment in addition to axial loads, as was the case in the 2008 bridge collapse in Illinois (Borello et al. 2009). Instead of posting timber piles with another timber section, using steel sections offers a high-strength and durable alternative. Three different retrofit configurations using wide-flange and round HSS sections were evaluated using finite element analysis. Fiber-reinforced polymer (FRP) composites offer another retrofitting alternative. In recent years, FRP composites have become a popular option in structural rehabilitation because of their high strength-to-weight ratio, durability, and versatility. They are especially attractive because the application of FRP does not require heavy machinery to install and is comparatively less labor-intensive. Previous studies

have shown that confinement of timber piles using FRP composites can effectively improve the strength, stiffness, and ductility (Caiza et al. 2012). In the case of abutment timber piles, it may not be possible to fully wrap the pile because of the abutment lagging. As part of the current study, the effectiveness of applying FRP retrofits to the tension face of abutment timber piles was examined analytically and experimentally. In experimental testing, the effect of initial timber condition was taken into consideration through extensive nondestructive tests using stress wave timing methods.

Despite the benefits, FRP composites are still not widely used in retrofitting timber structures. One area in which little research effort has been made is the long-term performance of FRP-strengthened structures. One of the main difficulties in conducting a study of this nature is obviously the amount of time required for the degradation to take place. The last part of this report addresses the long-term effectiveness of FRP wrapping in strengthening and protecting timber bridge piles. The problem of test duration was overcome by using an accelerated aging procedure to artificially induce degradation that would take years to occur naturally in the field in a much shorter period of time. This is done by simulating the exposure conditions at elevated severities.

1.2 REPORT OUTLINE

This report is composed of five main chapters:

- Chapter 2: Finite element analysis of timber pile retrofitting alternatives using typical steel sections adopted by the Illinois Department of Transportation (IDOT). The performances of three alternatives are evaluated in terms of deflections and load capacity.
- Chapter 3: A load rating method based on timber P–M interaction is proposed for abutment timber piles. The method is demonstrated using an FE model of a typical timber pile bridge. A method to incorporate flexural retrofitting of timber piles using FRP composites is introduced, and the effect of FRP retrofitting on the load rating is examined.
- Chapter 4: Experimental testing of FRP-retrofitted abutment timber piles is presented. The initial condition of the timber piles was assessed using stress wave timing techniques and accounted for in the design of the FRP retrofits. One unretrofitted and two FRP-retrofitted timber piles were tested under combined axial-bending loads.
- Chapter 5: The long-term performance of FRP-wrapped timber piles was investigated by subjecting test specimens to an accelerated aging procedure. The effect of long-term degradation on the compressive strength of retrofitted and unretrofitted timber piles was studied.
- Chapter 6: Summary and conclusions are presented.

CHAPTER 2: IDOT TIMBER PILE POSTING ALTERNATIVES

2.1 RETROFIT SCHEMES

Prior to examining a new retrofit technique for timber piles using fiber-reinforced polymers (FRPs), it was essential to first assess IDOT's state-of-practice. Three retrofit schemes often used by IDOT for deteriorated timber piles were analyzed using the finite element software ABAQUS (Dassault Systèmes Simulia Corp. 2011). The structural details are illustrated in Figure 2-1. Detailed drawings are provided in the appendix.

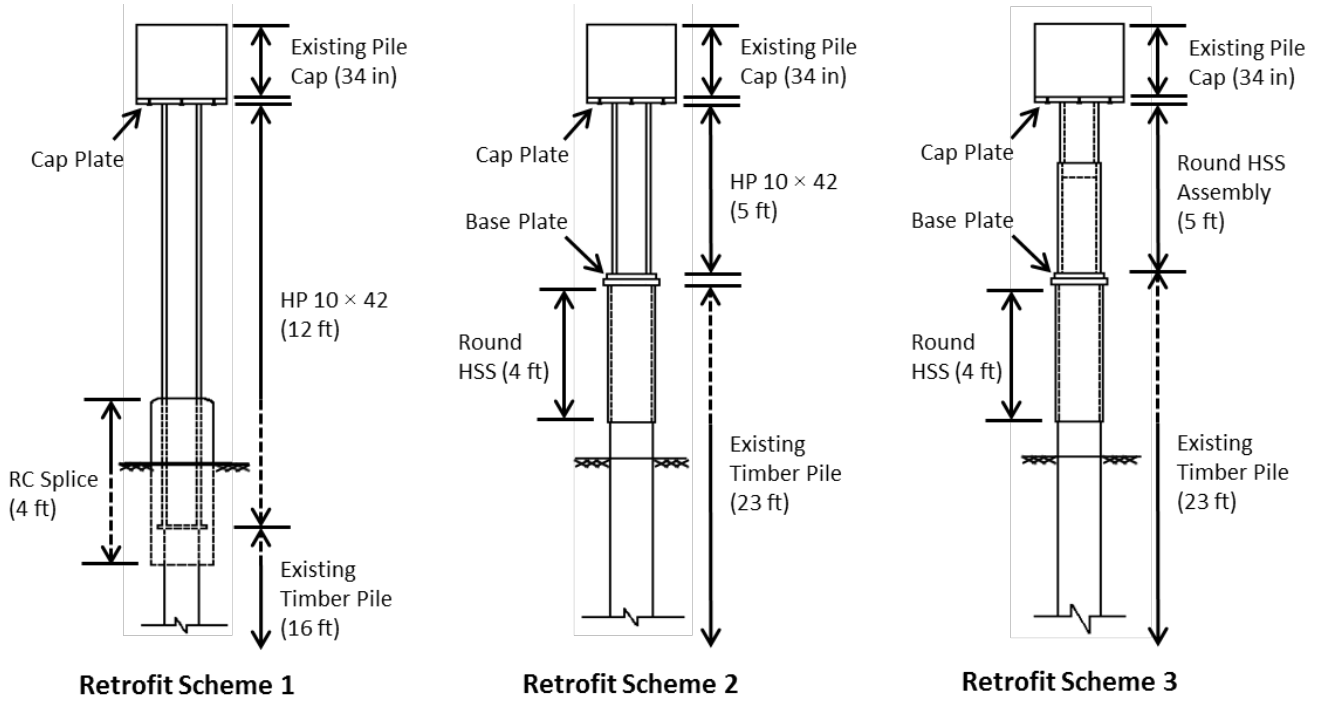

Figure 2-1. IDOT timber pile retrofit schemes.

Retrofit Scheme 1 is designed for cases where essentially the entire exposed length of the timber pile is deteriorated. The splice location is at or below the ground line and the deteriorated pile is replaced with a steel H-pile section (HP 10 × 42 or larger). The connection between the timber pile and H-pile is facilitated through a reinforced concrete splice. Retrofit Schemes 2 and 3 are for cases where only a segment of the exposed timber pile is deteriorated above the ground line. An H-pile (HP 10 × 42 or larger) segment is used in Retrofit Scheme 2, and an assembly of circular HSS (12 in. O.D. × 3/8 in. and 12 3/4 in. O.D. × 5/16 in. sections) is used in Retrofit Scheme 3 to replace the deteriorated section. A 4 ft long circular HSS section (14 in. O.D. × 3/8 in.) welded to steel base plates is fitted over the remaining timber pile stub to complete the connection. All joints between the steel members are welded. The cap plate is connected to the pile cap using ten 3/4 in. diameter wedge anchors. Refer to the structural drawings in the appendix.

2.2 FINITE ELEMENT ANALYSIS

2.2.1 Timber Pile Model

The timber pile models used in this analysis were based on the experimental test results from the 2008 forensic collapse investigation of timber pile bridge SN 019-5010 in DeKalb County, Illinois (Borello et al. 2009). The piles had an embedded length of 17 ft and extended another 11 ft above grade to a reinforced concrete pile cap. A constant diameter of 13.25 in. was assumed for the pile. The material behavior of wood obtained from tests on field-extracted specimens is shown in Figure 2-2. The exposed and embedded portions of the pile had slightly different peak stresses in compression.

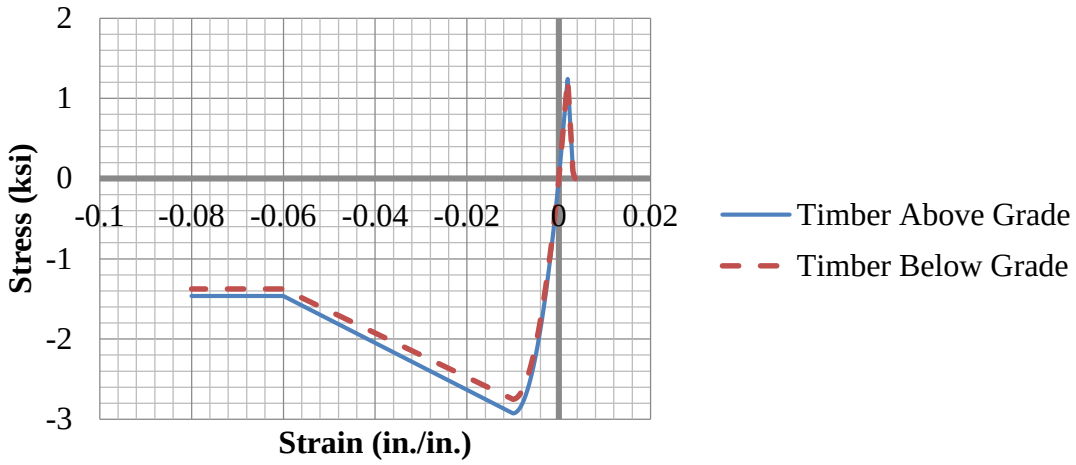

Figure 2-2. Timber material model.

The concrete-smeared cracking behavior was used in the finite element software ABAQUS to replicate the stress–strain relationship (Dassault Systèmes Simulia Corp. 2011). As shown in Figure 2-2, in compression, the wood behaves nonlinearly up to its peak stress then linearly softens to a perfectly plastic behavior at 50% of the peak stress. A brittle behavior was assumed in tension with a peak stress of approximately 1.25 ksi.

2.2.2 Soil–Pile Interaction

The soil–pile interaction was captured using elastic springs to represent the skin friction and lateral resistance. The soil springs were modeled using Cartesian connector elements in ABAQUS with varying stiffnesses. Eight soil springs were distributed around the circumference of the pile at 6 in. increments along the embedded length. The behavior of the soil springs is illustrated in Figure 2-3.

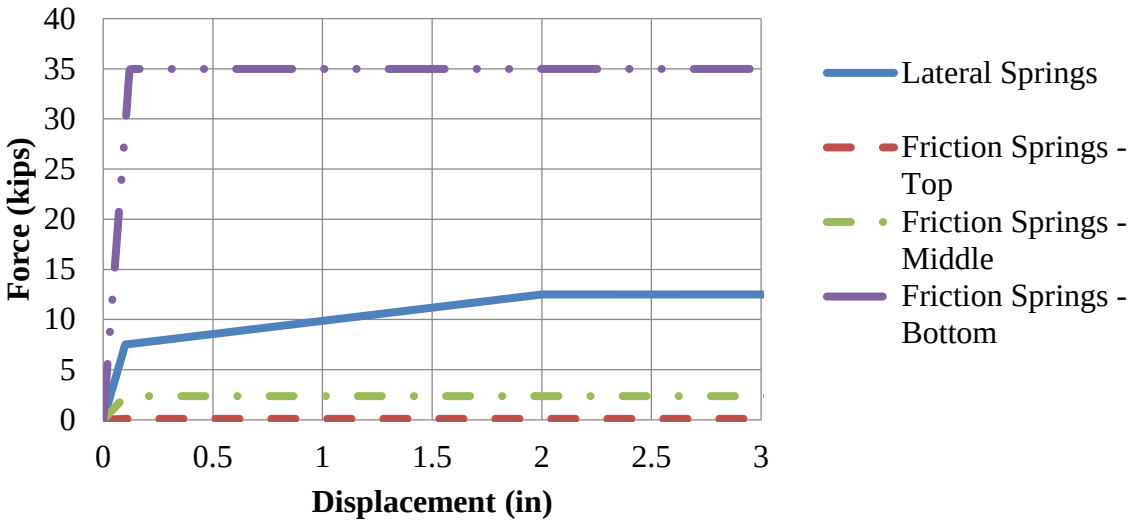

Figure 2-3. Soil spring models.

Although not shown, the vertical soil springs simulating skin friction have identical behavior in both compression and tension, which varies depending on the depth. The lateral springs have a trilinear behavior but have capacity in compression only. A fine mesh was defined over the embedded pile section to minimize adverse effects from stress concentrations caused by the soil springs. The arrangement of the soil springs is shown in Figure 1-4 with an overview of the complete timber pile model.

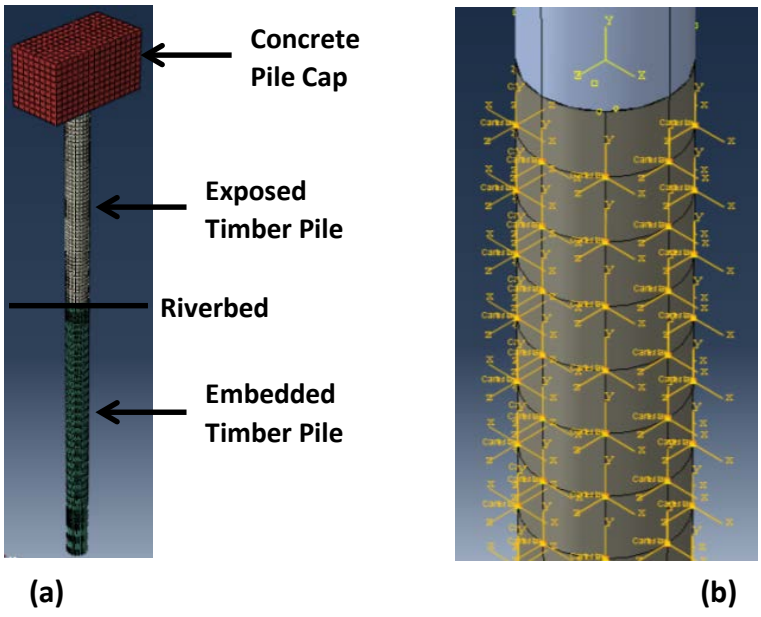

Figure 2-4. Typical timber pile analysis model: (a) complete timber pile model; (b) soil springs arranged along the embedded length of the pile.

The concrete-smeared cracking model was also used for the concrete pile cap with a peak compressive stress of 5 ksi. Based on the as-built drawings of the DeKalb County bridge, the pile cap was assumed to be 34 in. in depth (Borello et al. 2009). The reinforcing steel was not modeled. Tie constraints were defined at the interface between the pile and pile cap to simulate the timber pile embedment in the pile cap. It was assumed that a single pile supports a 5 ft tributary width of the pile cap. While the pile was free to translate vertically, it was assumed that the superstructure would be rigid enough to prevent lateral translations of the pile cap.

2.3.2 ABAQUS Retrofit Models

The retrofit options were modeled in a similar fashion to the timber pile model. The same material models were used for the timber and pile cap. Elastic soil springs were used along the embedded portion of the timber pile. The models created in ABAQUS and some key details are shown in Figure 2-5.

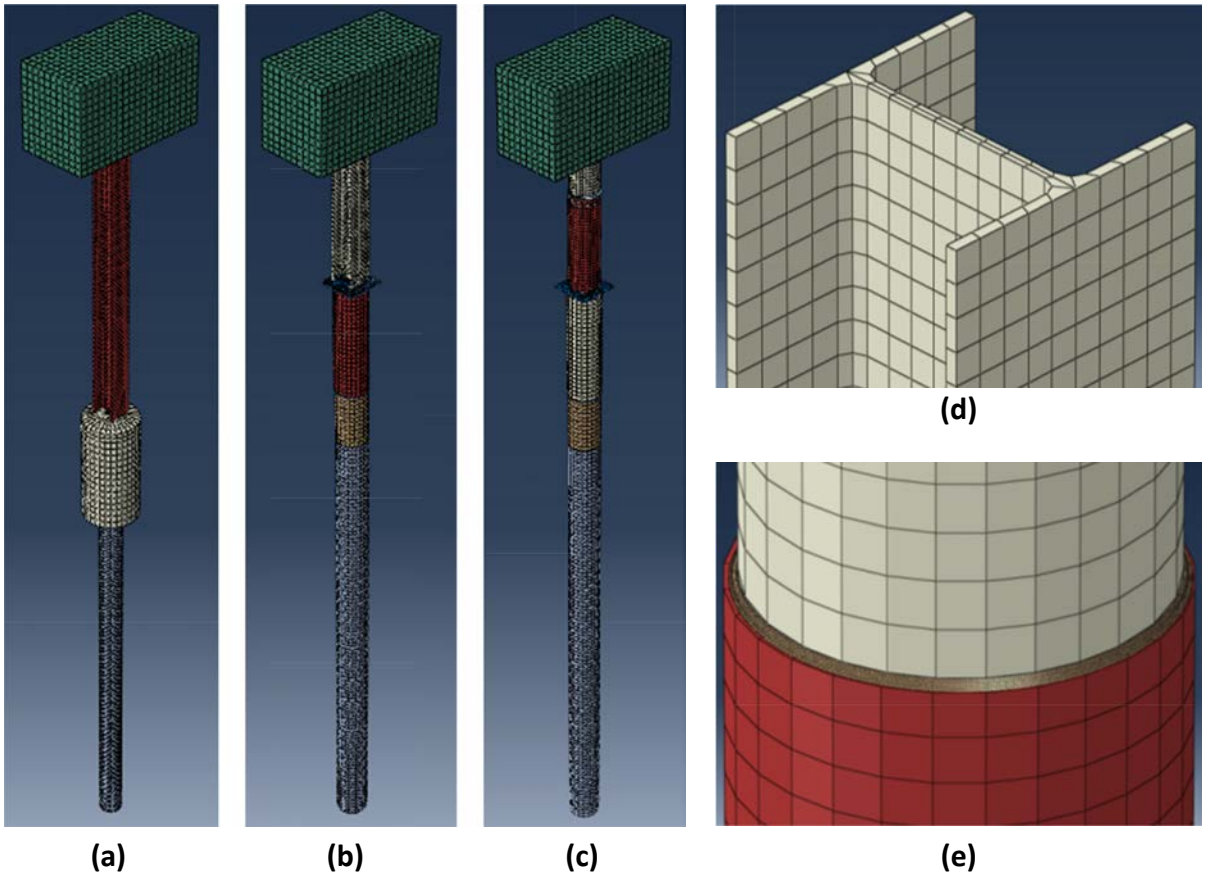

Figure 2-5. Finite element models created in ABAQUS: (a) Retrofit Scheme 1; (b) Retrofit Scheme 2; (c) Retrofit Scheme 3; (d) HP 10 × 42 section; (e) Retrofit Scheme 3 HSS assembly weld.

The timber pile stubs in Retrofit Schemes 2 and 3 fit snugly inside the HSS. A normal and frictional contact behavior was specified between the timber pile and HSS. Elastic–perfectly plastic behavior was assumed for all steel members. The steel material properties used are summarized in Table 2-1.

Table 2-1. Summary of Steel Material Properties

Member	Young's Modulus, E (ksi)	Yield Stress, F_y (ksi)
HP 10 × 42	29000	50
Timber Pile Stub HSS (14 in. O.D. × 3/8 in.)	29000	30
HSS Assembly (Retrofit Scheme 3)	29000	36 / 42
Plates	29000	36

All welds between the steel components were 1/4 in. fillet welds all around the joined members. A bilinear material behavior was assumed for the welds with a yield stress of 70 ksi with linear hardening, as shown in Figure 2-6. Tie constraints were used to fuse the weld geometry to the joined steel members.

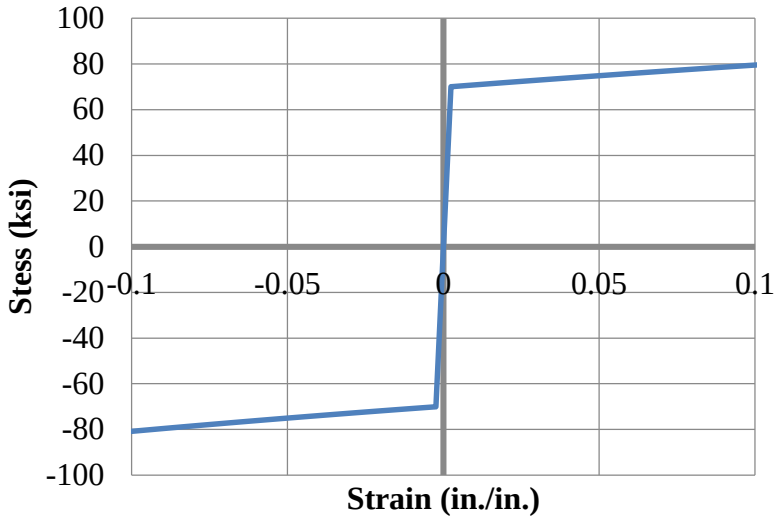

Figure 2-6. Weld material behavior.

Axial connectors were used to model the anchor bolts in the cap plate connection. The bolts were assumed to have a yield strength of 40 kips. In Retrofit Scheme 1, the reinforced concrete splice was modeled using the concrete-smeared cracking model with a peak stress of 3 ksi. The reinforcing bars were modeled using truss elements. The concrete section and reinforcing cage are shown in Figure 2-7. See the structural drawings in the appendix for details.

An embedded region constraint was defined for the reinforcement as well as the portions of the H-pile and timber pile embedded in the concrete splice.

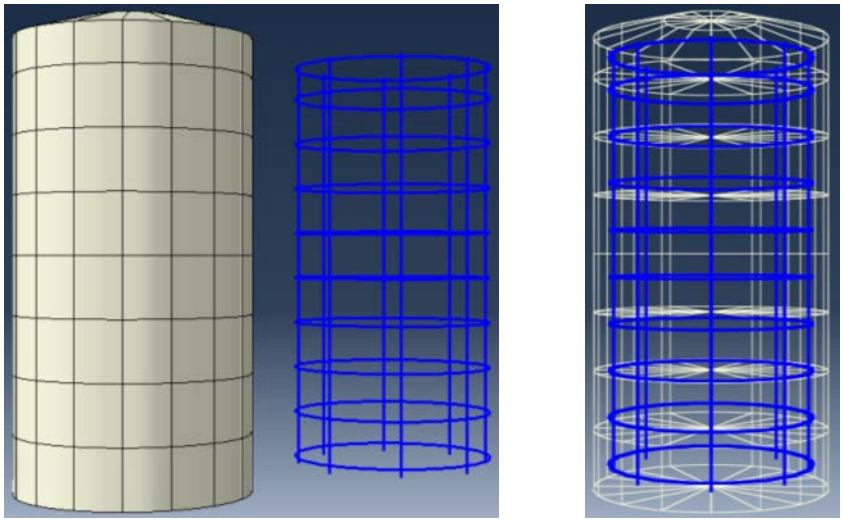

(a) (b)

Figure 2-7. Concrete section in Retrofit Scheme 1: (a) concrete section and reinforcement cage; (b) reinforcement embedded.

2.3.3 Loading

The critical loading case was obtained from the DeKalb County bridge collapse investigation (Borello et al. 2009). The study showed that the failure of the timber piles was caused by eccentric loading. The concentric dead load acting on a single pile was determined to be 32 kips. To simulate eccentric live load, a surface traction was applied to one-half of the pile cap such that the resultant load is acting through an eccentricity of 7.5 in., as shown in Figure 2-8.

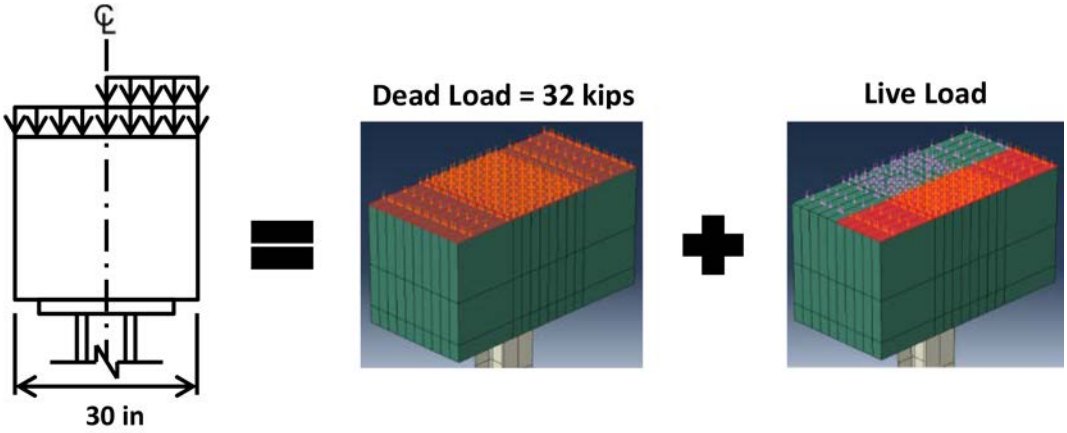

Figure 2-8. Eccentric loading pattern.

Both the dead and live loads were defined as nonfollower surface tractions in ABAQUS. Nonfollower tractions always act in a fixed direction rather than rotating with the surface. The live load was increased until failure.

2.4 ANALYSIS RESULTS

2.4.1 Timber Pile

The timber pile model was analyzed to provide a comparison. As expected, the analysis was terminated when the extreme tension fiber of the pile reached the tensile capacity as defined by the material model. The analysis results are summarized as plots in Figure 2-9.

Most of the deformation occurs above the riverbed, with the maximum deflection of 1.38 in. occurring at approximately 3 ft below the pile cap. Failure of the tensile fibers initiates at this location. The bending moment is maximum at the top of the pile cap and gradually reduces until the inflection point at approximately 2 ft above the river bed. This implies that the geometric nonlinearity arising from the deflection of the pile does not significantly increase the moment in the pile. The ultimate stress distribution in the cross-section at the pile tip and locations of maximum deflection above and below the riverbed are shown in Figure 2-10. In Figure 2-10(a), it is clear that the tensile extreme fiber has reached the ultimate stress but the compressive fiber has not. Below the riverbed, the pile is almost under pure compression.

As shown in the axial load-deflection plot in Figure 2-9, the ultimate axial load of the timber pile was 120 kips. Taking section cuts at several locations along the embedded length of the pile revealed that the vertical soil springs were effectively carrying some of the load. The total load carried by bearing at the pile tip was approximately 94 kips. Skin friction was responsible for the remaining 26 kips.

As exemplified by the deflected shape, the lateral soil springs were also effective at providing lateral support without the occurrence of high-stress concentrations.

2.4.2 Retrofit Schemes

As shown in Figure 2-11, all three retrofit schemes significantly improved the load capacity and stiffness of the piles. Because the entire exposed length is replaced with a steel section, Retrofit Scheme 1 had the lowest deflection, while Retrofit Scheme 2 achieved the highest ultimate load.

In both Retrofit Schemes 1 and 2, failure was caused by the buckling of the H-pile compression flange where the H-pile is bearing on the cap and base plates. As mentioned previously, the H-pile section HP 10 × 42 has noncompact flanges. Figure 2-12 shows the buckled H-pile sections.

Stress concentrations can be seen at the flange tips and near the flange–web intersection. In Retrofit Scheme 3, the ultimate strength was governed by the yielding of the HSS assembly in compression. As shown in Figure 2-13, under the given loading, compressive stresses are dominant throughout the HSS assembly and the top section has reached its yield stress.

As the load increased, small stress concentrations were noted in the welded connections in localized areas near geometric discontinuities, as illustrated in Figure 2-14. However, the stresses did not exceed the rupture strength, and the welds are not expected to be the governing element in the design.

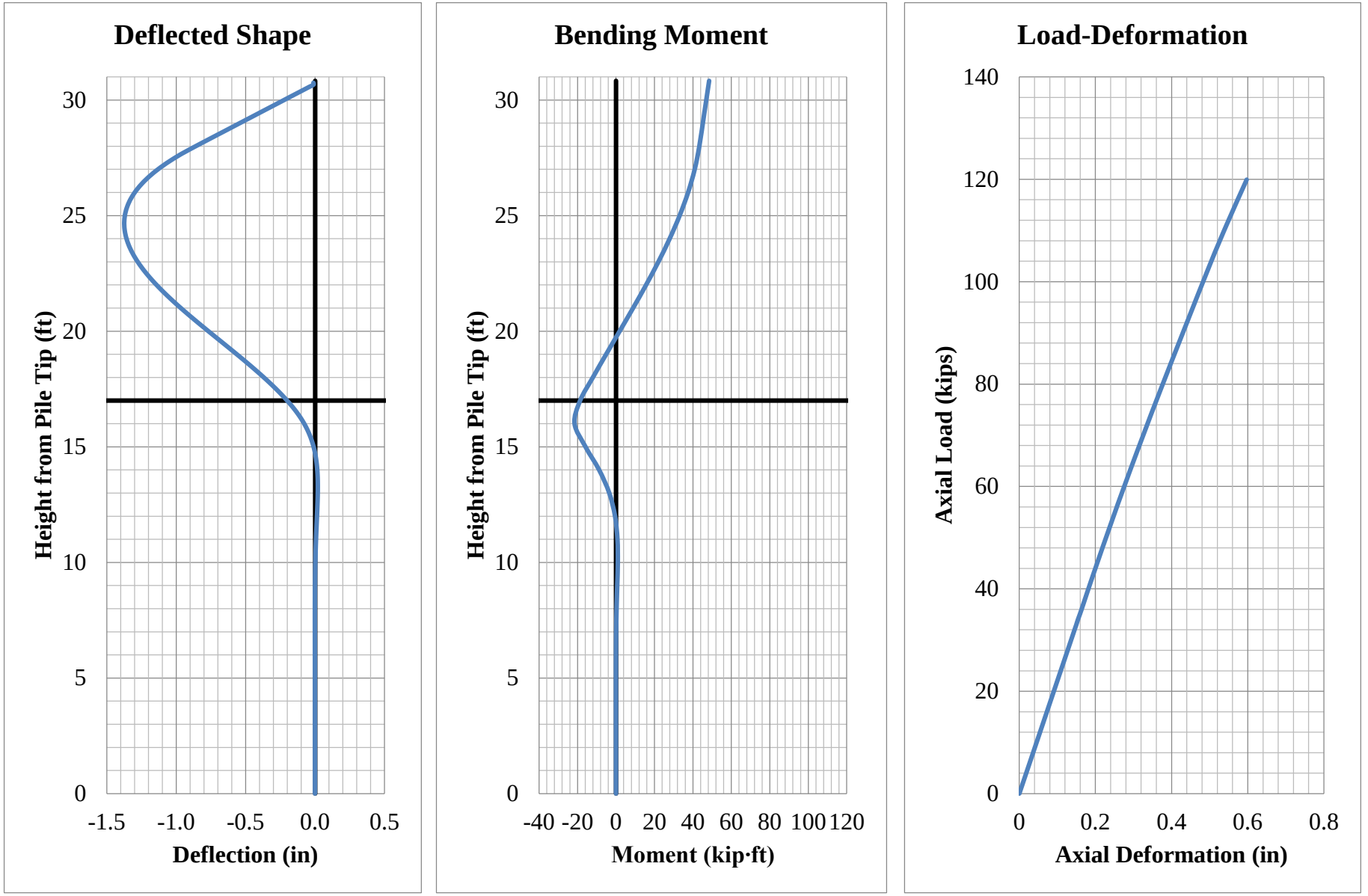

Figure 2-9. Timber pile analysis results.

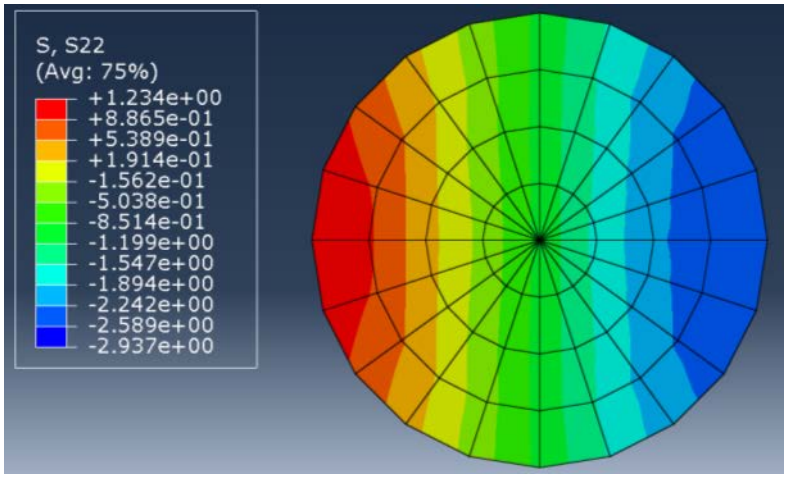

(a)

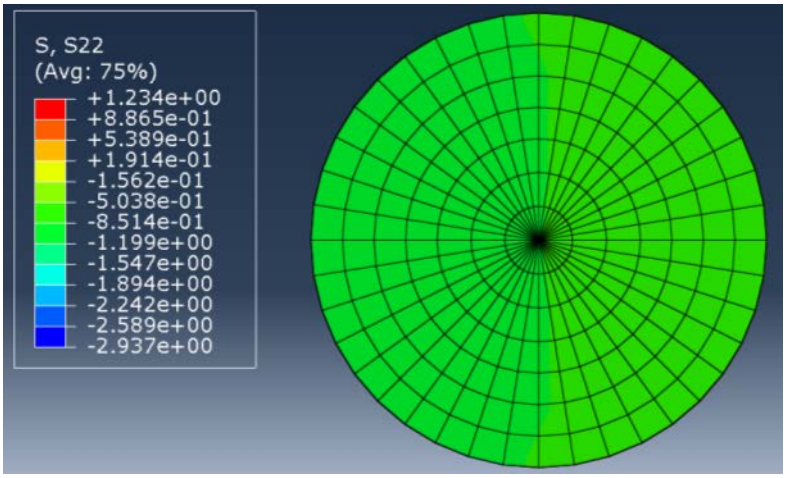

(b)

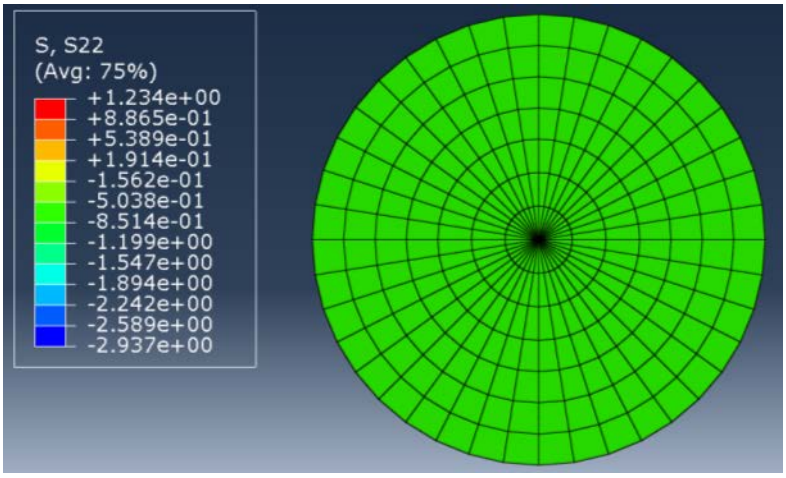

(c)

Figure 2-10. Cross-section stress at (a) maximum deflection above the riverbed; (b) maximum deflection below the riverbed; (c) pile tip.

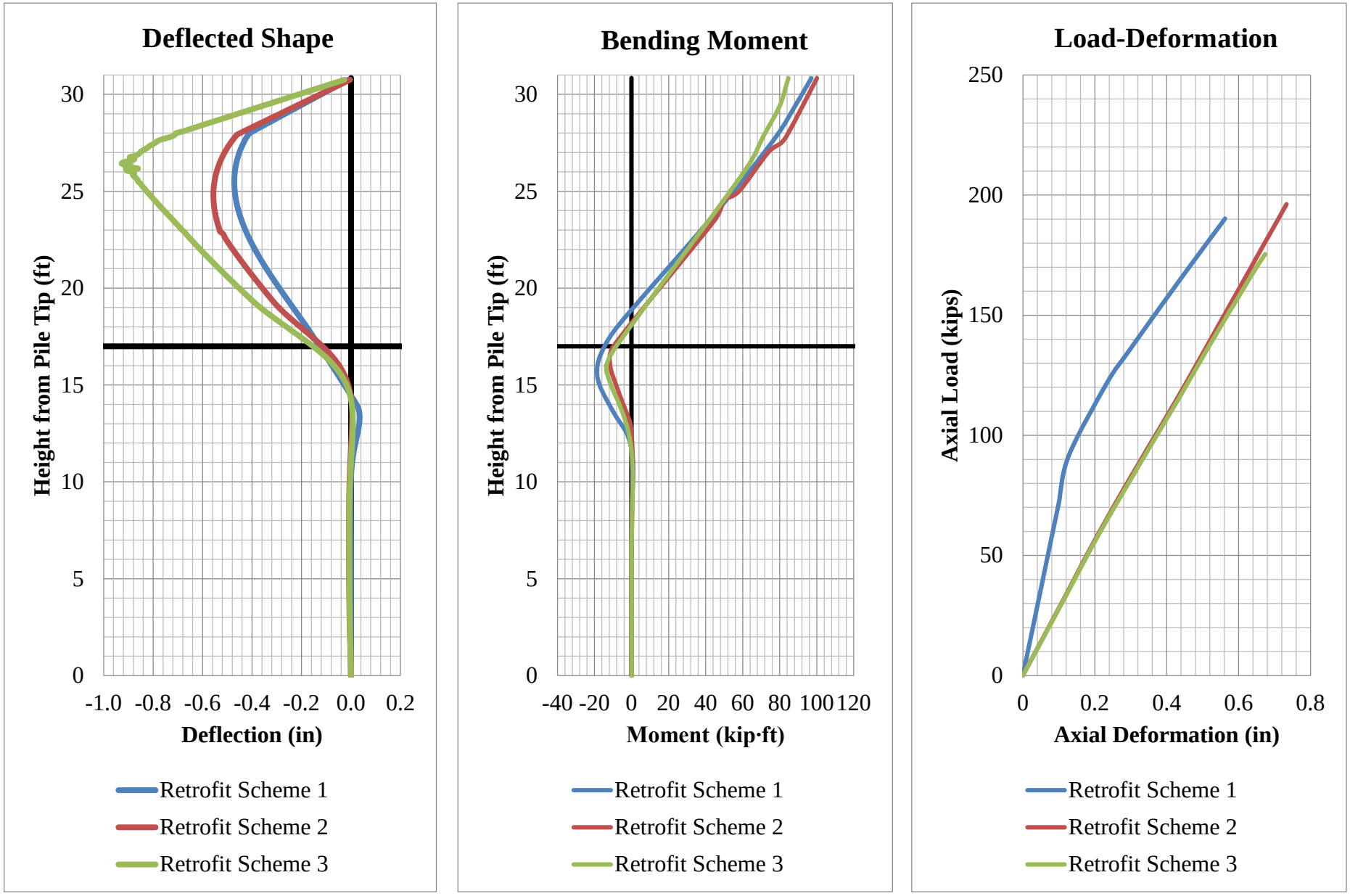

Figure 2-11. Retrofitted pile analysis results.

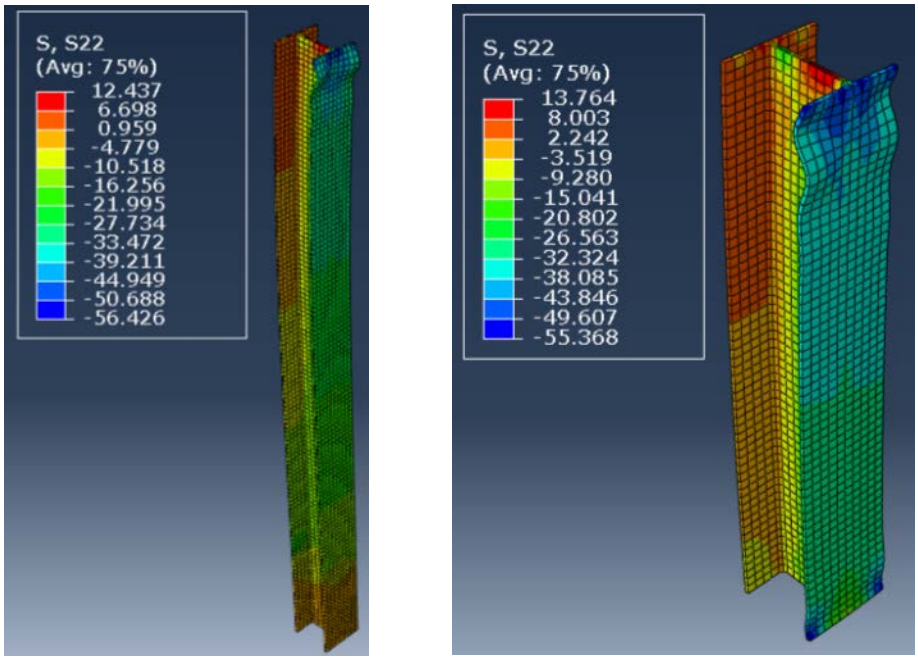

(a) **(b)**

Figure 2-12. HP 10 × 42 compression flange buckling: (a) Retrofit Scheme 1; (b) Retrofit Scheme 2.

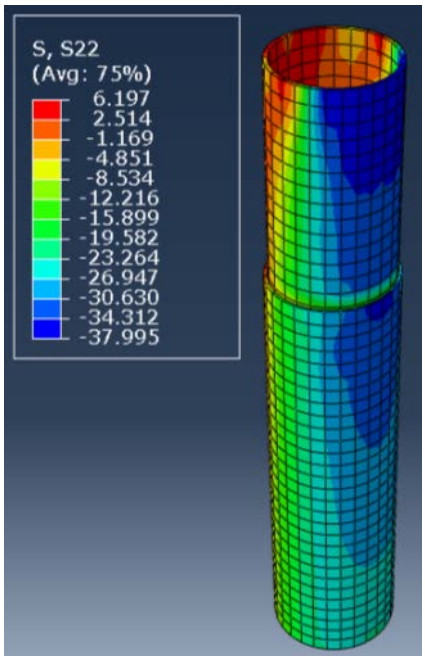

Figure 2-13. Compression yielding of the HSS assembly in Retrofit Scheme 3

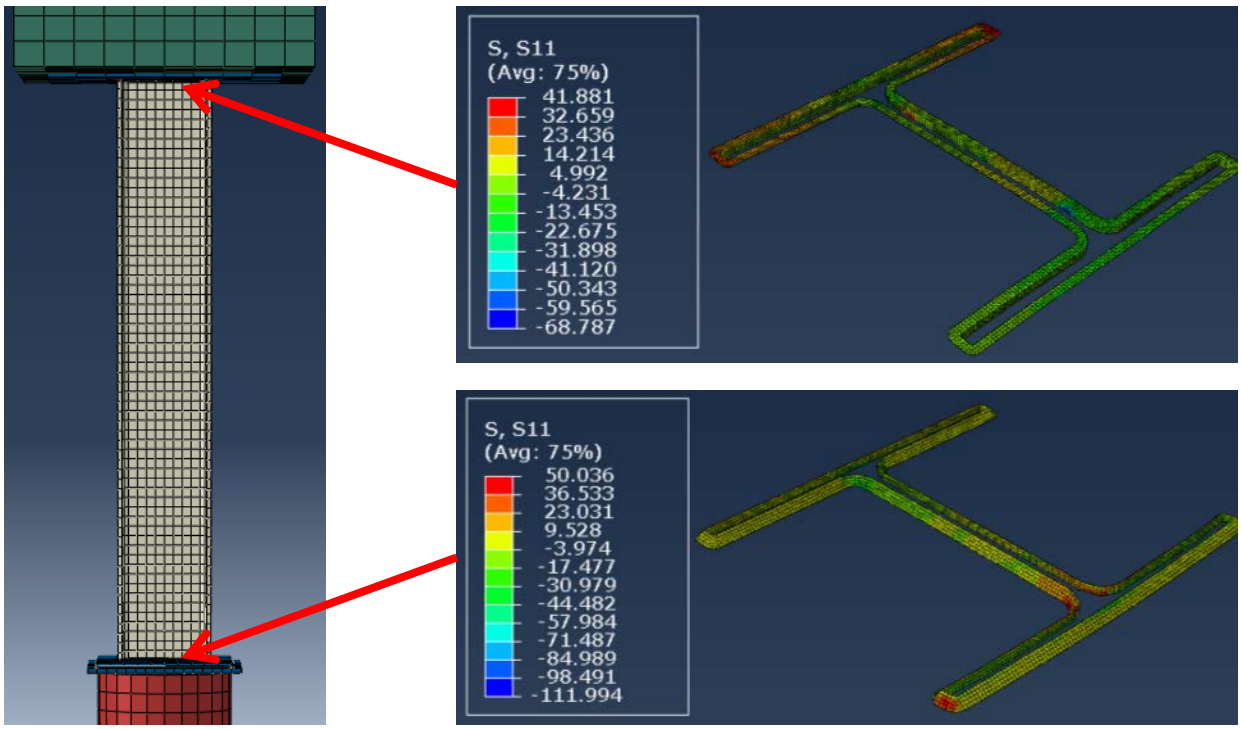

Figure 2-14. Maximum stresses in the fillet welds around the H-pile in Retrofit Scheme 2

The maximum forces in the anchor bolt elements connecting the top plate to the pile cap did not exceed 4.6 kips, which is far below the specified yield strength of 40 kips. The maximum principal stresses in the top plate were also far below the yield stress.

The bolted top plate connection in general had some flexibility. This is evident in the plot of the displaced shape in Figure 2-11, where small discontinuities can be seen at the pile cap–pile interface. In Retrofit Scheme 3 in particular, the maximum deflection occurred at the interface between the HSS assembly and cap plate. Given the stiff nature of the HSS assembly, most of the deflection was due to the flexibility of the cap plate.

In general, the retrofitted piles behaved under the eccentric loading case similarly to their behavior under the timber pile model. Maximum deflections occurred below the pile cap, and similar bending moment distributions were noted. The higher initial stiffness seen in the axial load-deformation plot of Retrofit Scheme 1 is attributed to the additional stiffness provided by the bearing soil springs at the bottom of the concrete splice. Once the plateau strength of the soil springs is reached, the overall pile stiffness approaches that of the other two retrofit schemes.

In all three retrofit schemes, the stresses in the remaining timber pile segments were not significant. In the case of Retrofit Scheme 1, the concrete splice effectively transferred the loads from the H-pile to the embedded timber pile, which was essentially under pure compression.

The stresses in the reinforced concrete splice were minimal. In Retrofit Schemes 2 and 3, there were localized stress concentrations in the timber pile stub where the steel members were bearing loads. Stresses in the timber pile sections are shown in Figure 2-15.

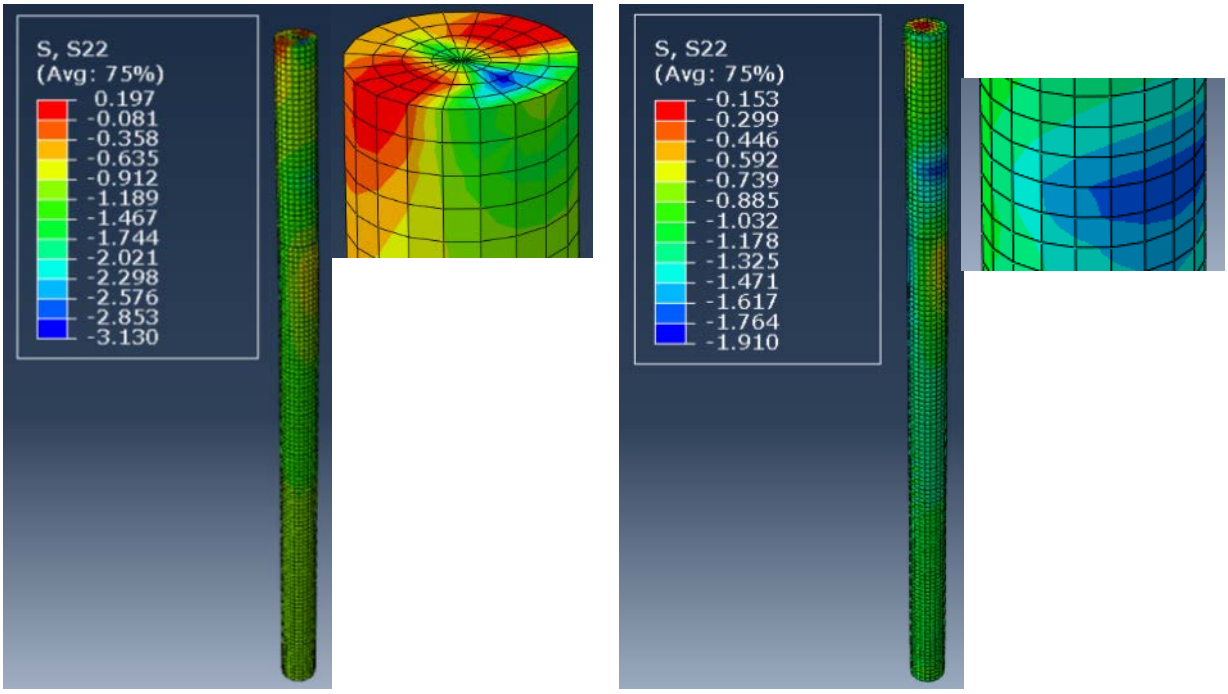

(a) **(b)**

Figure 2-15. Stresses in the timber pile segment: (a) Retrofit Scheme 2; (b) Retrofit Scheme 3.

The maximum loads sustained by the retrofit schemes were 190.6 kips in Retrofit Scheme 1, 196.2 kips in Retrofit Scheme 2, and 175.4 kips in Retrofit Scheme 3. Along the embedded portion of the existing timber pile, the vertical soil springs carried 19.2 kips of the total load for Retrofit Scheme 2 and 19.6 kips for Retrofit Scheme 3. In Retrofit Scheme 1, 96.9 kips of the total load was transferred into the vertical soil springs and bearing of the concrete splice on soil springs

2.5 CONCLUSIONS

Three retrofitting options for timber bridge piles were analyzed to evaluate their performance. An unretrofitted timber pile was also analyzed to provide a comparison. The timber pile was assumed to have a diameter of 13.25 in., an embedded length of 17 ft, and an unbraced length of 11 ft. The retrofits consisted of replacing deteriorated timber pile segments above the mudline with steel sections. A single pile was analyzed in each case using ABAQUS. The loading

consisted of a 32 kip dead load and an increasing live load applied through an eccentricity of 7.5 in. The results can be summarized as follows:

- The timber pile failed under flexure as the extreme tensile fiber reached its rupture stress. The unretrofitted timber pile failed at an ultimate load of 120 kips.
- Retrofit Scheme 1 was slightly stiffer than the other two retrofit options. The maximum deflection did not exceed 0.5 in. The failure was caused by the buckling of the H-pile flanges at the cap plate. Retrofit Scheme 1 sustained an ultimate load of 190.6 kips. The stresses in the connections and the reinforced concrete splice were minimal.
- Retrofit Scheme 2 achieved the highest ultimate load at 196.2 kips. Similar to Retrofit Scheme 1, failure was caused by the buckling of the H-pile flanges at the bearing points. There were stress concentrations at geometric discontinuities in the welds around the H-pile but the levels were not critical.
- The highest deflections were noted in Retrofit Scheme 3. The maximum lateral deflection of 0.9 in. occurred at the interface. The deflection was due primarily to the flexibility of the cap plate. Retrofit Scheme 3 failed at a maximum load of 175.4 kips as a result of the HSS assembly yielding under compression.
- In all three retrofit schemes, the connections and the remaining timber pile segment were not under significant stresses.

CHAPTER 3: LOAD RATING OF ABUTMENT TIMBER PILES

3.1 LOAD RATING PROCEDURE FOR AXIALLY LOADED PILES

The conventional load rating method for timber bridge piles was based on the assumption that the only applied load was a concentric axial force. The load rating factor was calculated as the ratio of the pile capacity to the demand imposed by an HS20-44 design truck, as shown below. Note this equation is applicable to other rating vehicles, with the live load force of that vehicle in the denominator as the Live Load.

$$Load\ Rating\ Factor = \frac{Pile\ Capacity - Dead\ Load}{HS20 - 44\ Live\ Load} \tag{3-1}$$

The dead and live load demands are typically computed through simple frame analysis. The pile capacity is given by the smaller of the allowable compressive strength of the timber pile itself or the geotechnical limit. The geotechnical capacity is generally given as the as-driven pile resistance. Each state department of transportation specifies different minimum pile-driving capacities (Andrawes and Caiza 2011). In most cases, the geotechnical capacity is much greater than the structural capacity of the timber pile. The allowable compressive stress on a timber pile loaded parallel to the grain is calculated according to the NDS as

$$F_c' = F_c C_D C_t C_u C_p C_{cs} C_{sp} \tag{3-2}$$

where, F_c is the reference allowable compression stress, C_D is the load duration factor, C_t is the temperature factor, C_u is the condition treatment factor, C_{cs} is the critical section factor, and C_{sp} is the single pile factor (AFPA 2005). C_p is the column stability factor given by

$$C_p = \frac{1 + (F_{cE}/F_c^*)}{2c} - \left[\left(\frac{1 + (F_{cE}/F_c^*)}{2c}\right)^2 - \frac{(F_{cE}/F_c^*)}{c}\right]^{\frac{1}{2}} \tag{3-3}$$

$$F_{cE} = \frac{0.822 E_{min}'}{(l_e/d)^2} \tag{3-4}$$

where, c is a constant equal to 0.85 for round timber piles, F_{cE} is the Euler critical buckling stress, F_c^* is obtained from Equation 3-2 by excluding C_p,and E_{min}' is calculated by multiplying the species-specific reference modulus of elasticity E_{min} by C_t. The allowable stress on a round timber pile is computed using an equivalent square section where d is the dimension of the equivalent square column. A load rating factor less than 1.0 signifies an inadequate pile.

The concentric load rating method as outlined above overlooks the potential of combined P–M interaction. As discussed in Borello et al. (2010), bending moments may be generated in timber pile bents as a result of deck eccentricity and asymmetric loading. Experimental results by Borello et al. (2010) showed that the ultimate load capacity of eccentrically loaded timber piles was 60% lower than that of concentrically loaded piles. To account for critical P–M interaction in eccentrically loaded timber piles, Andrawes and Caiza (2011) proposed a modification to the load rating equation where the maximum allowable stress in the timber pile is determined using a P–M interaction equation as shown below.

$$Modified\ Load\ Rating\ Factor = \frac{Live\ Load\ Stress\ Capacity,\ \ f_{cLL(max)}}{Stress\ due\ Live\ Load} \tag{3-5}$$

$$\left(\frac{f_{cDL}}{F'_{cDL}} + \frac{f_{cLL}}{F'_{cLL}}\right)^2 + \frac{f_{cLL}(6e_{LL}/d)[1 + 0.234(f_{cLL}/F_{cE})]}{F'_b[1 - (f_{cLL}/F_{cE})]} \leq 1.0 \tag{3-6}$$

Equation 3-6 is based on the P–M interaction equation outlined in the NDS (AFPA 2005). In Equation 3-5 and Equation 3-6, the lower- and uppercase variables represent the demands and capacities, respectively. Subscripts cLL and cDL represent the stress at the centroid related to live and dead loads. F'_b is the maximum allowable bending stress, F_{cE} is the Euler buckling stress, e_{LL} is the eccentricity of the live load, and d is the pile diameter. The allowable stresses are computed using NDS design equations. The allowable stresses under dead and live loads are distinguished by the load duration factor C_D. For F'_{cDL}, a permanent duration is used ($C_D = 0.9$), whereas for F'_{cLL}, a 2-month loading duration is used ($C_D = 1.15$). These values agree with AASHTO guidelines (AASHTO 2002). The allowable live load stress capacity in Equation 3-5 is obtained by solving for f_{cLL} in Equation 3-6. Based on the new load rating method, a parametric study was undertaken by Andrawes and Caiza (2011) in which a detailed finite element model of a timber pile bridge was analyzed with varying span length, deck eccentricity, pile length, and skew angle, and different levels of cross-sectional deterioration. The modified load rating method was shown to yield more conservative results in cases with moderate to high levels of deterioration.

3.2 PROPOSED LOAD RATING METHOD FOR ABUTMENT PILES

The load rating method proposed by Andrawes and Caiza (2011) is applicable only to timber piles under eccentric loading, which are typically found in bents or piers. There currently does not exist a load rating method for timber piles with lateral loads. Abutment timber piles are subjected to lateral loads from soil pressure and surcharge loads, as illustrated in Figure 3-1.

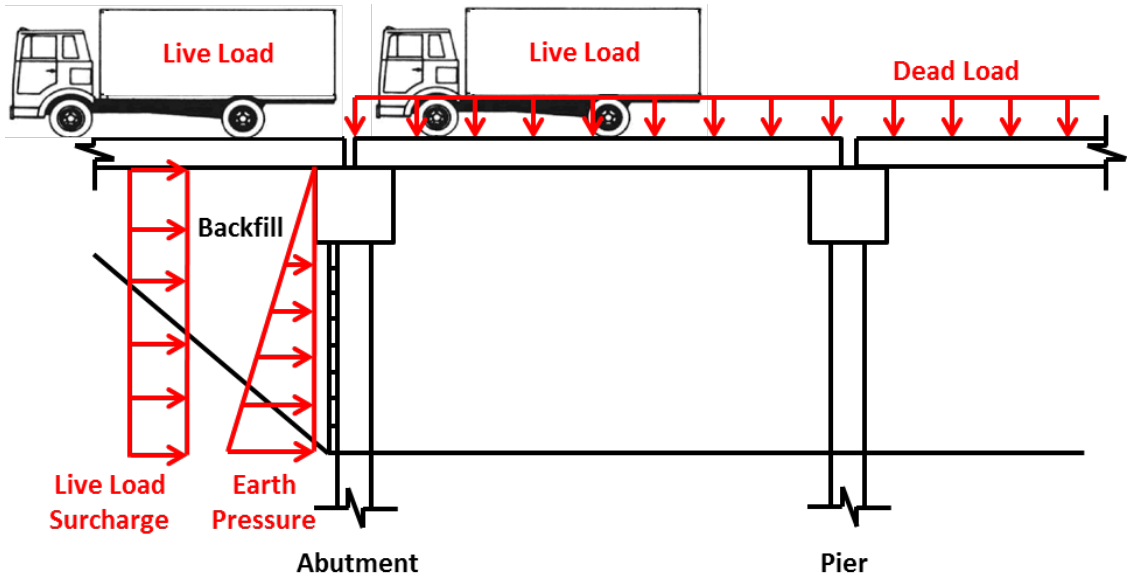

Figure 3-1. Loads applied on abutment timber piles.

The AASHTO LRFD Bridge Design Specifications require a live load surcharge to be applied to retaining walls when a vehicle load is applied on the surface of the backfill within a distance equal to one-half the wall height (AASHTO 2002). The live load surcharge is idealized as a uniformly distributed horizontal pressure, as shown in Figure 3-1. The surcharge vehicle does not impose a direct axial load on the abutment. In general, eccentric loading is not a concern in abutment piles. The modified load rating equation (Equation 3-5) proposed by Andrawes and Caiza (2011) was used as a basis for developing a load rating method for abutment piles. The following P–M interaction equation is proposed for calculating the allowable live load stress capacity, $f_{cLL(max)}$,

$$\left(\frac{f_{cDL}}{F'_{cDL}} + \frac{f_{cLL}}{F'_{cLL}}\right)^2 + \frac{(f_{bEP}/F'_{bEP} + f_{bLS}/F'_{bLS})}{1 - [(f_{cDL} + f_{cLL})/F_{cE}]} \leq 1.0 \qquad (3\text{-}7)$$

where f_{bEP} and F'_{bEP} are the bending stress capacity and demand caused by earth pressure, respectively; and f_{bLS} and F'_{bLS} are the bending stress capacity and demand related to vehicle surcharge, respectively. Stresses imposed by the permanent loads f_{cDL}, f_{cEP}, and f_{cLS} can be determined from structural analysis. Once these values are known, Equation 3-7 can be solved for f_{cLL} to determine the pile load rating. Per AASHTO guidelines, it is assumed that the cumulative live load duration is 2 months. This corresponds to an ASD load duration factor, C_D, of 1.15. This factor was used in computing the live load stress capacity, F'_{cLL}, and the flexural stress capacity related to vehicle surcharge, F'_{bLS}.

3.3. BRIDGE MODEL

To study the sensitivity of the proposed load rating method to certain geometric and structural parameters of bridges, a FE model of a multiple-span bridge was developed in ABAQUS. Three common cross-sectional deterioration profiles observed in timber piles were also considered.

3.3.1 Bridge Parameters

In the study of eccentrically loaded bridge timber piles, Andrawes and Caiza (2011) considered four geometric parameters: span length, deck eccentricity, pile length, and skew angle. In the case of abutment piles, span length, deck eccentricity, and skew angle are not critical factors. Therefore, the only geometric variable considered in the current study was the pile length. Based on a survey of construction drawings of existing timber pile bridges in the state of Illinois, a standard bridge model was developed using typical values. Most configurations consisted of two or three spans with precast or prestressed beam-slab systems and used reinforced concrete pile caps to transfer loads from the superstructure to the timber piles. Bridge model parameters used in this study are summarized in Table 3-1.

Table 3-1. Bridge Design Parameters Used in This Study

Parameter	Value
Span Length (ft)	30.7
Number of Piles per Abutment	7
Total Pile Length (ft)	21.0–23.0
Skew Angle (degrees)	25

A minimum pile penetration depth of 15 ft below the ground surface was specified in most cases. Therefore, the exposed pile length was taken to vary between 6 ft, 7 ft, and 8 ft in the study. All abutment and bent piles were assumed to have the same length. In some designs, deadman anchors were used to tie back the abutment pile caps and piles. However, they were not included in the model. The layout of the standard bridge model used in this study is depicted in Figure 3-2.

The standard bridge layout used in this study has two spans with precast concrete slab beams simply supported on reinforced concrete pile caps. The precast slab beams are 16 in. thick with a 5 in. thick wearing surface. Seven round red oak piles support the abutments and bent. All piles were assumed to be prismatic with a diameter of 12 in. The timber abutment lagging was assumed to extend from the pile cap soffit to the top of the soil. As shown in Figure 3-2, the deck measures 30 ft from edge to edge and carries two 10 ft wide traffic lanes. The deck is connected to the pile cap by dowel bars.

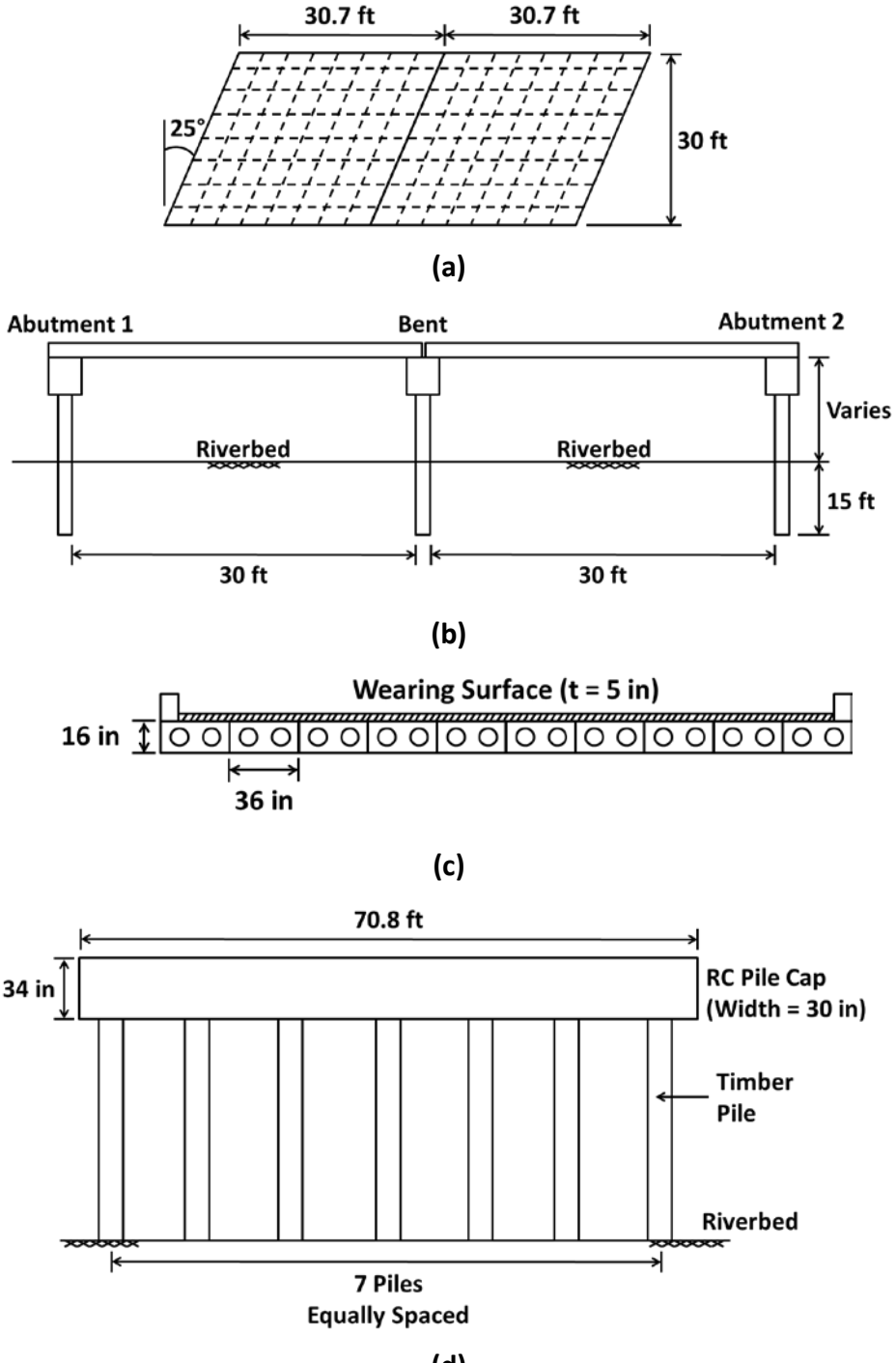

Figure 3-2. Layout of a typical timber pile bridge:
(a) deck, (b) bridge elevation, (c) deck cross-section, (d) typical timber pile bent.

3.3.2 Deterioration of Timber Piles

Timber materials used in exposed outdoor applications are typically treated with preservatives to prevent decay. Creosote is most commonly used in bridge timber piles. However, it is difficult to ensure that the preservative penetrates fully to the core of the pile. As a result, problems with decay, insect attack, and even boring animals can develop over the service life. These problems may lead to softening and severe section loss, which can have detrimental effects on the structural capacity of timber structures. Based on studies of timber pile specimens removed from service, three deterioration profiles were considered in this study. The profiles are illustrated in Figure 3-3. The damaged area was computed as a percentage of the gross cross-sectional area. The extent of deterioration was quantified by varying the dimensions shown.

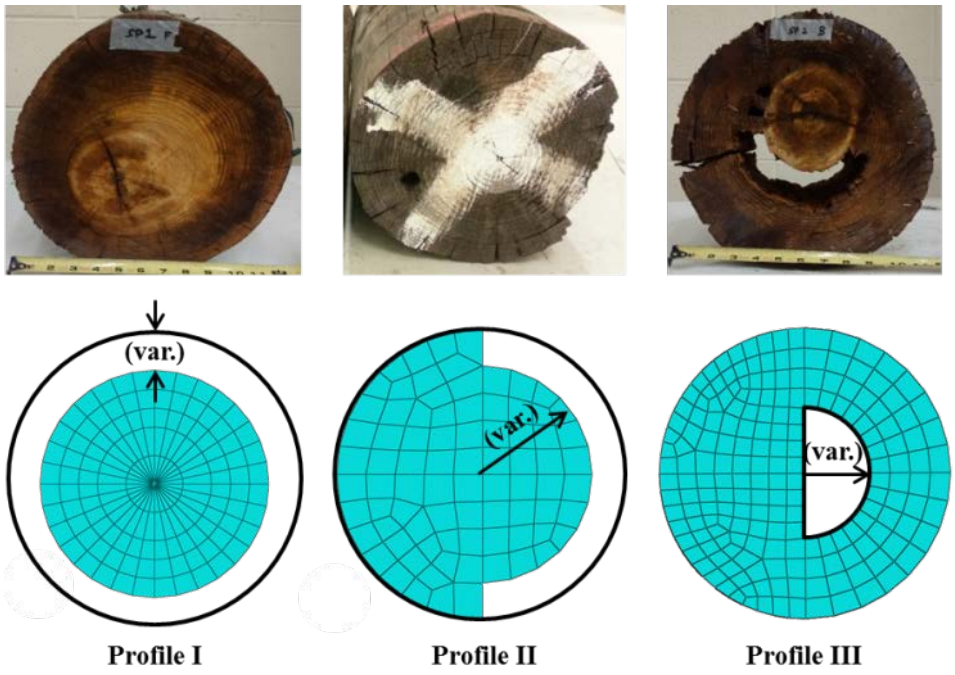

Figure 3-3. Timber pile deterioration profiles.

Profile I depicts uniform damage around the circumference of the pile. Profile II shows eccentric deterioration affecting only one-half of the pile. Profile III represents a case of internal deterioration. The internal void was assumed to have a semi-circular profile centered at the pile geometric center. In all three profiles, the remaining timber pile cross-section was assumed to be in good condition, with strength and mechanical properties unaffected by the deterioration. According to the Timber Pile Design and Construction Manual (AWPI 2002), environmental and biological degradation is a concern when the pile is exposed above the water table and subjected to wet–dry cycles. Therefore, it was assumed that the deterioration affected only the timber piles above grade. In the FE analyses, it was also assumed that every pile in an abutment had the same level of deterioration. The deteriorated timber pile sections were oriented such

that stresses were maximized. The level of damage in each profile was increased in 10% increments until the load rating was inadequate.

3.4 FINITE ELEMENT MODEL DESCRIPTION

3.4.1 Superstructure

As discussed above, the standard bridge model consisted of a precast concrete slab-beam superstructure. The deck was modeled using linear elastic shell elements in ABAQUS. A concrete elastic modulus of 3,800 ksi was assumed, and an equivalent shell thickness was determined from the flexural stiffness of the slab beam.

3.4.2 Pile Caps

Rectangular reinforced concrete pile caps measuring 34 in. deep and 30 in. wide were most commonly used. Timber piles were embedded 12 in. into the pile caps. Because the reinforced concrete pile caps at the abutments and bent are not structurally critical in the analysis and their local behavior is not significant to this study, the pile caps were modeled using discrete rigid shells. Rigid parts are governed by the motion of a reference node whose degrees of freedom are activated only when the rigid surfaces are used in contact interactions. The superstructure-to-pile-cap connection is typically made through dowel bars, but because the relative deformations and rotations at that joint are expected to be very small under normal loading conditions, the contact between the deck and pile cap was modeled using tie constraints.

3.4.3 Abutment Lagging

The abutment lagging is typically constructed using treated sawn lumber. Planks measuring 3 in. × 10 in. are typically specified in the existing construction drawings. The planks are fastened to each pile using spikes and tied together at the ends using nailer strips. In the FE model, the wall was modeled as a single part using linear elastic shell elements similar to the deck instead of modeling each discrete plank. It was assumed that the timber lagging extended from the bottom of the pile cap to the top of the ground surface. The elastic modulus of red oak (1,250 ksi) obtained from the NDS was used for the lagging. The planks were taken to be 3 in. thick. It was assumed that the lagging did not contribute any additional stiffness to the timber piles in the axial direction.

3.4.4 Timber Piles

The timber pile models used in this analysis were based on the experimental test results from Borello et al. (2009). The same material behavior as the one used in the FE analyses in Chapter 2 was used. The stress–strain behavior is plotted in Figure 2-2.

3.4.5 Soil–Pile Interaction

The soil–pile model was adapted from previous studies by Borello et al. (2009) and Andrawes and Caiza (2011). Discrete elastic spring elements were used to model skin friction and lateral resistance as described in Chapter 2. The lateral spring behavior plotted in Figure 2-3 was used.

In sufficiently long piles with lateral loading, failure occurs when a plastic hinge forms in the pile below the ground surface. For long free-headed piles in cohesionless soils, the expression below was developed by Broms (1964) for determining the depth from the ground surface to the location of the maximum bending moment in the pile.

$$f = 0.82\sqrt{\frac{P}{\gamma D K_p}} \tag{3-8}$$

where f is the depth to maximum bending moment, P is the total lateral force, γ is the soil unit weight, D is the pile diameter, and K_p is the Rankine passive earth pressure coefficient. Klaiber et al. (2004) showed that the simplified analysis method developed by Broms (1964) is adequate for the design of timber pile abutments. To simplify the FE model, the abutment timber piles were assumed to reach fixity at a depth, f, based on Equation 3-8 rather than modeling the full 15 ft embedment length. The friction springs were modeled as elastic–perfectly plastic. The depth dependent behavior of the friction springs is summarized in Table 3-2.

Table 3-2. Friction Soil Spring Behavior from Borello et al. (2009).

Depth	Yield Displacement (in.)	Yield Force (kips)
0 to 30 in.	0.1	0.10
36 in. to fixity	0.1	2.35

Cartesian connector elements were used to model the soil springs in ABAQUS. The springs were distributed at 6 in. increments along the embedded length.

3.4.6 Loading

The bridge model was subjected to three main load cases: (1) dead load (DL) applied as a uniformly distributed pressure on the deck, (2) vehicular live load (LL), and (3) earth pressure (EH) with live load surcharge (LS) applied to the abutment lagging. The HS20-44 truck load was used for the live load. The distance between the center and rear axles was taken as 14 ft. To maximize the axial load applied to the piles, two design trucks were placed as shown in Figure 3-4.

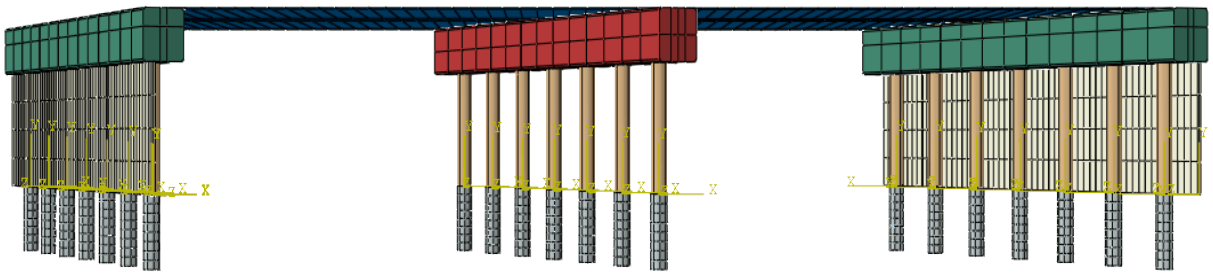

(a)

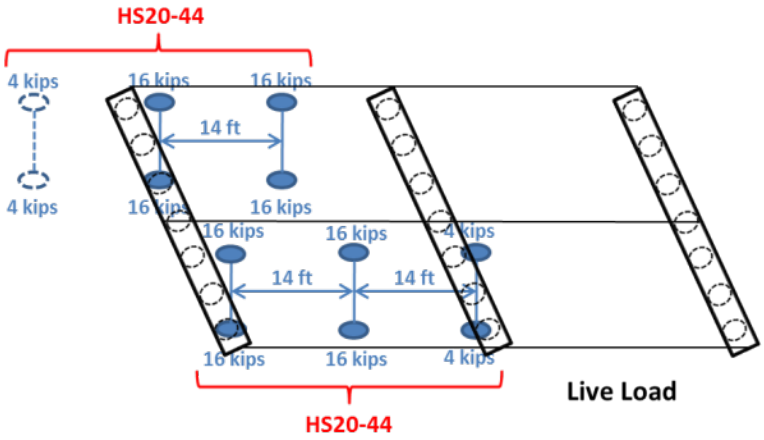

(b)

Figure 3-4. FE model of a typical timber pile bridge: (a) elevation of FE model; (b) live load vehicle load pattern.

The lateral earth pressure was calculated using the equivalent-fluid method with level backfill. The equivalent soil unit weight was varied in 0.005 kcf increments from 0.030 kcf to 0.060 kcf to cover a range of soil conditions. In addition to the earth pressure, the AASHTO Standard Specifications require the application of a live load surcharge load to be used in cases where vehicular loads are expected on the surface of the backfill. As per the guidelines in the AASHTO Standard Specifications (AASHTO 2002) a constant surcharge pressure equal to 2 ft of earth was used to represent live load surcharge. This yields a uniform lateral pressure distribution on the abutment lagging. The earth pressure was applied over the abutment backing wall and the backfill side of the abutment pile cap. In each load case, the coefficient of lateral earth pressure was back-calculated from the equivalent fluid soil unit weight and applied to the live load surcharge pressure. The live load surcharge was applied uniformly across the entire abutment wall, as specified in the AASHTO Standard Specification (AASHTO 2002).

3.5. BRIDGE MODEL LOAD RATING

3.5.1 Standard Bridge Model

The proposed load rating method for abutment piles is demonstrated in this section. The standard bridge model was analyzed with undeteriorated timber piles. It was assumed that red oak was used for all piles. Red oak is a common species of wood used in many heavy timber applications, including piles and railroad sleepers. The reference design values for red oak listed in the NDS are shown in Table 3-3, where F_c is the allowable compressive stress parallel to the grain, F_b is the allowable bending stress, F_v is the allowable shear stress parallel to the grain, E is the reference modulus of elasticity, and E_{min} is the reference modulus of elasticity used for beam and column stability calculations.

Table 3-3. Reference Design Values for Treated Red Oak Timber Piles Under Normal Load Duration and Wet Service Conditions (AWPA 2005)

F_c (ksi)	F_b (ksi)	F_v (ksi)	E (ksi)	E_{min} (ksi)
1.10	2.45	0.135	1,250	660

The allowable compressive stress parallel to grain under DL and LL is calculated using Equation 3-2. Based on reference values for red oak presented in the NDS, F'_{cDL} and F'_{cLL} are taken as 0.98 ksi and 1.23 ksi, respectively, for a pile with length 7 ft above the ground surface. The allowable bending stress is computed as

$$F'_b = F_b C_D C_t C_u C_F C_{sp} \tag{3-9}$$

where the factors C_D, C_t, C_u, and C_{sp} are the same as the allowable compressive stress calculation, and F_b is the reference allowable bending stress. C_F is the size factor equal to unity because the piles were assumed to have a constant diameter of 12 in. The allowable bending stress under earth pressure, F'_{bEP}, is equal to 2.21 ksi. The allowable bending stress under live load surcharge , F'_{bLS}, based a cumulative live load duration of 2 months as stated previously, is equal to 2.82 ksi. Typical analysis results are shown in Table 3-4 for a pile with 7 ft of exposed length subjected to an equivalent fluid soil pressure of 0.035 kcf. The load rating computed based on the P–M interaction equation, Equation 3-7, is compared with the conventional load rating method computed using Equation 3-1, in which only axial loads are assumed.

Table 3-4. Typical Analysis Results and Load Rating of the Standard Bridge Model

Pile	f_{cDL} (ksi)	f_{bEP} (ksi)	f_{bLS} (ksi)	f_{cLL} (ksi)	$f_{cLL\,(max)}$ (ksi)	Proposed Load Rating Factor	Conventional Load Rating Factor
1	0.065	0.872	0.504	0.065	0.671	10.3	14.1
2	0.083	0.862	0.478	0.077	0.663	8.6	11.7
3	0.100	0.824	0.462	0.090	0.665	7.4	9.8
4	0.117	0.823	0.461	0.102	0.645	6.3	8.5
5	0.135	0.819	0.460	0.114	0.625	5.5	7.4
6	0.152	0.852	0.472	0.126	0.584	4.6	6.6
7	0.169	0.858	0.497	0.138	0.552	4.0	5.9

As can be seen in Table 3-4, the bending stresses caused by earth pressure and live load surcharge are distributed relatively evenly amongst the piles. The stresses related to dead and live load are greatest in Pile 7. This is due to the bridge skew. As a result, Pile 7 is the most critical pile. Compared with the proposed load rating based on P–M interaction, the conventional method yields significantly higher load ratings. This shows that assuming all timber piles are loaded only in the axial direction is highly unconservative.

3.5.2 Sensitivity Study Results

The FE model of the standard bridge was used to generate load ratings under different levels of deterioration and soil conditions. The pile length above the ground surface was also varied between 6 ft, 7 ft, and 8 ft. For each case, the design allowable stresses were recalculated to reflect the geometric changes. The critical load rating is plotted in Figure 3-5 for each deterioration profile. A load rating factor less than 1.0 signifies a pile with inadequate structural capacity to resist the HS20-44 live load.

The effect of increasing backfill soil density is shown in Figure 3-5(a), (b), and (c). A constant pile length of 7 ft above the ground surface was used. It can be seen that the load rating follows the quadratic shape of the P–M interaction equation, Equation 3-7. Each curve represents the maximum load rating the critical timber pile with a given level of deterioration can achieve under lateral loads imposed by the range of backfill soil densities. The curves are not complete at high levels of deterioration because bending failure occurs; hence, there is zero live load capacity. For deterioration Profile I, the critical load rating factor falls below 1.0 at 10% deterioration at equivalent soil density γ_{eq} greater than 0.050 kcf. Up to approximately 20% cross-sectional deterioration, the results are similar for Profiles I and II. However, at 30%, it can be seen that Profile II is more critical. Internal deterioration as depicted by Profile III can be very problematic because it can be very difficult to detect during field inspections without advanced tools and techniques. However, in comparison to the other deterioration profiles, it is able to sustain larger loads for a given level of deterioration. The relatively large drop in load rating from 20% deterioration to 30% suggests that deterioration Profile III causes more rapid loss of strength as the deterioration progresses. It is important to note that the bending stress

contribution to the P–M interaction in Equation 3-7 is generally much larger than that of the axial loads because of second-order amplification effects and because the axial compression components are squared to capture the shifting of the neutral axis (Steiger and Fontana 2005).

The effect of pile length on the load rating is shown in Figure 3-5(d), (e), and (f). An equivalent soil unit weight of $\gamma_{eq} = 0.035$ kcf was used in all cases. Increasing the pile length yields similar trends in the critical load rating as increasing the backfill soil unit weight. For a given pile length and level of deterioration, Profile II yields the lowest critical load rating. Increasing the pile length not only affects the magnitude of the lateral load but also its stability. Because most abutment timber piles are not braced in the out-of-plane direction, second-order effects may significantly impact the structural integrity of long piles with dense backfill.

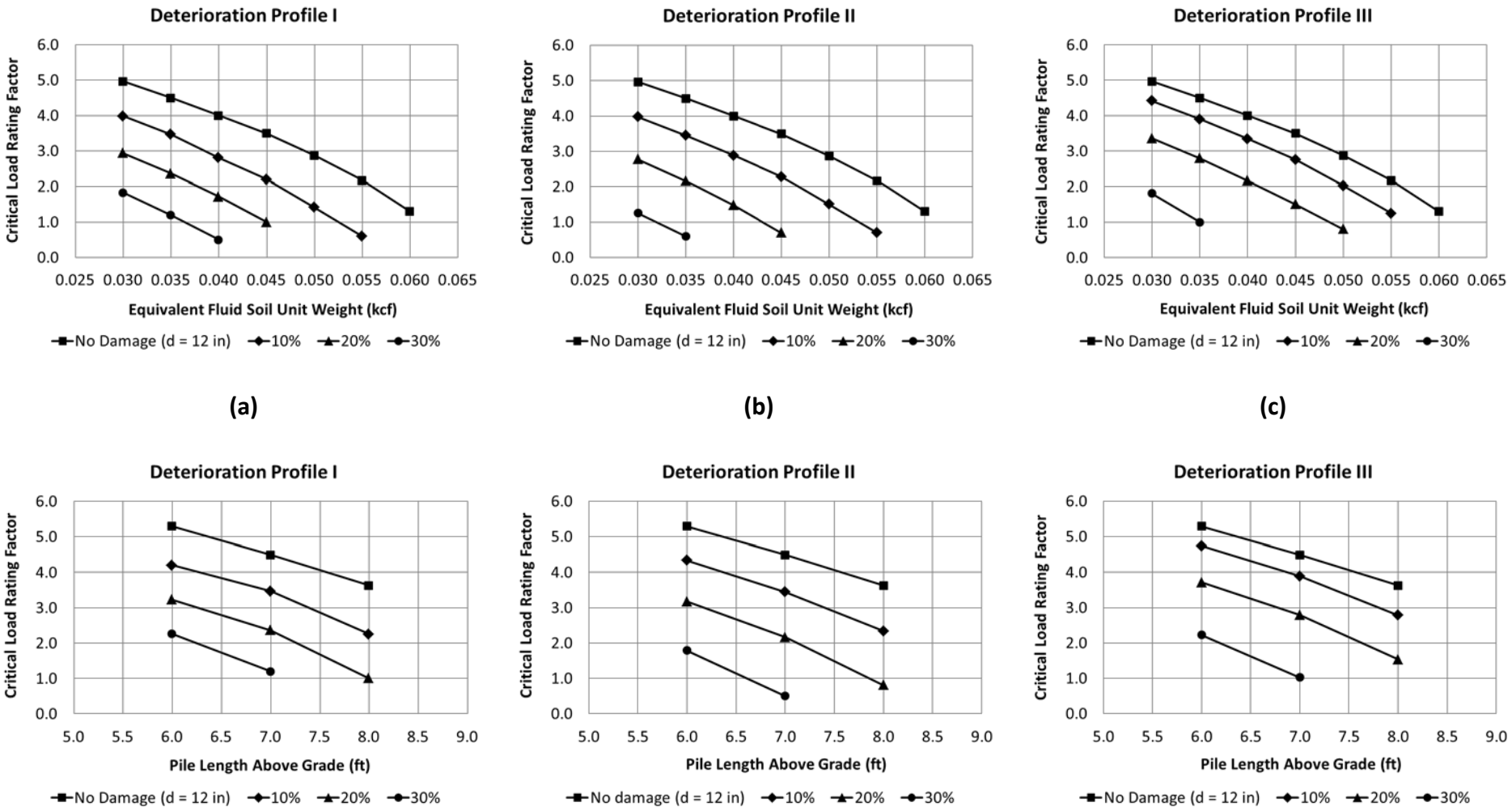

Figure 3-5. Load rating sensitivity study results.

3.6 FRP RETROFIT

3.6.1 Design

The performance of timber structural members retrofitted with FRP composites has been studied by many researchers. Confinement with FRP wraps has been shown to significantly improve the strength and ductility of timber piles (Hagos 2001; Lopez-Anido et al. 2003; Caiza et al. 2012). In the case of bridge abutment timber piles, it is not possible to fully wrap the pile with FRP because of the abutment lagging. Therefore, FRP retrofits to abutment timber piles may be feasible only in the form of stiffening strips or shells to the exposed side of the pile that is in tension. In general, the presence of defects in wood such as knots and checks causes timber members to be much weaker in tension than in compression. As a result, the behavior of timber members in bending is typically governed by tension (Buchanan 1984). In the current study, an FRP composite shell fully encompassing one-half of the timber pile was considered as a retrofitting alternative. The thickness of the composite was varied to determine the effect of FRP retrofitting on the load rating of abutment timber piles. The retrofit scheme is illustrated in Figure 3-6.

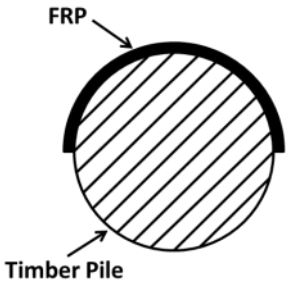

Figure 3-6. Half-shell FRP retrofit scheme considered in this study.

3.6.2 Modified Allowable Bending Stress

Because of material nonlinearity and size effects, it is difficult to determine the true maximum flexural stress of timber (Buchanan 1984). Traditionally, the allowable bending stress for timber members has been determined by assuming linear elastic behavior and computing the modulus of rupture. The nominal bending moment capacity of timber structural members is computed this way in the AASHTO Standard Specifications (AASHTO 2002). A similar elastic design approach was taken to determine the moment capacity of FRP-retrofitted timber piles, as illustrated in Figure 3-7.

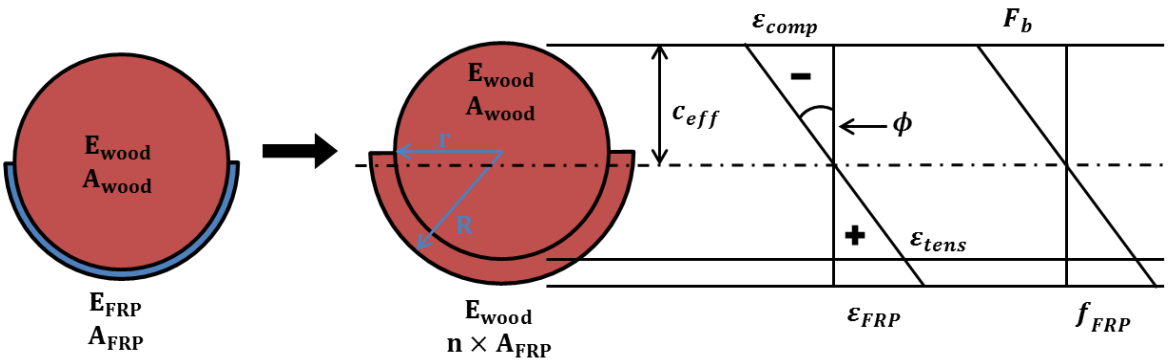

Figure 3-7. Elastic design approach for abutment pile FRP retrofit design.

The FRP composite was transformed into an equivalent thickness of timber using the modular ratio. Linear stress–strain behavior was assumed and using basic mechanics, the moment capacity of the section was determined as

$$M = E_{wood} I_{eff} \phi = E_{wood} I_{eff} \frac{\varepsilon_{comp}}{c_{ef}} = E_{wood} I_{eff} \frac{(F_b / E_{wood})}{c_{eff}} \quad (3\text{-}9)$$

where M is the bending moment capacity of the retrofitted section, E_{wood} is the timber pile elastic modulus, I_{eff} is the transformed section moment of inertia, and ϕ is the section curvature. ε_{comp} is the strain at the extreme compression fiber, c_{eff} is the depth to the neutral axis measured form the compressive fiber, and F_b is the design allowable bending stress obtained from the NDS. This FRP retrofitting method is expected to improve the bending moment capacity of the timber piles but will not offer significant contributions in the axial direction. To account for the improved moment capacity provided by the FRP, the moment calculated using Equation 3-9 is then projected onto an unretrofitted timber pile section to obtain a modified allowable bending stress, as shown in Figure 3-8.

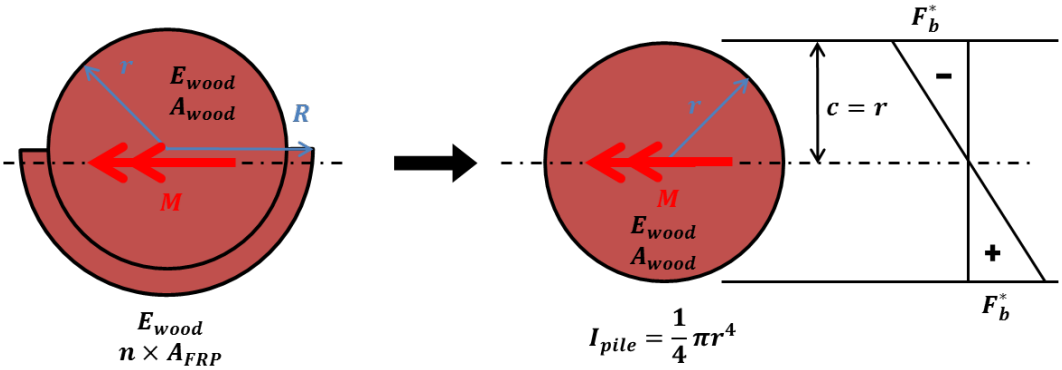

Figure 3-8. Projection of the bending moment obtained from transformed section analysis onto an unretrofitted timber pile section.

As shown in Figure 3-8, the modified allowable bending stress is computed assuming linear elasticity and the neutral axis at mid-height of the timber cross-section. Although this is not an exact representation of the actual bending stresses in the timber pile at failure, it conservatively captures the increased moment capacity of the retrofitted pile. The study by Buchanan (1984) shows that, owing to size effects, the failure stress in a timber beam in bending increases as the portion of the cross-section under tension decreases. Therefore, assuming a high neutral axis location as in the method described above provides a conservative representation of the flexural strength of the retrofitted timber pile.

3.6.3 Effect on Critical Load Rating

The modified allowable bending stress was computed using the procedure described above for a 7 ft timber pile with deterioration Profile I. The reference allowable bending stress, F_b, in Equation 3-9 was taken to be 2.45 ksi, which corresponds to red oak. An elastic modulus of 660 ksi was assumed for the timber pile. A constant FRP thickness of 0.25 in. was assumed with elastic modulus of 1,800 ksi, typical for GFRP composites. For 0%, 10%, 20%, and 30% cross-sectional deterioration, the bending moment capacity of the retrofitted section and the modified allowable bending stress are shown in Table 3-5.

Table 3-5. Modified Allowable Reference Bending Stress for a Red Oak Timber Pile Retrofitted with a Half-Shell FRP

Deterioration Level (%)	Unretrofitted Timber Pile Cross-Sectional Area (in^2)	FRP Transformed Cross-Sectional Area, A_{eff} (in^2)	c_{eff} (in)	I_{eff} (in^4)	M (kip·ft)	F_b^* (ksi)
0	113.1	126.2	6.4	1281.5	40.8	2.88
10	101.8	114.2	6.1	1050.1	35.1	2.92
20	90.5	102.4	5.8	845.8	29.8	2.94
30	79.2	90.3	5.4	658.1	24.9	3.01

The modified allowable bending stresses in Table 3-5 were taken as the reference bending stress in computing the allowable bending stress under earth pressure and live load surcharge using Equation 3-9. The critical load rating for the FRP-retrofitted timber piles is compared with unretrofitted timber piles in Figure 3-9 for various soil conditions.

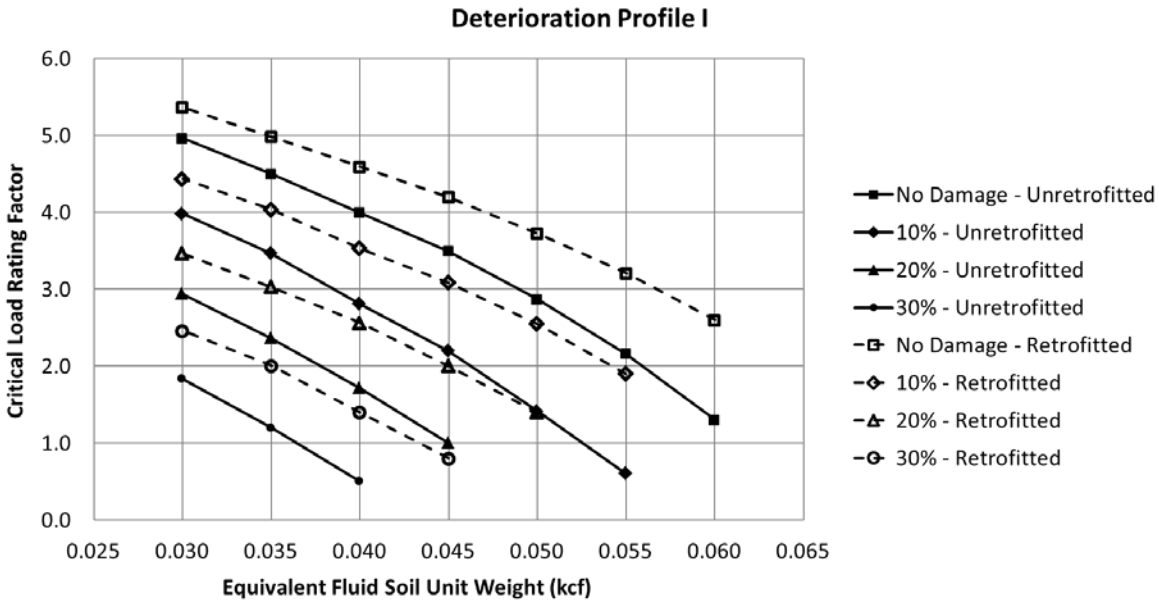

Figure 3-9. Comparison of critical load ratings for unretrofitted and retrofitted timber piles with deterioration Profile I.

In Figure 3-9, the curves plotted with solid lines represent unretrofitted timber piles, while those with dotted lines are the piles retrofitted with FRP. For each level of damage, the curve for the FRP-retrofitted timber piles is shifted up and the slope becomes more gradual. The critical load rating is adequate with 30% cross-sectional damage for equivalent fluid soil density γ_{eq} greater than 0.040 kcf. In comparison, the unretrofitted timber pile has very little capacity at 30% deterioration. Increasing

the volumetric ratio of FRP further increases the critical load rating. Using the proposed load rating method and the method for determining the modified allowable bending stress, the exact volumetric ratio of FRP needed to achieve a desired load rating can be determined.

3.7 CONCLUSIONS

The conventional method for determining the load rating for bridge timber piles assumes only axial loads are applied. The live load capacity is computed as the axial load capacity of the timber pile minus the dead load demand. In the study by Andrawes and Caiza (2011), it was shown that this assumption is not conservative for eccentrically loaded timber piles. Although the behavior of timber piles under P–M interaction is critical, there does not exist a load rating method applicable to abutment timber piles that must resist lateral earth pressure and surcharge loads as well as gravity loads. As part of the current study, a modified allowable stress load rating method that does account for combined axial–flexural loading was developed. Using an FE model of a typical timber pile bridge, the effect of backfill soil unit weight, pile length, and deterioration on the load rating was studied. Additionally, a simplified method for computing the allowable bending stress of an FRP-retrofitted timber pile was demonstrated. The main findings from the study are summarized below.

- It was shown that, compared with the conventional load rating method, the new load rating method gives much more conservative results.
- Bridge skew affects the distribution of axial loads from dead and live loads such that the piles closest to the obtuse angle are the most critical. Distribution of lateral forces from earth pressure and live load surcharge are not affected by the skew.
- The load rating follows the quadratic behavior of the P–M interaction equation.
- In general, deterioration Profiles I and II, representing external section loss, led to more critical load ratings than Profile III, which modeled internal damage. For all three deterioration profiles, 10% deterioration was enough to cause the critical load rating to drop to inadequate levels under high equivalent fluid soil pressures.
- Retrofitting the tension face with FRP improves the bending moment capacity of timber piles. To incorporate this into the load rating method, a modified allowable bending stress was computed based on elastic design assumptions.
- A 0.25 in. thick GFRP half-shell retrofit was considered for deterioration Profile I. The modified bending stress for the deteriorated sections was greater than the reference design bending stress in the NDS by more than 18%. This increased the critical load rating by at least 17%.

CHAPTER 4: EXPERIMENTAL TESTING OF FRP RETROFITS FOR ABUTMENT TIMBER PILES

As shown by the results in Chapter 3, deterioration of the abutment timber piles can lead to significant reductions in the load capacity. Because abutment piles are restrained on one side by the backing wall, not a lot of options are feasible. Because the bending behavior of timber is generally governed by tension, using FRP composites to strengthen the tension face of timber piles may be an effective retrofitting strategy. However, unlike other conventional structural materials, obtaining an accurate condition assessment on which to base retrofit designs on is very difficult for timber structures. In this chapter, the effectiveness of FRP retrofits for abutment piles is evaluated experimentally. The condition of the timber pile was determined using a nondestructive stress wave timing technique, and the results were directly incorporated into the retrofit design and interpretation of the results.

4.1 TIMBER PILE SPECIMENS

Three red oak piles removed from service were used in the study. The NDS reference design values for red oak can be found in Table 3-5. It was unclear how long these piles were in service for and what the service conditions were. Visual inspection of the piles found no signs of decay or damage to the exterior of the specimens. Minor splitting was common across all three specimens. The timber pile specimens are shown in Figure 4-1.

Figure 4-1. Timber pile specimens used in experimental testing of FRP retrofits.

Timber piles are tapered as a result of natural tree growth. For the purposes of this study, the pile cross-section was idealized as being perfectly circular despite being non-uniform. The diameter of the pile at each stress wave measurement location was estimated by measuring the circumference of the pile. All three specimens were very similar in size. Specimen details are summarized in Table 4-1.

Table 4-1. Timber Pile Specimen Details

Specimen	Average Pile Diameter (in)	Density, ρ (lb/in^3)
SP1	10.7	0.0269
SP2	11.0	0.0268
SP3	10.7	0.0265

One specimen was tested as-is to determine the baseline performance. Two specimens were retrofitted using GFRP composites before testing. To gain an understanding of the internal condition of the piles and obtain a quantifiable measure of the condition of the piles, a nondestructive stress wave timing test method was used.

4.2 INITIAL CONDITION ASSESSMENT

4.2.1 Stress Wave Timing

Conventional inspection methods including visual inspection and hammer sounding are limited to identifying deterioration close to the surface and may be subjective. The Forest Products Laboratory (FPL) has evaluated nondestructive inspection tools for condition assessment of in situ wood (Ross et al. 2004). Stress wave timing is a method in which decay and other deteriorations are detected by measuring the velocity at which a stress wave propagates through a material. It is based on the principle that stress waves propagate rapidly through stiff, solid materials and more slowly through soft, flexible materials. The fundamental concept behind the stress wave timing method is illustrated in Figure 4-2.

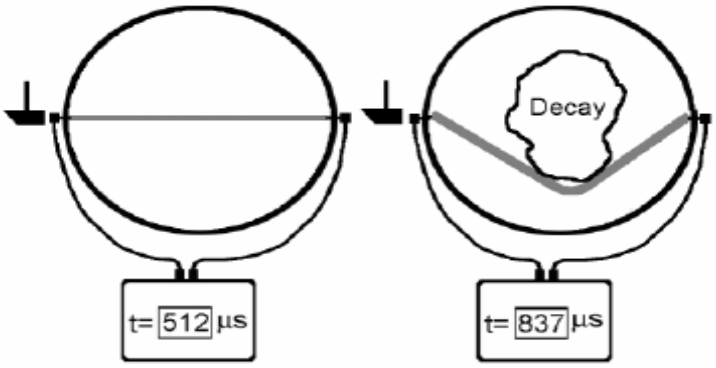

Figure 4-2. Stress wave timing concept (Wang et al. 2004).

As shown in Figure 4-2, a stress wave is induced in a specimen on one side by impacting the specimen or using ultrasonic pulses. The time it takes for the stress wave to be detected by a receiver at a known distance away from the source is measured. In this study, an ultrasonic pulse velocity (UPV) instrument was used. The instrument consisted of two 50 kHz piezoelectric transducers and a receiver that measured the transmission time. Typical stress wave transmission times through timber vary depending on the species, grain direction, and moisture content. However, as outlined in Wang et al. (2004), there are some well-established reference values. The reference stress wave transmission times for undeteriorated red oak are summarized in Table 4-2.

Table 4-2. Stress Wave Transmission Times Through Undeteriorated Red Oak

Reference	Moisture Content (%)	Stress Wave Transmission Time [µs/m [µs/ft)]	
		Parallel to Grain	Perpendicular to Grain
Smulski 1991	11	262–200 (80–61)	—
Armstrong et al. 1991	4–6	226–177 (69–54)	646–571 (197–174)
Jung 1979	12	302–226 (92–69)	—

As a result of the unique microstructure of wood, the stress wave velocity varies greatly, depending on the direction of measurement. Stress wave velocity measurements can be interpreted in two ways. First, measurements taken across the cross-section in directions tangent and perpendicular to the grain can be used to generate tomographic images that may be used to identify internal damage or decay. The study by Wipf et al. (2007) verified the accuracy of this method. However, a large number of sampling points is needed in order to generate an accurate image of the cross-section. This may not be feasible in the field for abutment timber piles because of the backing wall. In the current study, six measurements were taken across the cross-section at seven evenly spaced locations along the length of the pile for each specimen. The study by Divos and Szalai (2002) showed that the minimum size of an internal defect that can be detected using six measurements across the cross-section is approximately 8% of the cross-sectional area.

Stress wave velocity measurements in the longitudinal direction parallel to the grain offer a more direct representation of the structural condition of timber piles. Using one-dimensional wave theory, stress wave velocity in the longitudinal direction can be related to the elastic modulus of a material as follows (Kim et al. 2000):

$$V = \sqrt{\frac{E}{\rho}} \tag{4-1}$$

Equation 4-1 represents the propagation of longitudinal and flexural waves through a thin rod where V is the stress wave velocity, E is the dynamic elastic modulus, and ρ is the material density. To use Equation 4-1, stress wave velocities must be measured directly on the cross-section through the length of a specimen. The dynamic elastic modulus is a property of a material under vibratory conditions. Although it cannot be directly used to compute the strength of a material, it is a good indicator of its stiffness.

After all tests were completed, the piles were cut into five segments and longitudinal stress wave velocities were measured. Because wood is neither a homogeneous nor isotropic material, obtaining an accurate prediction of the mechanical behavior based on such assumptions may be inaccurate. However, studies have shown that the speed and attenuation of stress waves through timber are strongly related to the mechanical properties (Ross and Pellerin 1994; Ross et al. 1997). For the purposes of the current study, this simplification presents a suitable measure of the timber pile condition.

4.2.2 Stress Wave Timing Results

Six stress wave velocity measurements were taken through the cross-section at seven locations along the length of the pile for each pile. Although the number of measurements is not sufficient to develop a detailed tomographic image of the cross-section, the values provide a good indication of the internal condition. The average stress wave velocity at each cross-section along the length is plotted in Figure 4-4.

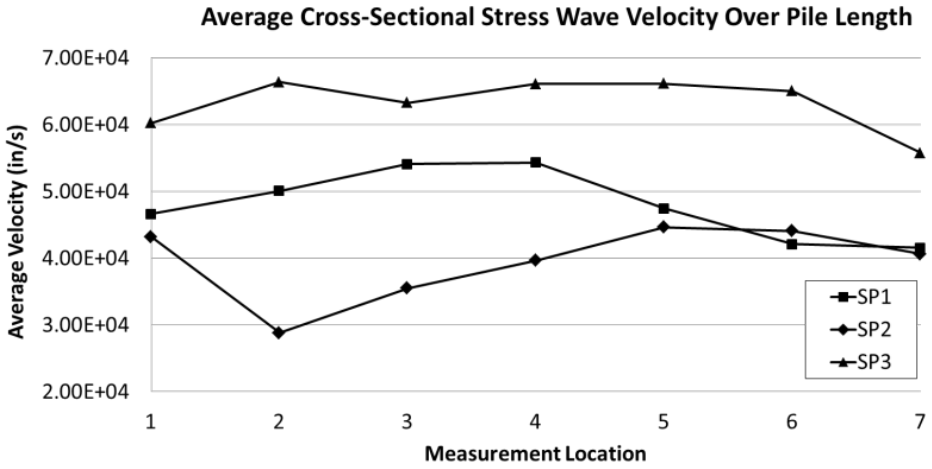

Figure 4-4. Average stress wave velocity along pile length.

The average stress wave velocity in SP2 at Location 2 was considerably lower compared with the rest of the pile. This suggests there exists some localized internal defect or damage at that location. Similarly, in SP1, the stress wave velocities drop near locations 6 and 7. Overall, the plot of average stress wave velocity clearly shows that the condition of specimens SP1 and SP2 were inferior to those of specimen SP3. The average longitudinal stress wave velocities measured on the cross-sections of the pile specimens after they were tested and cut were 1.83×10^5 in/s, 1.71×10^5 in/s, and 1.96×10^5

in/s for SP1, SP2, and SP3, respectively. Using these values in Equation 4-1, the dynamic moduli estimated from the longitudinal stress wave velocity are 27.6×10^6 psi, 24.1×10^6 psi, and 31.8×10^6 psi, respectively. The general trend shows that SP3 was in the best overall condition and SP2 was in a much worse condition.

As explained above, Equation 4-1 is based on one-dimensional wave theory, which is a significant simplification considering timber is an orthotropic, defect-filled material. Nonetheless, numerous studies have shown it is strongly correlated to timber condition (Emerson 1999). Therefore, the stress wave timing results were used as a direct measure of the timber pile quality in this study.

4.3 FRP RETROFIT

4.3.1 Materials

In this study, a GFRP woven roving fabric and epoxy resin were used to fabricate the FRP composite. The FRP was applied to the timber piles using the wet layup technique. The GFRP fabric was 0.025 in. thick with an elastic modulus of 1,800 ksi. Although the woven fabric consists of fibers in the longitudinal and transverse directions, the transverse fibers have no flexural stiffness contribution. The epoxy resin was a medium viscosity, two-part resin with a pot life of 60 min. The materials used to fabricate the FRP composite are identified in Table 4-3.

Table 4-3. FRP Composite Material Properties

GFRP Woven Roving	Thickness: 0.025 in. Density: 0.63 oz/ft^3 Elastic Modulus: 1,800 ksi Ultimate Strain: 1%
Epoxy Resin	Density: 9.2 lb/gal Tensile Strength: 9.8 ksi Ultimate Strain: 1.9%

4.3.2 Retrofit Design

In the case of abutment piles, it is not feasible to do a full FRP wrap because of the retaining wall. Therefore, FRP retrofits for abutment timber piles can be applied only to the open side, which corresponds to the tension side. The behavior of timber members in bending is typically governed by tension because defects in the wood such as knots and checks greatly reduce the tensile strength. Compressive strength is not significantly affected by defects (Buchanan 1984). The FRP retrofit in this case would effectively improve the strength of the timber pile in bending but will not provide any additional compressive strength. It is common to design timber members in bending assuming linear elastic behavior in both tension and compression. This is a conservative approach because accounting

for inelasticity in compression causes the neutral axis to shift toward the tension fiber. In this study, two FRP configurations were considered, as shown in Figure 4-6.

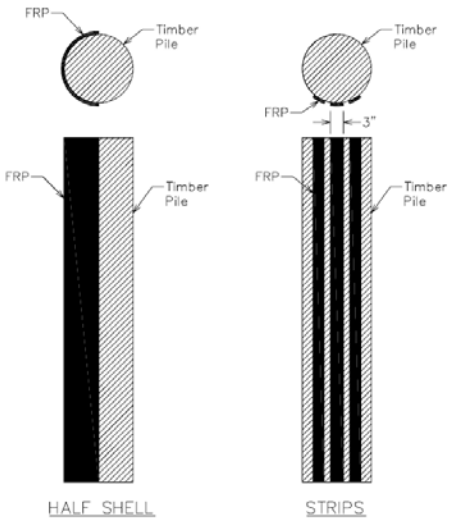

Figure 4-6. Possible FRP retrofitting configurations for abutment timber piles.

The first configuration is a uniform half-shell encompassing one-half of the timber pile. In the second configuration, 3 in. wide FRP strips of identical thickness were evenly spaced around one side. In both cases, the FRP was applied to the full length of the pile. Because it was shown that timber pile specimen SP3 was in the best condition, it was tested as-is and used as the control specimen. The half-shell FRP configuration was applied to specimen SP2, and the strip configuration to specimen SP1.

Currently there are no guidelines available on designing FRP retrofits for timber piles. In the Phase I study conducted by Caiza et al. (2012), a simplified elastic method was used to derive the thickness of FRP needed in a full FRP shell to restore the flexural stiffness of timber piles. Based on providing full FRP wraps, it was shown that the timber pile specimens used in that study required between 6 and 10 layers of FRP. In the current study, 10 layers (0.25 in.) of FRP was used in both retrofitting schemes shown in Figure 4-6. Prior to applying the FRP composite to the piles, the surfaces of the timber piles were cleaned with a wire brush to remove any dirt and debris. The fabric was cut to size and saturated with resin using rollers. Once applied, the FRP was allowed to cure for at least 72 hours before testing. The retrofitted specimens are shown in Figure 4-8.

(a) (b)

Figure 4-8. FRP-retrofitted timber pile specimens: (a) SP1; (b) SP2.

4.4 EXPERIMENTAL TESTING

4.4.1 Test Setup

From a survey of several existing timber pile bridges in Illinois, it was determined that the average exposed pile length above the ground surface was approximately 7 ft. The test specimens were cut to 9 ft, and the ends were embedded 12 in. in reinforced concrete pile caps. To apply combined bending and axial loads to the pile specimens, a post-tensioning scheme was used, as shown in Figure 4-9.

A reinforced concrete pile cap was cast over the ends of the timber piles, as shown, to transfer the loads into the piles. Back-to-back MC18×58 steel sections were used on top of the pile caps to ensure the piles did not punch through. Post-tensioning rods (1.5 in. diameter) were fitted through the C-channels and pile caps 12 in. away from the pile centerline. The tests were conducted by first imposing a constant bending moment then applying a concentric axial force. The bending moment was induced by tensioning just one of the rods using a bolt stretcher. This eccentric load was then anchored off, and both rods were tensioned from the opposite end using hydraulic jacks. The concentric load was increased until the onset of nonlinear behavior. Each pile was tested up to the elastic limit under eccentric loads varying from 10 kips up to 35 kips. The forces applied on the piles were monitored using load cells. As shown in Figure 4-9, strains in the timber and FRP were measured at the extreme fibers at quarter and mid-length, and linear variable displacement transducers (LVDTs) were placed at the ends of the pile caps to measure the total axial deformations. The tests were conducted with the timber piles lying horizontally. Form oil was used to minimize friction between the pile caps and the floor.

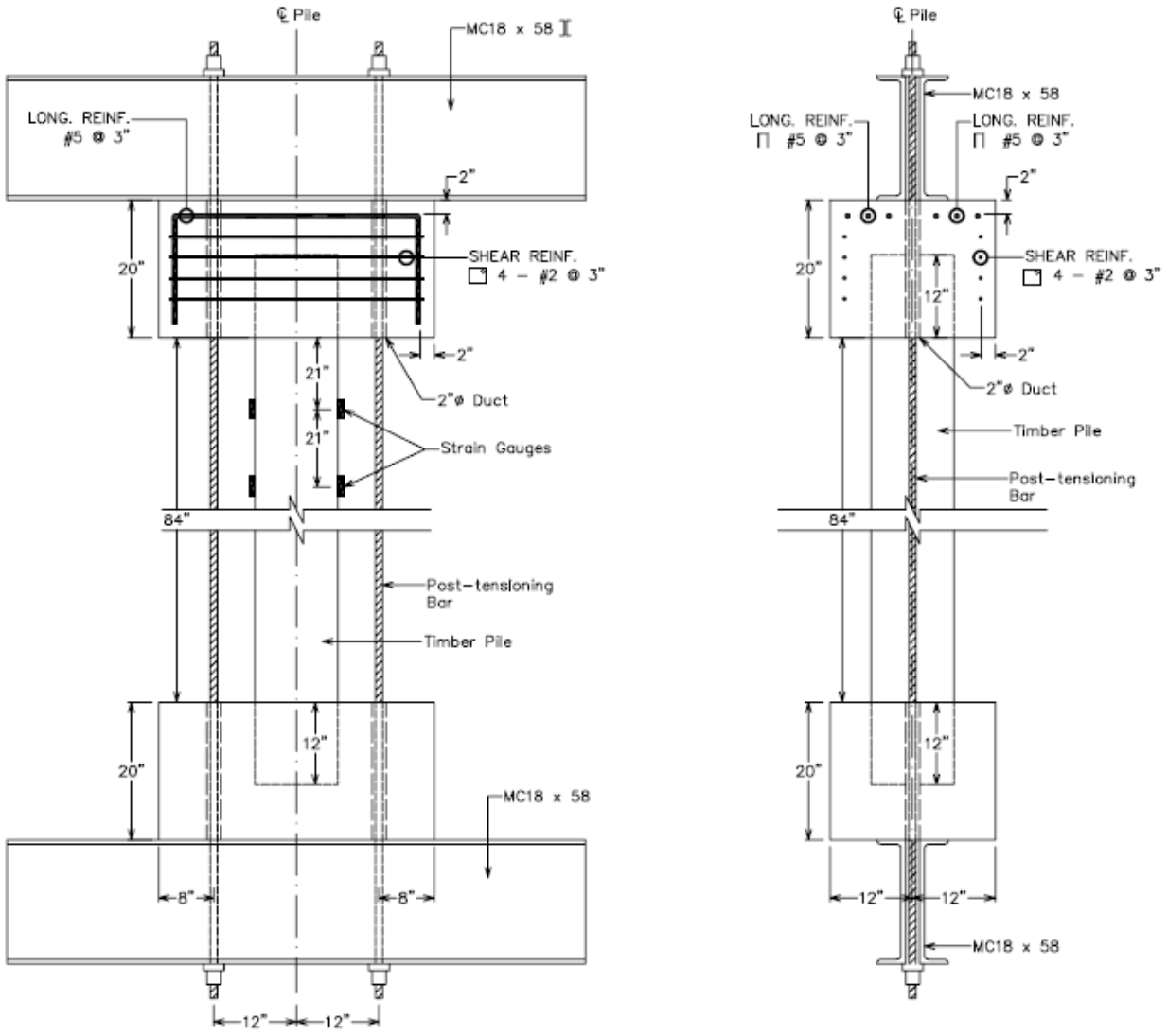

Figure 4-9. P–M interaction test setup.

4.4.2 Results

As explained above, each specimen was loaded with a prescribed eccentric load applied through an eccentricity of 12 in. then an increasing concentric load up to the point of nonlinearity. The maximum total force at the proportional limit was taken as the ultimate load. This limit was based on the assumption of linear elasticity, which forms the basis of the flexural design of timber piles. This does not represent the true ultimate capacity of the timber piles. At high loads, significant bending in the timber piles was clearly noticeable, with audible cracking of the FRP composite. The curvature at mid-height caused by the application of the eccentric load is plotted against the resulting bending moment in Figure 4-10. The curvature was computed using strains measured at the extreme fibers of the specimen.

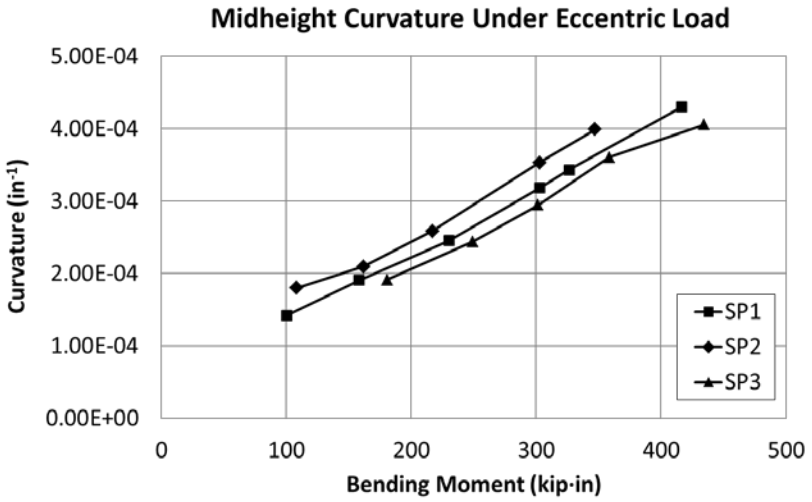

Figure 4-10. Mid-height curvature caused by the eccentric load.

As can be seen, the curvature caused by the eccentric loads in each specimen was very similar. Compared with the unretrofitted specimen SP3, the curvatures in the retrofitted specimens SP1 and SP2 were only 4% and 11% higher, respectively. This shows that despite the additional stiffness provided by the FRP retrofit, the behavior is still strongly influenced by the timber pile condition. After each loading scheme, the specimens were visually inspected. However, there was no visible damage to the timber piles or the FRP composite, even at very high loads. The cracking of the FRP heard during testing was most likely from the resin because no visible fiber fractures were noted. The ultimate P–M interaction behavior is plotted in Figure 4-11.

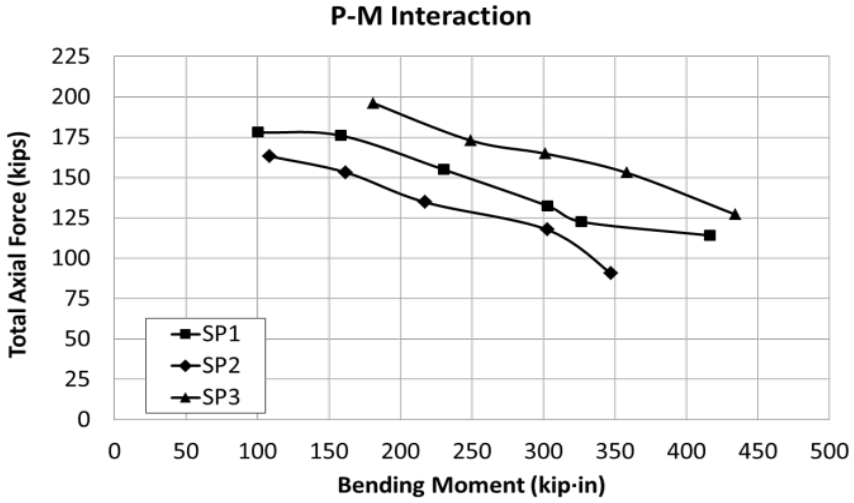

Figure 4-11. Peak total axial force attained under each bending moment.

The observed P–M interaction follows the expected behavior with the peak axial force decreasing with increasing bending moment. For a given level of applied bending moment, the total axial force attained by the FRP half-shell specimen SP2 is approximately 30% lower than the unretrofitted specimen SP3. The difference is approximately 15% between the FRP strip specimen SP1 and SP3. However, directly comparing the test results is problematic because of the discrepancy in timber condition. The loading was kept in the linear elastic range, and the timber piles were similar in size; therefore, these results suggest that there is a high discrepancy in the elastic modulus of the timber piles. To neutralize the results based on the timber condition, the axial force and bending moment were normalized and nondimensionalized using Euler buckling load and design bending moment capacity. The normalization loads were computed as shown below.

$$P = \alpha \frac{\pi^2 EI}{L^2} \tag{4-4}$$

$$M = \alpha F_b S \tag{4-5}$$

In Equation 4-4, E is the reference minimum elastic modulus for red oak obtained from the NDS, I is the moment of inertia of each timber pile, and L is the effective length. In Equation 4-5, F_b is the design allowable bending stress for red oak from the NDS, and S is the timber pile section modulus. In both equations, α is a condition scaling factor computed as the ratio of the dynamic elastic modulus of a specimen to a reference value. For $\alpha = 1.0$, Equation 4-4 represents the Euler buckling strength of an undeteriorated pile, and Equation 4-5 is undeteriorated bending moment capacity. In this case, it was assumed that SP3 represented the ideal timber condition and was used as the reference timber pile. The condition scaling factors and resulting normalization loads are summarized in Table 4-5.

Table 4-5. Condition Scaling Factors and Normalization Loads

Specimen	Dynamic Elastic Modulus (psi)	Scaling Factor, α	Euler Buckling Load (kips)	Scaled Euler Buckling Load (kips)	Bending Moment Capacity (kip·in)	Scaled Bending Moment Capacity (kip·in)
SP1	28.0×10^6	0.87	162.2	141.1	292.6	254.6
SP2	24.4×10^6	0.76	180.9	139.3	317.5	244.5
SP3	31.8×10^6	1.0	162.2	162.2	292.6	292.6

Both the Euler buckling strength and design bending moments are good normalization factors in this case because they are both based on elastic behavior. In effect, dividing the test results by the scaled values in Table 4-6 normalizes the results to the reference timber condition. The normalized test results are shown in Figure 4-12.

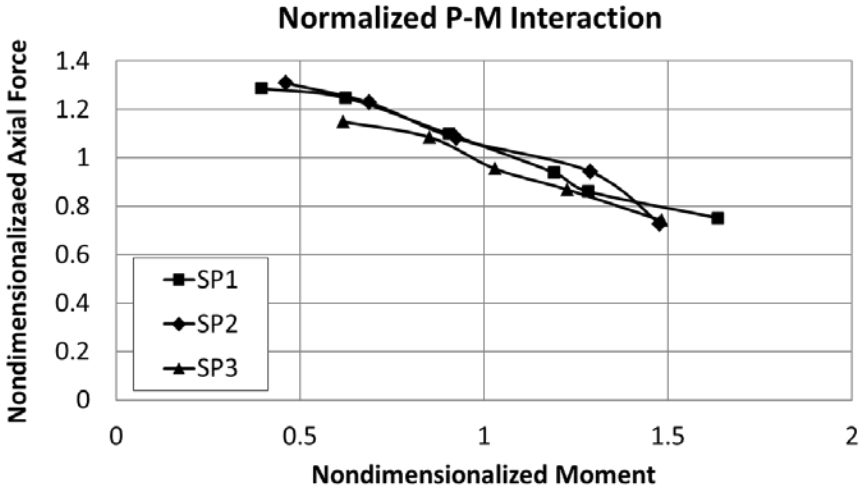

Figure 4-12. Normalized test results.

The normalized values represent the magnitude by which the FRP retrofits could improve the strength if all three timber piles were in a condition identical to SP3. Therefore, these results show that the 0.25 in. thick FRP retrofitting would increase the axial capacity of SP1 and SP2 beyond that of SP3 by an average of approximately 7%. The performance improvement provided by the FRP retrofits appear marginal, but increasing the thickness of the FRP retrofits or using materials with higher strength would improve the strength further. Overall, the normalized results suggest that at the elastic limits to which the specimens were tested, the difference in the performance of the FRP half-shell and FRP strips is not significant. The test results also clearly show that a good understanding of the timber pile condition is necessary to design an effective retrofit.

4.5 CONCLUSIONS

The effectiveness of using FRP composites to strengthen timber structures has been studied by many researchers. However, there does not exist a universal design guideline for FRP retrofits to timber. For deteriorated bridge abutment timber piles, full confinement using FRP is not possible because of the backing wall. Therefore, FRP retrofits can be applied only to the tension face of the piles. In this study, the effectiveness of the retrofitting technique was experimentally tested using three full-size timber piles, denoted SP1, SP2, and SP3. The specimens were loaded with an initial eccentric load to induce a bending moment, then an increasing concentric load was applied until the proportional limit in behavior. Unlike other conventional structural materials, one of the main difficulties in designing an effective retrofit for timber piles is obtaining an accurate assessment of the timber condition. To account for the timber condition in the design of the FRP retrofits, extensive nondestructive testing was done on the timber piles using a stress wave timing technique. That technique consisted of measuring the stress wave propagation velocity through the specimens. Using a one-dimensional simplification, the stress wave velocities were then used to compute the dynamic elastic modulus of the timber piles. The dynamic elastic modulus was used as an indicator of the timber pile condition. The observations and findings from the study are summarized below.

- Stress wave timing results showed that timber pile specimen SP3 was in good condition. Therefore, SP3 was used as the reference timber pile and tested as-is with no retrofitting.
- In comparison, the dynamic moduli of SP1 and SP2 were lower than that of SP3 by 13% and 31%, respectively. This suggests that SP2 was considerably deteriorated.
- As part of the study, FRP retrofits were designed for SP1 and SP2. The tension side of SP1 was retrofitted using GFRP strips. The tension side of SP2 was retrofitted with a GFRP half-shell. Based on tests completed in Phase I an FRP thickness of 0.25 in. was used for both cases.
- Under bending moments, the mid-height curvatures were comparable between all three specimens. On average, the curvature in specimens SP1 and SP2 was 4% and 11% higher, respectively, than SP3. This suggests that despite the additional stiffness provided by the FRP retrofit, the behavior is still strongly influenced by the timber pile condition.
- The P–M interaction curves generated for each pile showed that for a given level of applied bending moment, the axial load capacity of SP1 and SP2 was approximately 15% and 30% lower than SP3 respectively.
- The test results were normalized using the Euler buckling load and design bending moment capacity, both scaled using dynamic elastic moduli ratios to account for the timber condition. The results showed that for a given timber condition, 0.25 in. thick FRP strip and half-shell retrofits would increase the axial capacity by 7%. Increasing the thickness of the FRP would yield higher strength improvements. The normalized results suggest that the performance of the FRP strip and half-shell retrofits are comparable.
- To design effective FRP retrofits, the timber condition must be assessed accurately and integrated into the design.

CHAPTER 5: LONG-TERM PERFORMANCE TESTING OF FRP RETROFITTED TIMBER PILES

Although it has been shown by many research studies that FRP composites can be used to effectively strengthen timber structures, their use still has not been very widely adopted, especially for outdoor applications such as timber bridges. One of the main obstacles in applying FRP retrofits for timber bridges is the uncertainty regarding their long-term performance. Durability tests are difficult to conduct simply because the time required to monitor natural degradation is prohibitive. Therefore, an accelerated aging procedure was used to study how FRP retrofits could protect and strengthen timber piles against severe long-term environmental deterioration. The accelerated aging procedure simulates natural degradation conditions at elevated severities to shorten the time required to induce damage in test specimens. The effect of the accelerated aging on the compressive strength and ductility of unretrofitted and FRP-wrapped timber piles was examined.

5.1 TEST SPECIMENS

5.1.1 Timber Piles

Because this study was aimed at investigating existing timber piles that are in need of rehabilitation, it was essential to use specimens from piles that have been in service for a considerable amount of time. The specimens used in this study were cut from eight field-extracted red oak piles. The piles used in this study ranged in diameter from 8.7 in. to 12.5 in. While the exact age of the piles was not known, it was indicated that they were treated with creosote in 1993. Ports drilled for creosote injection were clearly visible and had been properly plugged. The piles were cut into specimens 24 in. in height. In total, 24 specimens were prepared. Figure 5-1 shows typical timber specimens used in this study.

Figure 5-1. Typical red oak pile specimens used in the study.

In general, the outside surfaces of the piles showed signs of moderate weathering. Splitting ranging from a few millimeters wide up to a centimeter was noted throughout the specimens, both along grain boundaries and across grains. Inspection of the specimen cross-sections revealed that although the overall level of creosote retention was high, in some specimens it had not fully penetrated to the core. Moderate to severe decay was observed in some piles, which had led to section loss. The decay

was typically limited to localized areas affecting only a few individual specimens. The moisture content of the specimens was determined through oven drying to be between 11% and 14%.

5.1.2 FRP Wrapping

FRP retrofitting in the field can be done using prefabricated composite shells or using the wet layup method (Mirmiran et al. 2008). Prefabricated shells are relatively easier to implement in the field; however, they are more difficult to bond properly to the timber. Furthermore, it is difficult to fit one shell to multiple timber piles because of variations in the timber diameter. Therefore, all specimens were prepared using the wet layup method. In this study, the same GFRP woven roving fabric described in Chapter 4 was used with three different resins to fabricate the FRP composite. Although the woven fabric consists of fibers in the longitudinal and transverse directions, the longitudinal fibers do not contribute to providing lateral confinement. The resins used were (1) polyester resin, (2) standard epoxy resin, and (3) epoxy resin formulated with a special moisture-tolerant curing agent. The two epoxy resins had comparable characteristics. In general, epoxy resins are more expensive than polyester but offer higher strength and better bond. Material properties of the constituents are listed in Table 5-1.

Table 5-1. FRP Composite Material Properties

GFRP Woven Roving	Thickness: 0.635 mm Density: 0.67 kg/m^3 Elastic Modulus: 124,000 MPa Ultimate Strain: 1%
Polyester Resin	Density: 1.1 kg/L Tensile Strength: 55 MPa Ultimate Strain: 2.1%
Standard Epoxy Resin	Density: 1.1 kg/L Tensile Strength: 67.8 MPa Ultimate Strain: 1.9%
Moisture-Tolerant Epoxy Resin	Density: 1.0 kg/L Tensile Strength: 61.4 MPa Ultimate Strain: 2.5%

Prior to applying the FRP, the surfaces of the timber piles were cleaned with wire brushes to remove any dirt and debris. The fabric was cut into sheets tailored to each specimen then wrapped around the timber and saturated with resin using rollers. Each layer was overlapped 3 in. at the ends, with each subsequent layer being offset by 90 degrees to ensure that the seams did not coincide. The saturated FRP was smoothed out to remove any air pockets. The FRP was allowed to cure for at least 48 hr before testing. The FRP wet layup process is illustrated in Figure 5-2.

(a) **(b)**

Figure 5-2. FRP wet layup process: (a) cutting the fabric; (b) resin application.

In an earlier study conducted by Caiza et al. (2012), it was determined that similar timber piles required a 0.25 in. thick (ten layers) GFRP wrap with standard epoxy resin to recover the deteriorated flexural stiffness. The study by Caiza et al. used the same type of FRP fabric as the current study, and each layer of FRP was 0.025 in. thick. In the current study, five layers and ten layers of FRP were considered to determine the effect of varying the FRP thickness. For the specimens fabricated with the moisture-tolerant epoxy resin, wet and dry surface conditions were also considered. To simulate a wet initial pile condition, the timber was submerged under water for 48 hr and drip dried for 1 hr before applying the FRP. A summary of the test specimens is provided in Table 5-2. Each specimen is identified according to a specimen number from SP1 to SP24 followed by its resin type, number of FRP layers, and accelerated aging status. Resin type designation N represents unretrofitted timber pile specimens, while P, E, and M correspond to the polyester, standard epoxy, and moisture-tolerant epoxy resins, respectively. In the moisture-tolerant epoxy resin specimens, the lowercase letter d or w following the resin type refers to dry and wet initial surface conditions, respectively. Lastly, specimens ending in U were tested as-is without being subjected to accelerated aging, while those ending in A were aged.

Table 5-2. Summary of Test Specimens

Resin Type	Specimen Designation	No. of FRP Layers
No FRP	SP1-NA SP2-NA SP3-NU SP4-NU	—
Polyester Resin	SP5-P5A SP6-P5A SP7-P5U	5
	SP8-P10A SP9-P10A SP10-P10U	10
Standard Epoxy Resin	SP11-E5A SP12-E5A SP13-E5U	5
	SP14-E10A SP15-E10A SP16-E10U	10
Moisture-Tolerant Epoxy Resin	SP17-M5dA SP18-M5wA SP19-M5dU SP20-M5wU	5
	SP21-M10dA SP22-M10wA SP23-M10dU SP24-M10wU	10
Total Number of Specimens	24	

5.2 STRESS WAVE TIMING

To better assess the condition of the timber pile samples before testing and determine how the initial condition of the timber affects the overall performance of the FRP retrofit, a nondestructive stress wave timing method was used. The same equipment described in Chapter 4 was used. In this case, measurements were taken in the longitudinal direction of the specimens parallel to the grain. The ultrasonic pulse velocity (UPV) equipment used in this study is shown in Figure 5-3(a). Measurements were taken at five equally spaced points across the cross-section in the direction parallel to the grain, as shown in Figure 5-3(b).

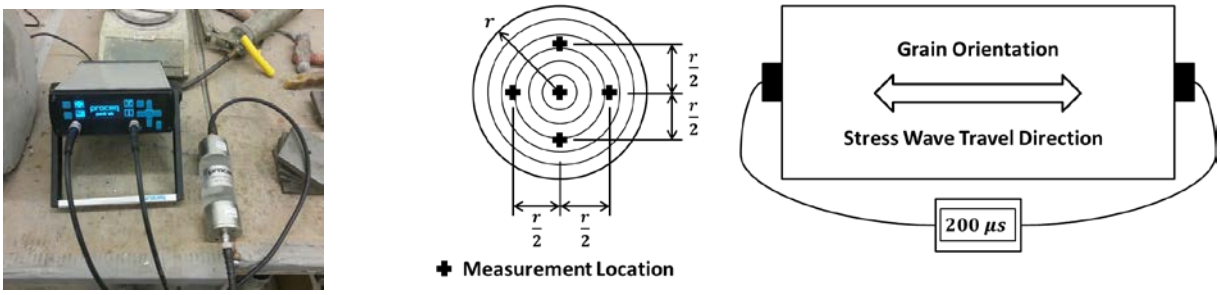

(a) (b)

Figure 5-3. Stress wave timing parallel to grain: (a) UPV instrument; (b) schematic of test setup.

The measured stress wave transmission times were compared with the reference values shown in Table 4-1. The reference stress wave transmission times for undeteriorated red oak parallel to the grain range from 54 μs/ft to 92 μs/ft, depending on the moisture content.

In total, measurements were taken on 13 specimens prior to subjecting them to accelerated aging. To evaluate the effect of accelerated aging on the stress wave transmission time, measurements were also taken after the procedure on four specimens. The average stress wave transmission times are summarized in Table 5-3.

Table 5-3. Average Stress Wave Transmission Times Through Timber Pile Specimens Parallel to Grain

	Average Transmission Time (μs/ft)	
Specimen	Before Accelerated Aging	After Accelerated Aging
SP1-NA	65.7	—
SP2-NA	64.3	—
SP5-P5A	84.8	—
SP6-P5A	69.4	—
SP11-E5A	93.1	—
SP12-E5A	73.9	—
SP17-M5dA	69.7	75.3
SP18-M5wA	66.3	71.0
SP19-M5dU	69.6	—
SP21-M10dA	67.2	74.7
SP22-M10wA	67.8	75.5
SP23-M10dU	65.0	—
SP24-M10wU	67.7	—

Overall, most specimens were in good condition relative to the reference values. However, relatively high transmission times were observed in specimens SP5-P5A and SP11-E5A. These two specimens were cut from the same timber pile. When these specimens were load tested, it was revealed that they were severely decayed. The data from these specimens were excluded as outliers. Measurements taken on specimens after accelerated aging showed that the aging increases the stress wave transmission time by as much as 11%, indicating the introduction of further deterioration in the timber. Although an accurate mathematical expression does not exist for the relationship between stress wave transmission times and the mechanical properties of wood, the initial condition assessment may provide a basis on which to determine the strength of retrofit required in future applications.

5.3 ACCELERATED AGING

One of the main challenges in this study was simulating the effects of environmental degradation. Because it was not feasible to achieve this in real-time through years of actual field exposure, an accelerated aging procedure was used to artificially induce the degradation in the lab. One such procedure was developed by Chow et al. (1986) for artificially weathering red oak railroad sleepers. As identified by Chow et al., checking or splitting caused by repeated wet–dry cycles and decay are the principal causes of wood railroad sleeper failure. Although the loading conditions are different, these are problems common to all heavy timber structures. The accelerated aging procedure involves alternating steps of soaking, steaming, oven drying, and freezing at extreme temperatures to rapidly induce swelling and shrinkage stresses, and to cause wood fiber degradation (Chow et al. 1986)). These exposure conditions were shown to be effective in reducing the hardness and modulus of elasticity perpendicular to the grain. In a detailed comparison of red oak crossties ranging from new to more than 30 years old and those subjected to the accelerated aging procedure, it was determined that six cycles of the accelerated aging are roughly equivalent to 20 years of field exposure (Chow et al. 1987). A six-cycle accelerated aging protocol similar to the one developed by Chow et al. is described in ASTM D1037-12 Standard Test Methods for Evaluating Properties of Wood-Base Fiber and Particle Panel Materials (ASTM 2012). The ASTM standard consists of similar exposure conditions but does not call for vacuum or pressurized soaking. Because it is difficult to create vacuum or pressurized conditions for large timber specimens, the ASTM procedure was used in this study. The accelerated aging procedure adopted in this study is described in Table 5-4.

Table 5-4. ASTM D1037 Accelerated Aging Procedure Adopted in This Study

Condition	Duration	Purpose
Soaking (120 ± 3°F)	1 hr	Causes swelling
Steaming (200 ± 5°F)	3 hr	Degradation of wood fibers
Freezing (10 ± 5°F)	20 hr	Simulates winter conditions
Oven Drying (210 ± 3°F)	3 hr	Causes shrinkage and splitting
Steaming (200 ± 5°F)	3 hr	Degradation of wood fibers
Oven Drying (210 ± 3°F)	18 hr	Causes shrinkage and splitting

The setup for the accelerated aging procedure consisted of a large tank fitted with a temperature-controlled water heater, a steam box fitted with a steam generator, a chest freezer, and a conventional aggregate oven, as shown in Figure 5-4.

(a) (b) (c) (d)

Figure 5-4. Test setup for the ASTM D1037 accelerated aging procedure adopted in this study: (a) heated water tank; (b) steam box with steam generator; (c) chest freezer; (d) aggregate drying oven.

To prevent any moisture ingress through the ends of the pile specimens during the accelerated aging procedure and to ensure level surfaces for load testing, a thin layer (< 0.25 in.) of quick-setting mortar was applied to both ends. The mortar had a specified compressive strength of 4 ksi after 24 hr. The mortar layer was not intended to be load carrying.

Visual inspection of the FRP-strengthened specimens after accelerated aging revealed no significant damage to the FRP composite itself except for some discoloration caused by the seepage of creosote. In the as-is timber pile specimens, splitting was more prevalent, but there were no other visual signs of major deterioration. However, as shown in Table 5-3, the accelerated aging procedure led to increased stress wave transmission times in specimens SP17-M5dA, SP18-M5wA, SP21-M10dA, and SP22-M10wA. This is an indication of the additional damage induced in the timber piles by the accelerated aging.

5.4 TEST RESULTS

Each specimen was tested in uniaxial compression using a 600 kip MTS servo-controlled machine. The testing frame was instrumented with an internal load cell and a linear variable differential transducer (LVDT). An additional 10 in. gauge extensometer was attached to the side of the specimen. The load was applied at a constant cross-head rate of 0.05 in. per minute. In total, 20 FRP-wrapped specimens were tested. However, when tested under load, it was revealed that four specimens: SP5-P5A, SP8-P10A, SP11-E5A, and SP20-M5wU were severely decayed at the core which could not have been caused by the accelerated aging procedure. These specimens are not included in the discussions because they failed prematurely.

5.4.1 As-Is Timber Piles

Unretrofitted timber pile specimens SP3-NU and SP4-NU were tested as-is to examine their behavior. The failure of the wood occurred in two stages: (1) splitting of the grains, and (2) crushing and buckling of the wood fibers. These failure patterns are illustrated in Figure 5-5.

Figure 5-5. Failure of unretrofitted timber specimens.

Externally, both specimens were in relatively good condition prior to the testing, without extensive checking or splitting. An inspection of the failed specimens revealed no signs of internal decay. The average peak stress of specimens SP3-NU and SP4-NU was 2.13 ksi, and the average elastic modulus was 220 ksi. The average peak stress of the two specimens was almost two times higher than the reference allowable compressive stress (Table 3-5). However, the average elastic modulus was about 65% lower than the reference elastic modulus, E_{min}. The stress–strain relationships observed in the unretrofitted timber specimens are shown in Figure 5-6.

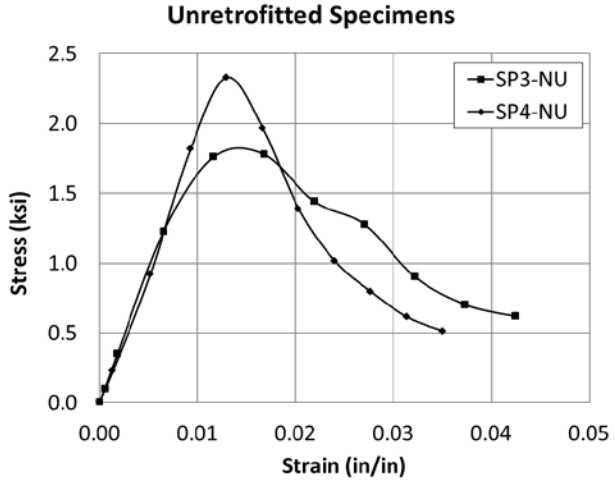

Figure 5-6. Stress–strain behavior of unretrofitted as-is timber piles.

5.4.2 FRP Retrofitted Piles Without Accelerated Aging

In many cases during the testing of FRP-strengthened timber piles, small localized ruptures developed in the FRP composite at various points in the test that led to sudden but minor drops in the stress. Because FRP composites are brittle, complete rupture of the FRP occurred very suddenly. However, it was noted that even when the FRP failed, the timber inside was still relatively sound. Therefore, the specimens were loaded until the timber pile itself failed. A typical test progression up to failure is illustrated in Figure 5-7 for specimen SP19-M5dU.

(a) **(b)** **(c)** **(d)**

Figure 5-7. Typical FRP-strengthened specimen damage progression: (a) beginning of loading; (b) initial longitudinal rupture of the FRP; (c) rupture propagation; (d) complete rupture of the FRP and crushing of the timber pile.

Test results of two unretrofitted specimens and seven FRP-wrapped specimens, all without accelerated aging, are plotted in Figure 5-8. As illustrated in Figure 5-8, compared with the as-is timber piles, the FRP-strengthened specimens performed considerably better. Both the strength and ductility were significantly improved.

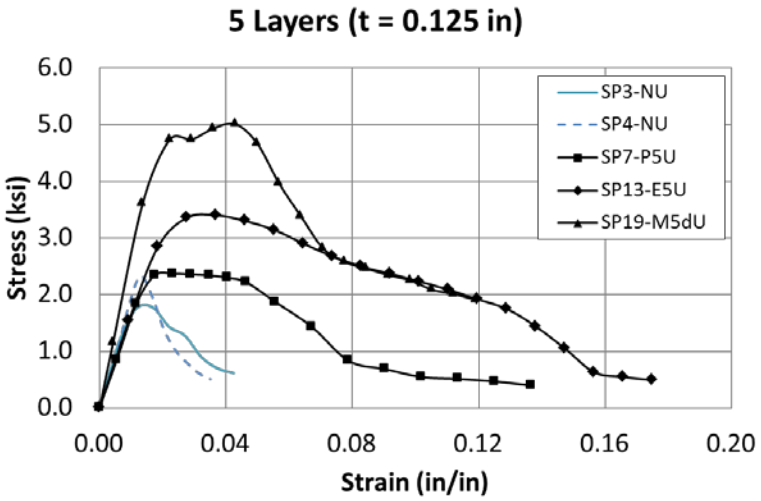

Specimen	Ductility Ratio
SP3-NU	1.5
SP4-NU	1.4
SP7-P5U	2.9
SP13-E5U	2.4
SP19-M5dU	2.8

(a)

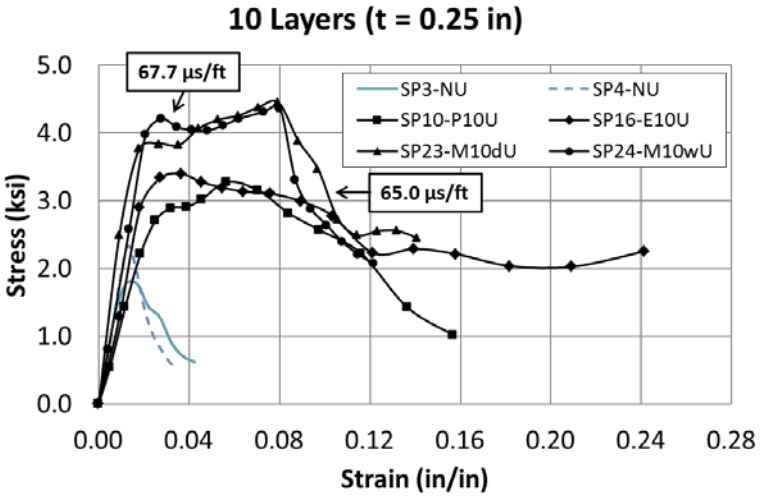

Specimen	Ductility Ratio
SP3-NU	1.5
SP4-NU	1.4
SP10-P10U	3.6
SP16-E10U	3.7
SP23-M10dU	4.5
SP24-M10wU	4.5

(b)

Figure 5-8. Performance of FRP-strengthened timber piles not subjected to accelerated aging: (a) five layers; (b) ten layers.

Ductility in this study was assessed based on the ductility ratio, which is defined as the ratio between the ultimate strain and the strain at onset of nonlinear behavior. Ultimate strain is defined in this study as the strain at the post-peak stress stage corresponding to a 20% drop from the peak stress. The five- and ten-layer FRP specimens had average peak stresses of 3.63 ksi and 3.87 ksi, respectively. On average, this represents an increase of 70% and 82% respectively for the five- and ten layer FRP specimens compared with the unretrofitted specimens. As illustrated in the figure, increasing the thickness of the FRP did not yield a proportional increase in the peak stress, but the ten-layer FRP specimens were considerably more ductile than the five-layer specimens. The average ductility ratios of the five- and ten-layer specimens were 2.7 and 4.0, respectively. Compared with the average ductility of 1.4 observed in the as-is specimens, the ductility was improved by more than 90%. Compared with the increase in peak stress, the FRP strengthening did not lead to drastic changes in the modulus of elasticity. The average elastic moduli in the five- and ten-layer specimens were 236 ksi and 222 ksi, respectively. As mentioned above, this can be attributed to the fact that the primary function of the FRP composite under the axial load was to provide confinement in the radial direction. Although the glass fabric used was bi-directional, the fibers in the longitudinal direction were not directly bearing and consequently did not provide any additional stiffness.

For specimens SP23-M10dU and SP24-M10wU, the average stress wave transmission times through the timber pile are noted in Figure 5-8(b) as 65.0 µs/ft and 67.7 µs/ft, respectively. These values are comparable to the reference values presented in Wang et al. (2004) and indicate that both timber piles were in good condition. Because both piles were in similar initial condition and retrofitted with the same amount of FRP, it is clear that the surface condition of the timber prior to applying the FRP did not have a significant effect on the performance of the moisture-tolerant epoxy resin.

5.4.3 Effect of Accelerated Aging

Although the internal effects of the accelerated aging on the unretrofitted timber piles could not be directly observed, the aging procedure caused extensive splitting. Test results for unretrofitted specimens with and without accelerated aging are compared in Figure 5-9. From these results, it is clear that the accelerated aging leads to reductions in the strength.

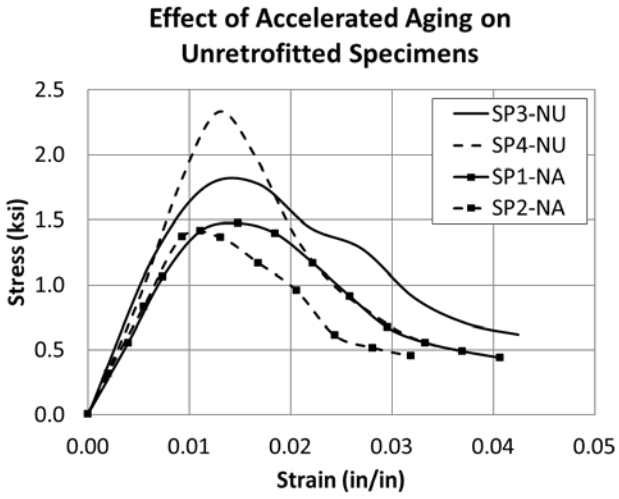

Figure 5-9. Unretrofitted timber piles, as-is and after accelerated aging.

Compared with the specimens that did not go through accelerated aging, the aging procedure led to an average reduction of 31% in peak stress and 17% in the elastic modulus for the as-is specimens. Stress wave timing indicated that both specimens SP1-NA and SP2-NA shown in Figure 5-9 were initially in very good condition before the accelerated aging procedure.

As discussed previously, the accelerated aging procedure did not visibly damage the FRP composites. However, an increase in the stress wave transmission time suggests that additional degradation was induced in the timber piles (Table 5-3). The test results for the FRP-retrofitted timber piles subjected to accelerated aging are shown in Figure 5-10. It could be noted that with the exception of the five-layer polyester resin specimens, the accelerated aging led to a loss in peak stress between 10% and 34% in the FRP-retrofitted specimens compared with the unaged specimens.

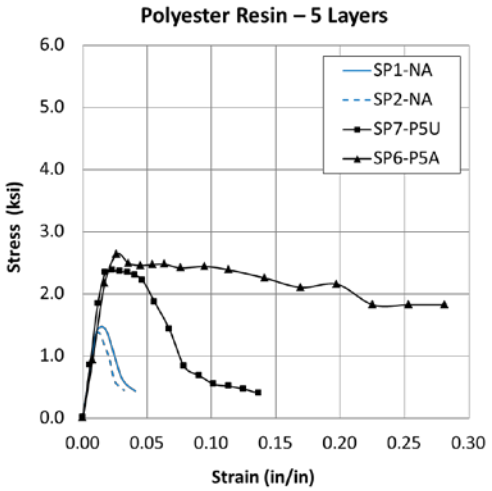

(a)

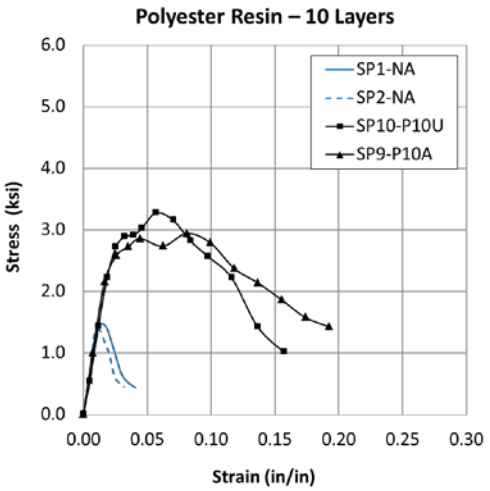

(b)

Specimen	Ductility Ratio
SP1-NA	1.5
SP2-NA	1.4
SP3-NU	1.5
SP4-NU	1.4
SP6-P5A	5.9
SP7-P5U	2.9
SP9-P10A	4.4
SP10-P10U	2.6

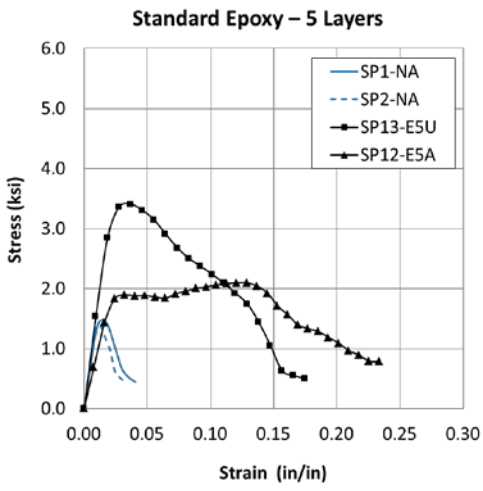

(c)

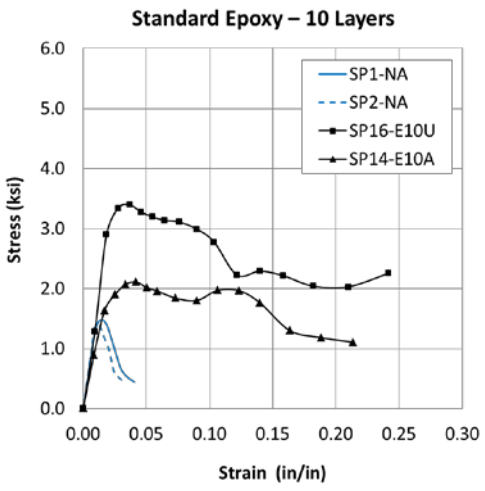

(d)

Specimen	Ductility Ratio
SP1-NA	1.5
SP2-NA	1.4
SP3-NU	1.5
SP4-NU	1.4
SP12-E5A	6.0
SP13-E5U	2.4
SP14-E10A	5.6
SP16-E10U	3.7

Figure 5-10. Stress–strain behavior of unretrofitted and FRP-strengthened timber piles subjected to accelerated aging: (a) five-layer polyester resin; (b) ten-layer polyester resin; (c) five-layer standard epoxy resin; (d) ten-layer standard epoxy resin.
[FIGURE CONTINUES, NEXT PAGE]

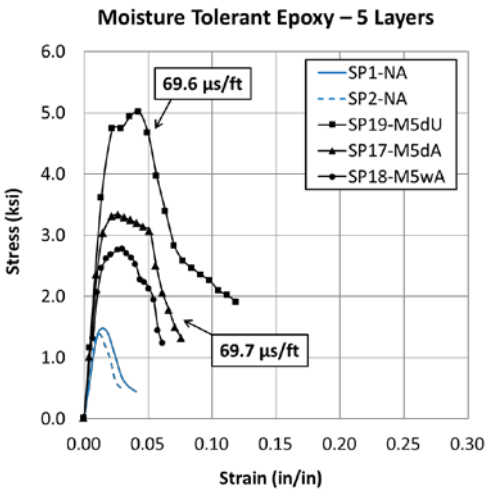

(e)

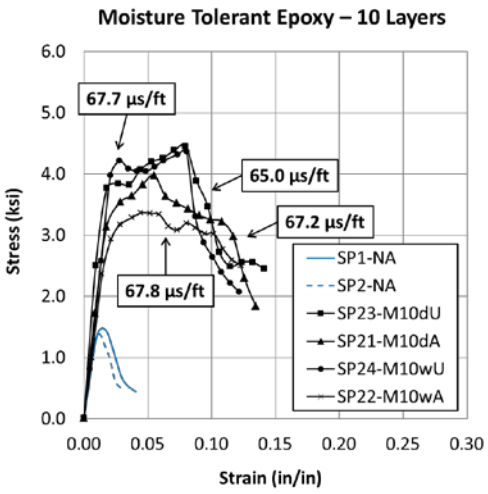

(f)

Specimen	Ductility Ratio
SP1-NA	1.5
SP2-NA	1.4
SP3-NU	1.5
SP4-NU	1.4
SP17-M5dA	2.8
SP18-M5wA	2.4
SP19-M5dU	2.8
SP21-M10dA	3.8
SP23-M10dU	4.5
SP22-M10wA	4.4
SP24-M10wU	4.5

Figure 5-10 [continued]. Stress–strain behavior of unretrofitted and FRP-strengthened timber piles subjected to accelerated aging: (e) five-layer moisture-tolerant epoxy; (f) ten-layer moisture-tolerant epoxy.

Comparing the plots for each resin type in Figure 5-10, it can be seen that in general, higher levels of ductility were obtained from FRP composites fabricated with polyester and standard epoxy resin than with the moisture-tolerant epoxy. However, the moisture-tolerant epoxy specimens attained higher peak stresses both before and after accelerated aging. Overall, with the exception of the standard epoxy specimens, increasing the FRP thickness led to improved strength retention after accelerated aging. The average strength loss related to aging in the five-layer specimens was 35% compared with 15% in the ten-layer specimens. Therefore, applying a thicker FRP retrofit in the field may be beneficial for long-term environmental degradation. The accelerated aging did not affect the ductility of the FRP-retrofitted specimens.

In Figure 5-10(a), it can be seen that specimen SP7-P5U failed at much lower strains compared with the other retrofitted specimens. The FRP in specimen SP7-P5U ruptured at lower strain levels and failed to properly confine the timber pile. In the ten-layer specimens, although the accelerated aging caused a drop in the peak stress, the ductility ratio and stiffness were unaffected. It can also be seen that the ten-layer specimen SP9-P10A retained a 10% higher peak stress compared with the five-layer specimen SP6-P5A when subjected to accelerated aging.

Compared with the polyester or moisture-tolerant epoxy FRP, the relatively poor performance of the standard epoxy resin specimens subjected to accelerated aging could be attributable to the poor initial condition of the timber. Specimen SP12-E5A shown in Figure 5-10(c) had an initial stress wave transmission time of 73.9 µs/ft. In comparison, the initial stress wave transmission times for the two unretrofitted specimens SP1-NA and SP2-NA subjected to accelerated aging shown in Figure 5-10 were 65.7 µs/ft and 64.3 µs/ft, respectively. This suggests that specimen SP12-E5A was more severely deteriorated prior to testing. However, SP12-E5A achieved a 37% higher peak stress and showed a significant improvement in the ductility compared with the unretrofitted specimens.

It can be seen in Figure 5-10(e) that specimens SP19-M5dU and SP17-M5dA had almost identical stress wave transmission times, indicating that they were in similar initial condition. Similarly, in Figure 5-10(f), the initial condition of specimens SP22-M10wA and SP24-M10wU was comparable. However, after the accelerated aging procedure, the peak stresses of SP17-M5dA and SP22-M10wA were lower than their unaged counterparts by 34% and 23%, respectively.

Despite the reductions in peak stress observed after accelerated aging, the FRP-wrapped timber piles still performed significantly better under accelerated aging than the unretrofitted timber piles. This shows that the FRP retrofit can effectively improve the structural properties of severely damaged timber piles and that this efficacy is expected to be maintained despite the harsh environmental and service conditions of the piles.

5.5 CONCLUSIONS

The effectiveness of FRP strengthening of timber piles after long-term degradation was investigated by testing field-extracted red oak timber piles wrapped with GFRP composites. FRP thickness, resin type, and timber pile initial condition were the three main parameters examined in this study. An accelerated aging technique was used to induce artificial deterioration equivalent to approximately 20 years of field exposure. Twenty timber pile specimens were wrapped with five or ten 0.025 in. thick layers of GFRP composite fabricated with polyester, standard epoxy, or a moisture-tolerant resin. Prior to testing, the initial condition of the timber piles was evaluated using a nondestructive stress wave timing technique. Including the four unretrofitted specimens, a total of 24 specimens were tested in uniaxial compression in the direction parallel to the grain. The following conclusions could be drawn from the study:

- The accelerated aging procedure was shown to cause substantial degradation in timber piles. The accelerated aging did not visibly damage the FRP composites.
- Without accelerated aging, using five and ten layers of FRP improved the peak strength of the timber piles by 70% and 82%, respectively, compared with the unretrofitted specimens.
- In general, increasing the thickness of the FRP did not result in a proportional increase in the strength but it did have a direct impact on the ductility. Because the primary function of the FRP composite was to provide confinement, the retrofit did not affect the stiffness.
- The ductility ratios for each resin type were comparable. The surface condition did not have a major influence on the bonding of the moisture-tolerant epoxy resin.
- On average, strength loss after accelerated aging was 35% in the five-layer specimens and 15% in the ten-layer specimens. Despite the reductions in peak stress, the FRP-wrapped timber piles still performed significantly better than the unretrofitted timber piles after accelerated aging. Therefore, applying a thicker FRP retrofit in the field may be beneficial for mitigating long-term environmental degradation.
- The average ductility ratios of the five- and ten-layer specimens were 2.7 and 4.0, respectively. Compared with the as-is specimens, the ductility is improved by more than 90%. The accelerated aging did not affect the ductility of the FRP-retrofitted specimens.

- The moisture-tolerant epoxy resin attained higher strength than the polyester or standard epoxy resin. The peak strength of the moisture-tolerant resin specimens was higher than the other FPR retrofitted specimens by at least 30%, and 5% without and with accelerated aging, respectively.

CHAPTER 6: SUMMARY AND CONCLUSIONS

The current phase (Phase II) of the project, Strengthening of Bridge Wood Piling Retrofits for Moment Resistance, focused on load rating and FRP retrofitting abutment timber piles and the long-term performance of FRP-wrapped timber piles. The findings and observations from the study are summarized below.

Three timber pile retrofitting schemes using steel sections were evaluated; the results were discussed in Chapter 2.

- Retrofit Scheme 1 was slightly stiffer than the other two retrofit options. The maximum deflection did not exceed 0.5 in. The failure was caused by the buckling of the H-pile flanges at the cap plate. Retrofit Scheme 1 sustained an ultimate load of 190.6 kips. The stresses in the connections and the reinforced concrete splice were minimal.
- Retrofit Scheme 2 achieved the highest ultimate load at 196.2 kips. Similar to Retrofit Scheme 1, failure was caused by the buckling of the H-pile flanges at the bearing points. There were stress concentrations at geometric discontinuities in the welds around the H-pile, but the levels were not critical.
- The highest deflections were noted in Retrofit Scheme 3. The maximum lateral deflection of 0.9 in. occurred at the interface. The deflection was primarily caused by the flexibility of the cap plate. Retrofit Scheme 3 failed at a maximum load of 175.4 kips because of the yielding of the HSS assembly under compression.

In Chapter 3, a P–M interaction-based load rating method was proposed for abutment timber piles. A method for accounting for FRP retrofits was also discussed. A detailed FE model of a typical timber pile bridge was used to demonstrate the load rating and the effectiveness of FRP retrofitting.

- The new load rating method gives more conservative results compared with the conventional load rating method.
- Section deterioration Profiles I and II, representing external section loss, led to more critical load ratings than Profile III, which modeled internal damage. For all three deterioration profiles, 10% deterioration was enough to cause the critical load rating to drop to inadequate levels under at-rest soil conditions.
- A 0.25 in. thick GFRP half-shell retrofit was considered for deterioration Profile I. The modified bending stress for the deteriorated sections was greater than the reference design bending stress in the NDS by more than 18%. This increased the critical load rating by at least 17%.

In Chapter 4, experimental testing results of FRP-retrofitted abutment timber piles were discussed. Extensive stress wave timing measurements were taken to assess the initial condition of the timber.

- Stress wave timing results showed that timber pile specimen SP3 was in good condition. Therefore, SP3 was used as the reference timber pile and tested as-is with no retrofitting.
- In comparison, the dynamic moduli of SP1 and SP2 computed using longitudinal stress wave propagation velocities were lower than that of SP3 by 12% and 23%, respectively. This suggests that SP2 was considerably deteriorated.
- Based on the FRP retrofit designs adopted in Phase I, a constant FRP thickness of 0.25 inches was used to retrofit the tension side of SP1 with GFRP strips. SP2 with a GFRP half-shell.
- The P–M interaction curves were normalized to the reference condition of SP3. The results showed that for timber condition consistent with that observed in SP3, the FRP strip retrofit and FRP half-shell retrofit would increase the axial capacity of the pile by approximately 7%. Higher FRP thicknesses are needed to provide further improvements.

The long-term performance of FRP-wrapped timber piles was investigated by subjecting test specimens to an accelerated aging procedure and examining its effect on the compressive strength of retrofitted and unretrofitted timber piles. The results were discussed in Chapter 5 are summarized as follows:

- The accelerated aging procedure was shown to cause substantial degradation in timber piles but did not visibly damage the FRP composites.
- Without accelerated aging, using five and ten layers of FRP improved the peak strength of the timber piles by 70% and 82%, respectively, compared with the unretrofitted specimens.
- On average, strength loss after accelerated aging was 35% in the five-layer specimens and 15% in the ten-layer specimens. Despite the reductions in peak stress, the FRP-wrapped timber piles still performed significantly better than the unretrofitted timber piles after accelerated aging.
- Compared with the unretrofitted specimens, FRP wrapping improved the ductility by more than 90%. The accelerated aging did not affect the ductility of the FRP-retrofitted specimens.

REFERENCES

American Association of State Highway and Transportation Officials (AASHTO). (2002). Standard specifications for Highway Bridges. Washington, DC.

American Association of State Highway and Transportation Officials (AASHTO). (2010). LRFD bridge design specifications. Washington, DC.

American Forest and Paper Association (AFPA). (2005). National Design Specification (NDS) for Wood Construction, Washington DC.

American Wood Preservers Institute (AWPI), Timber Piling Council (2002). Timber Pile Design and Construction Manual. AWPI. Vancouver, WA.

Andrawes, B., and Caiza, P. (2011). Bridge Timber Piles Load Rating under Eccentric Loading Conditions. Journal of Bridge Engineering, 17(4), 700-710.

Armstrong, J.P.; Patterson, D.W., and Sneckenberger, J.E. (1991). Comparison of three equations for predicting stress wave velocity as a function of grain angle. Wood and Fiber Science. 23(1): 32.43.

ASTM Standard D1037 (2012). Standard Test Methods for Evaluating Properties of Wood-Base Fiber and Particle Panel Materials. ASTM International, West Conshohocken, PA, DOI: 10.1520/D1037-12, www.astm.org.

Borello, D. J., Andrawes, B., Hajjar, J. F., Olson, S. M., and Hansen, J. (2010). Experimental and analytical investigation of bridge timber piles under eccentric loads. Engineering Structures, 32(8), 2237-2246.

Borello, D. J., Andrawes, B., Hajjar, J., Olson, S. M., Hansen, J., and Buenker, J. (2009). Forensic collapse investigation of a concrete bridge with timber piers. Illinois Center for Transportation (ICT).

Broms, B. B. (1964). Lateral resistance of piles in cohesionless soils. Journal of the Soil Mechanics and Foundations Division, 90(3), 123-158.

Buchanan, A. H. (1984). Strength model and design methods for bending and axial load interaction in timber members. Doctoral dissertation. University of British Columbia. Vancouver, British Columbia, Canada.

Caiza, P., Shin, M., and Andrawes, B. (2012). Load Rating and Retrofit Testing of Bridge Timber Piles Subjected to Eccentric Loading. FHWA-ICT-12-014.

Chow, P., Lewis, S. L., Reinschmidt, A. J., and Barenberg, E. J. (1987). Effects of Natural and Accelerated Aging on Oak Crossties. American Wood-Preservers' Association Proceedings

Chow, P., Reinschmidt, A.J., Barenberg, E. J., and Lewis, S.L. (1986) Laboratory Tests on Artificial Weathering of *Quercus* rubra Crossties. Int. Res. Gr. On Wood Pres. Doc. IRG/WP/2252. Sweden. 7 p.

Dassault Systèmes Simulia Corp. (2011). ABAQUS 6.11. Vélizy-Villacoublay Cedex, France

Divos, F., and Szalai, L. (2002). Tree evaluation by acoustic tomography. In Proceedings of the 13th international symposium on nondestructive testing of wood (pp. 251-256). Forest Products Research Society, Madison, WI.

Emerson, R. N. (1999). Nondestructive evaluation of timber bridges. Doctoral Dissertation. Washington State University. Pullman, WA.

Hagos, M. W. (2001). Repair of heavily decayed timber piles using glass fiber-reinforced polymers (GFRP) and cementitious grout. M.S. Thesis, University of Manitoba, Winnipeg, Manitoba, Canada.

Jung, J. (1979). Stress wave grading techniques on veneer sheets. Gen. Tech. Rep. FPL.GTR.27. Madison, WI: U.S. Department of Agriculture, Forest Service, Forest Products Laboratory.

Kim, Y. R., Ranjithan, S. R., Donato, P. J., and Murphy, C. M. (2000). Nondestructive evaluation of the structural condition of timber piles. Final Report, North Carolina Department of Transportation, FHWA/NC/2000-004.

Klaiber, F. W., White, D. J., Wipf, T. J., Phares, B. M., and Robbins, V. W. (2004). Development of Abutment Design Standards for Local Bridge Designs–Vol. 1: Development of Design Methodology. Iowa Department of Transportation Project TR–486.

Lopez-Anido, R., Michael, A. P., and Sandford, T. C. (2003). Experimental characterization of FRP composite-wood pile structural response by bending tests. Marine Structures, 16(4), 257-274

Mertz, D. (2012). Steel Bridge Design Handbook: Load Rating of Steel Bridges. Federal Highway Administration (FHWA) Report No. FHWA-IF-12-052 - Vol. 18. FHWA, Washington, DC.

Mirmiran, A., Shahawy, M., Nanni, A., Karbhari, V. M., Yalim, B., and Kalayci, A. S. (2008). Recommended construction specifications and process control manual for repair and retrofit of concrete structures using bonded FRP composites (No. Project 10-59B).

Ross, R. J., and Pellerin, R. F. (1994). Nondestructive testing for assessing wood members in structures. General Technical Report FPL-GTR-70, Forest Products Laboratory, US Department of Agriculture.

Ross, R. J., Degroot, R. C., Nelson, W. J., and Lebow, P. K. (1997). The relationship between stress wave transmission characteristics and the compressive strength of biologically degraded wood. Forest products journal, 47(5), 89-93.

Ross, R. J., White, R. H., Pellerin, R. F., Wang, X., and Brashaw, B. K. (2004). Wood and timber condition assessment manual. Forest Products Laboratory (FPL). Madison, WI.

Smulski, S.J. (1991). Relationship of stress wave and static bending determined properties of four northeastern hardwoods. Wood and Fiber Science. 23(1): 44.57.

Steiger, R., and Fontana, M. (2005). Bending moment and axial force interacting on solid timber beams. Materials and structures, 38(5), 507-513.

Wang, X., Divos, F., Pilon, C., Brashaw, B. K., Ross, R. J., and Pellerin, R. F. (2004). Assessment of decay in standing timber using stress wave timing nondestructive evaluation tools: A guide for use and interpretation. Forest Products Library (FPL). Madison, WI.

Wipf, T. J., Klaiber, F. W., White, D. J., and Koskie, J. (2007). Investigation of Steel-Stringer Bridges: Superstructures and Substructures, Volume II (No. IHRB Project TR-522).

APPENDIX A: TIMBER PILE POSTING ALTERNATIVES

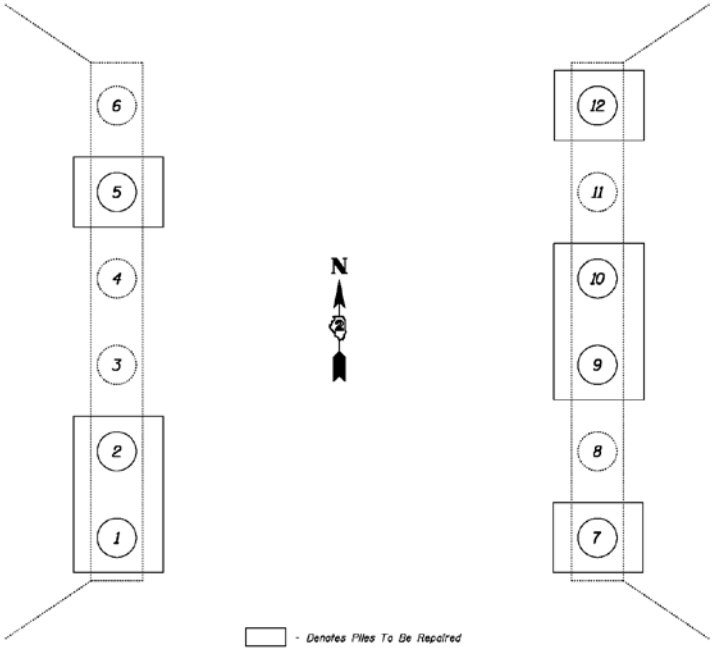

GENERAL NOTES

Plan dimensions and details relative to existing plans are subject to nominal construction variations. The Contractor shall field verify existing dimensions and details affecting new construction and make necessary approved adjustments prior to construction or ordering of materials. Such variations shall not be cause for additional compensation for a change in scope of the work, however, the Contractor will be paid for the quantity actually furnished at the unit price bid for the work.

All structural steel used for timber pile repairs shall be unpainted.

All traffic shall be removed from the structure during repair.

The Contractor shall provide support and/or shoring systems for the cap and superstructure in the area of timber pile repair.

Existing backing planks shall be notched as required for plate installation.

All hardware shall be hot-dipped galvanized and have a minimum bending yeild strength Fyb of 45,000 psi.

Asbuilt plans must be provided to the Bureau of Bridges and Structures upon completion of the project, indicating which Alternate Method was used.

TIMBER PILE REPAIR CONSTRUCTION METHOD

1. Provide temporary support for the superstructure before starting repairs.
2. Only one pile shall be repaired at a time to ensure stability of the substructure unit. The Contractors Sequence of Construction shall be approved by the Engineer prior to the start of construction.
3. Cut off timber pile level, through a non-deteriorated cross section, to allow full bearing contact with the bottom base plate of the steel pile assembly (Alternate 1) or Pile Stub Assembly (Alternate 2 & 3). Remove section of timber pile. Top of remaining timber pile shall be coated with Copper Naphthenate meeting the material requirements of AWPA Standard M4-06.
4. Top of deteriorated timber pile section shall be removed or cut flush with the bottom of the existing pile bent cap.
5. Install Bottom Base Plate (Alternate 1) or Pile Stub Assembly (Alternate 2 & 3). Bottom base plate shall bear on pile in a level position. Field measure the length required for the steel pile assembly (Alternate 1 & 2) or Steel Sleeve Assembly (Alternate 3), allowing for the ½" bottom base plate.
6. Cut steel pile assembly (Alternate 1 & 2) or Steel Sleeve Assembly (Alternate 3) to required length and grind ends to be field welded. ½" cap plate should be shop welded to the steel pile.
7. Place steel pile assembly (Alternate 1 & 2) or Steel Sleeve Assembly (Alternate 3) in the removed pile location. Position the steel pile on bottom base plate. Field weld the steel pile to bottom base plate at locations shown.
8. Connect cap plate to the existing pile bent cap. Use shop fabricated cap plates as a template for drilling holes into the existing pile bent cap. Provide shims for tight fit if necessary. Install ¾" wedge anchors or lag screws as required.
9. Repeat procedures for all remaining piles to be repaired

DESIGN SPECIFICATIONS

2002 AASHTO

DESIGN STRESSES

FIELD UNITS (NEW CONSTRUCTION)

f'c = 3,500 psi (Concrete Pile Encasement)
fy = 60,000 psi (Reinforcement)
fy = 36,000 psi (Structural Steel)
unless otherwise noted

LOADING HS15-44 - NEW CONSTR.

TIMBER PILE REPAIRS
MEYERS BRIDGE
SHATTUCK RD. OVER MOSQUITO CREEK
BOONE COUNTY
STRUCTURE NO. 004-3048

Expires: November 30, 2014

DESIGNED JSB	EXAMINED	DATE -	STATE OF ILLINOIS DEPARTMENT OF TRANSPORTATION		F.A. RTE.	SECTION	COUNTY	TOTAL SHEETS	SHEET NO.
CHECKED JAE	ENGINEER OF STRUCTURAL SERVICES								
DRAWN JSB	PASSED						CONTRACT NO.		
CHECKED SBC	ENGINEER OF BRIDGES AND STRUCTURES			SHEET NO. 1 OF 4 SHEETS			ILLINOIS FED. AID PROJECT		

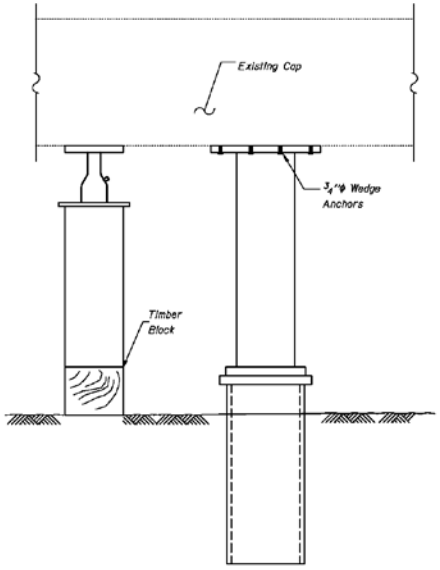

TEMPORARY SUPPORT

Temporary support must be less than half the spacing to the adjacent pile but not to exceed 3'-0".

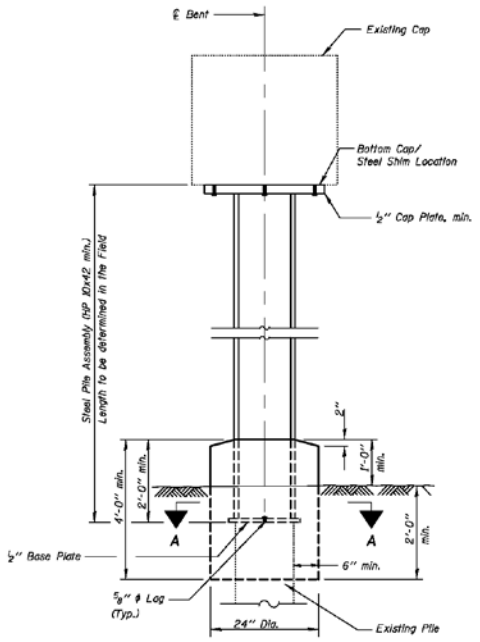

SIDE VIEW

REPAIR ALTERNATE 1

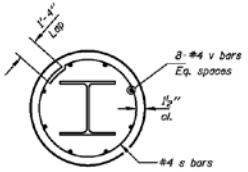

SECTION A-A

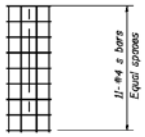

REINFORCEMENT

Note: See Sheet 4 of 4 for additional details.

DESIGNED JSB CHECKED JAE DRAWN JSB CHECKED SBC	EXAMINED _____ DATE - ENGINEER OF STRUCTURAL SERVICES PASSED _____ ENGINEER OF BRIDGES AND STRUCTURES	STATE OF ILLINOIS DEPARTMENT OF TRANSPORTATION	PILE REPAIR DETAILS EXISTING STRUCTURE NO. 004-3048 SHEET NO. 2 OF 4 SHEETS	F.A. RTE.	SECTION	COUNTY	TOTAL SHEETS / SHEET NO.
						CONTRACT NO.	
						ILLINOIS FED. AID PROJECT	

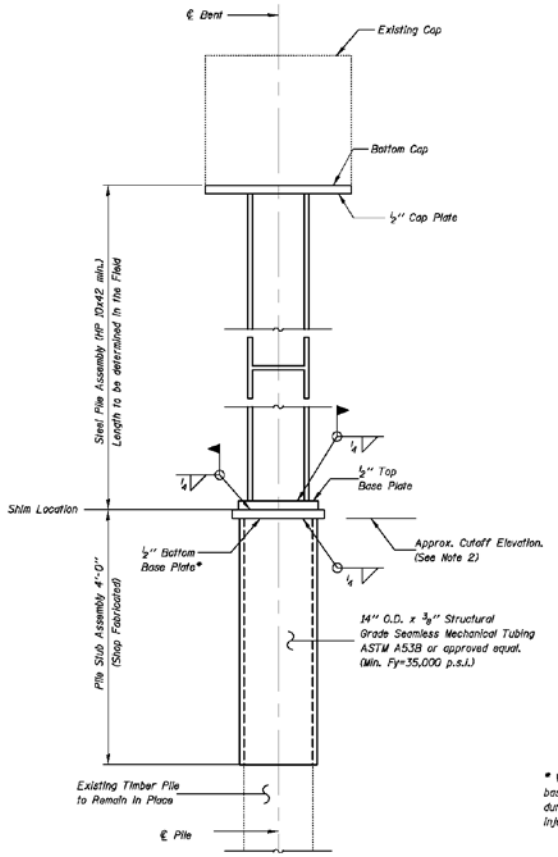

SIDE VIEW

REPAIR ALTERNATE 2

* Vent holes should be provided in bottom base plate to allow air and water to escape during installation. Holes may also be used to inject epoxy if required for stability.

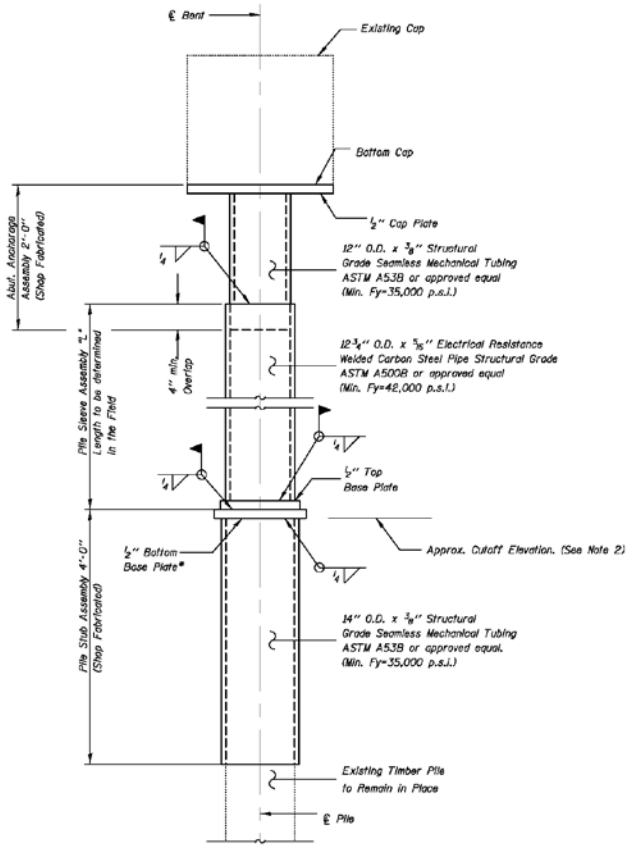

SIDE VIEW

REPAIR ALTERNATE 3

Note: See Sheet 4 of 4 for additional details.

DESIGNED JSB CHECKED JAE DRAWN JSB CHECKED SBC	EXAMINED _____ DATE - ENGINEER OF STRUCTURAL SERVICES PASSED _____ ENGINEER OF BRIDGES AND STRUCTURES	STATE OF ILLINOIS DEPARTMENT OF TRANSPORTATION	PILE REPAIR DETAILS EXISTING STRUCTURE NO. 004-3048 SHEET NO. 3 OF 4 SHEETS	F.A. RTE.	SECTION	COUNTY CONTRACT NO. ILLINOIS FED. AID PROJECT	TOTAL SHEETS / SHEET NO.

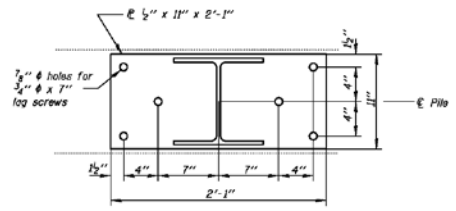

CAP PLATE DETAIL

(For Timber Abutment/Pier Cap)

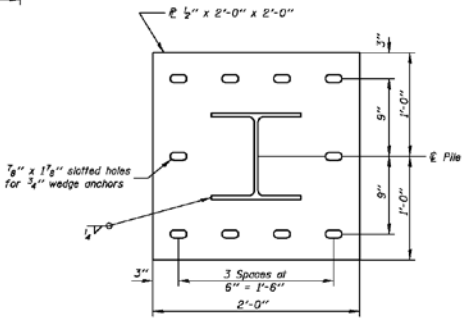

CAP PLATE DETAIL

H-Pile shown; Structural Tubing similar

(For Concrete Abutment/Pier Cap)

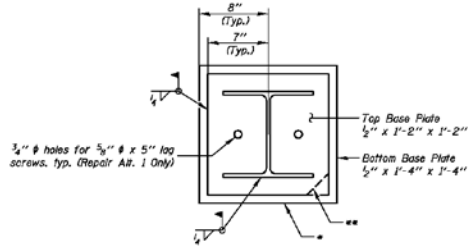

BASE AND SHIM PLATE

H-Pile shown; Structural Tubing similar

* Bottom Base Plate is not required for Repair Alternate 1.

** Plate corners may be clipped for Repair Alternate 1 to provide clearance within concrete encasement.

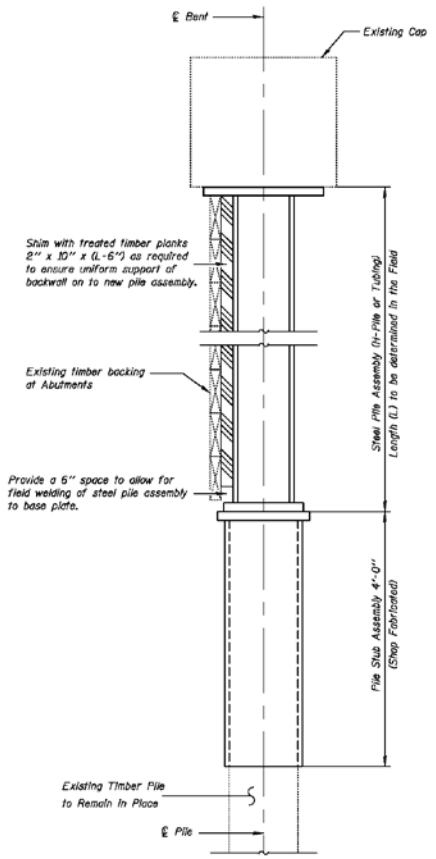

SECTION AT ABUTMENT

Repair Alternate 2 shown; Others similar.

DESIGNED JSB CHECKED JAE DRAWN JSB CHECKED SBC	EXAMINED _____ DATE _____ ENGINEER OF STRUCTURAL SERVICES PASSED _____ ENGINEER OF BRIDGES AND STRUCTURES	STATE OF ILLINOIS DEPARTMENT OF TRANSPORTATION	PILE REPAIR DETAILS EXISTING STRUCTURE NO. 004-3048 SHEET NO. 4 OF 4 SHEETS	F.A. RTE.	SECTION	COUNTY CONTRACT NO. ILLINOIS FED. AID PROJECT	TOTAL SHEETS	SHEET NO.

APPENDIX B: FRP RETROFIT TESTING RESULTS

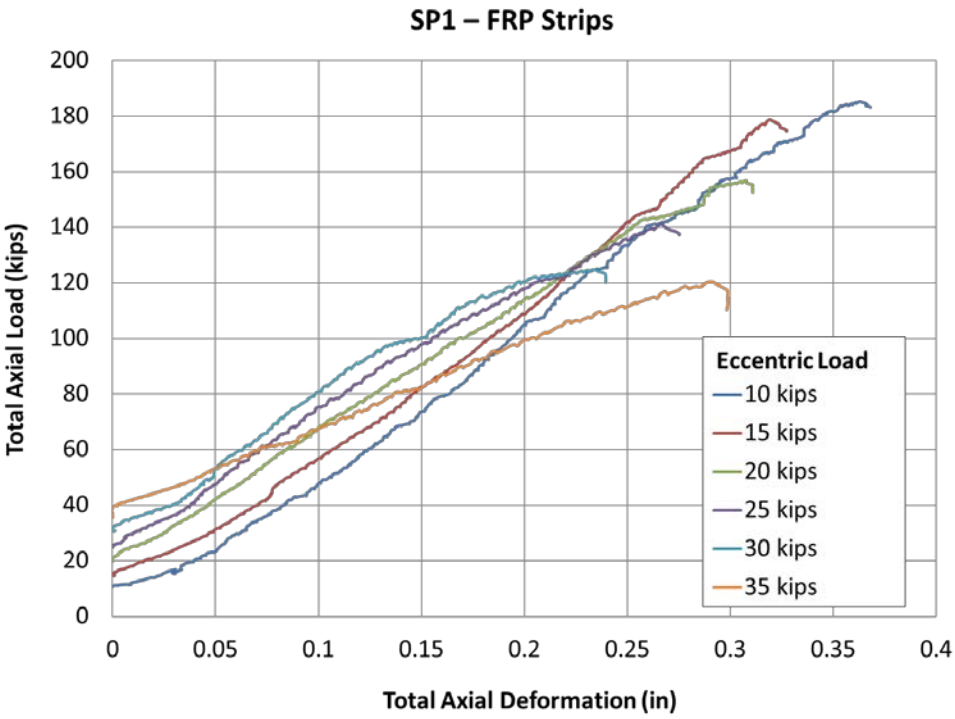

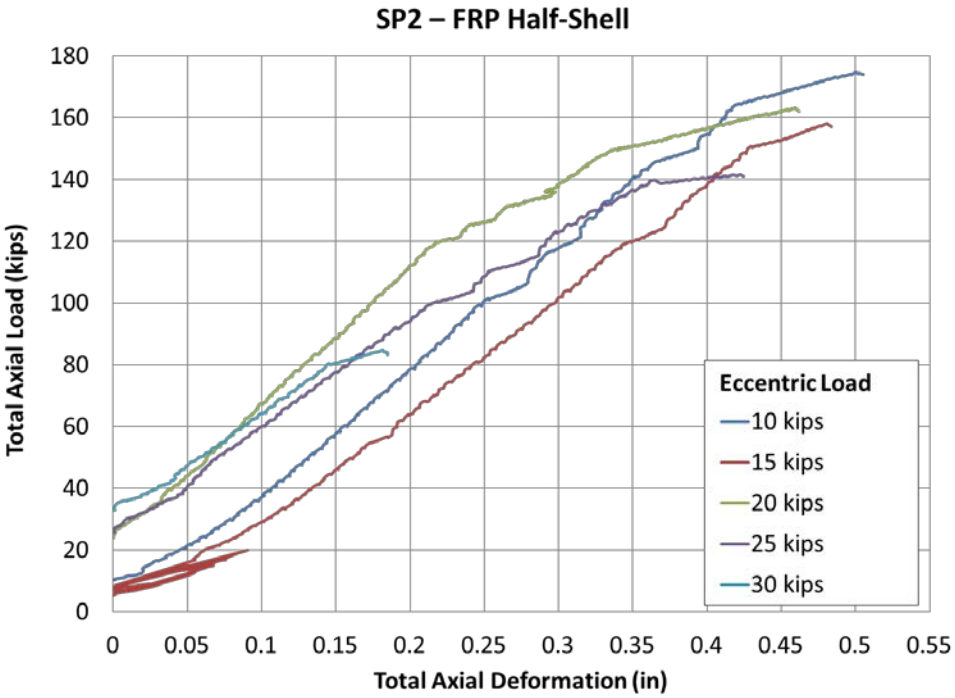

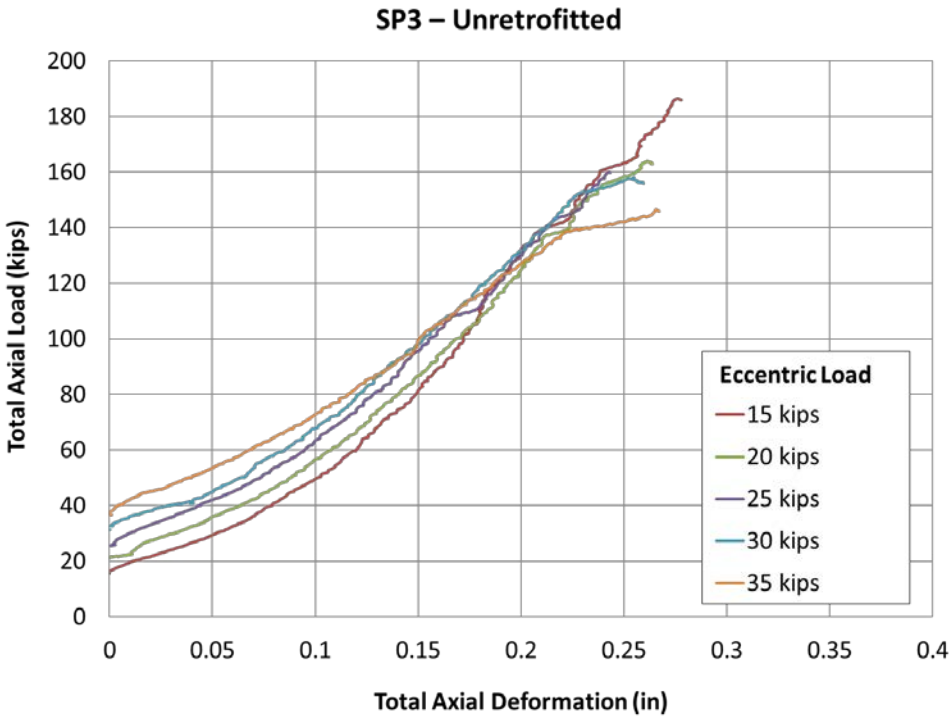
SP3 – Unretrofitted
Total Axial Load (kips)
200
180
160
140
120
100
80
60
40
20
0
0
0.05
0.1
0.15
0.2
0.25
0.3
0.35
0.4
Total Axial Deformation (in)
Eccentric Load
15 kips
20 kips
25 kips
30 kips
35 kips


Illinois Department
of Transportation


ILLINOIS
UNIVERSITY OF ILLINOIS AT URBANA-CHAMPAIGN